Tetraconodontines and suines (Artiodactyla: Suidae) from the earliest Vallesian site of Castell de Barberà (Vallès-Penedès Basin, NE Iberian Peninsula)

Sharrah McKenzie[1] · Sara G. Arranz[1] · Sergio Almécija[2,3,1] · Daniel DeMiguel[4,5,1] · David M. Alba[1,*]

[1] Institut Català de Paleontologia Miquel Crusafont, Universitat Autònoma de Barcelona, Edifici ICTA-ICP, c/ Columnes s/n, Campus de la UAB, 08193 Cerdanyola del Vallès, Barcelona, Spain

[2] Division of Anthropology, American Museum of Natural History, Central Park West at 79th Street, New York, NY 10024, USA

[3] New York Consortium in Evolutionary Primatology, New York, NY, USA

[4] ARAID foundation, Zaragoza, Spain

[5] Universidad de Zaragoza, Departamento de Ciencias de la Tierra, and Instituto Universitario de Investigación en Ciencias Ambientales de Aragón (IUCA), Pedro Cerbuna 12, 50009 Zaragoza, Spain

***Corresponding author:**
David M. Alba
david.alba@icp.cat

ORCIDs:
Sharrah McKenzie: 0000-0002-8259-3756
Sergio Almécija: 0000-0003-1373-1497
Daniel DeMiguel: 0000-0001-6138-7227
David M. Alba: 0000-0002-8886-5580

Abstract

The earliest Vallesian (~11.2 Ma) site of Castell de Barberà (CB) figures prominently in the paleoanthropological literature because of the co-occurrence of pliopithecoid and hominoid primates. However, the rest of the fauna remains understudied. In the case of suids, fossils of *Albanohyus castellensis* and *Listriodon splendens* have been described in detail, but those of suines and tetraconodontines need revision. Here, we describe more than 200 remains (both published and unpublished) of these suid subfamilies from CB, including mostly isolated teeth and some dentognathic fragments, to justify their taxonomic attribution. We conclude that CB records the suine *Propotamochoerus palaeochoerus* and the tetraconodontines *Parachleuastochoerus valentini* and *Versoporcus steinheimensis*—contrasting with previous reports that the latter was the only large tetraconodontine present there. The remains of *Pa. valentini* confirm the distinctiveness of this species and reinforce the contention that it is not a junior synonym of *Conohyus simorrensis*, while those of *Versoporcus* lead us to conclude that *Versoporcus grivensis* is a junior subjective synonym of *V. steinheimensis*. We further conclude that many remains previously included in *Conohyus doati* belong instead to *Pa. valentini*, although the species is considered a nomen dubium because its lectotype might belong to either *Conohyus* or *Versoporcus*.

Keywords *Parachleuastochoerus* · *Versoporcus* · *Propotamochoerus* · Late Miocene · Spain.

Introduction

The site of Castell de Barberà

Castell de Barberà (CB) is one of the most renowned fossil sites from the Vallès-Penedès Basin (NE Iberian Peninsula), particularly in the paleoprimatological literature (Crusafont Pairó and Hürzeler 1969; Crusafont-Pairó 1975a; Crusafont-Pairó and Golpe-Posse 1981a, 1982a; Harrison 1991; Golpe Posse 1993; Andrews et al. 1996; Alba et al. 2011, 2019; Alba 2012; Alba and Moyà-Solà 2012; Almécija et al. 2012; Marigó et al. 2014; Arias-Martorell et al. 2021), as it is not only the type locality of a pliopithecoid primate species but one of the few sites where pliopithecoids and hominoids co-occur (see discussion in Sukselainen et al. 2015; Alba et al. 2017; DeMiguel et al. 2021). Besides primates, the rest of the vertebrate fauna from CB has been the subject of multiple studies devoted to amphibians (Villa et al. 2019), reptiles (Luján et al. 2016), and some other mammals, particularly carnivorans (Petter 1976; Crusafont-Pairó and Golpe-Posse 1981b, b; Golpe-Posse 1981a, b, 1984; de Beaumont and Crusafont 1982; Robles et al. 2010, 2013; Robles 2014), artiodactyls (Golpe-Posse 1971, 1972, 1975, 1977, 1978; Moyà-Solà 1983; Azanza and Menéndez 1990; Van der Made 1990a, b, 1996a, b, 1997; Sánchez and Morales 2006; Sánchez et al. 2019), perissodactyls (Crusafont-Pairó and Golpe-Posse 1974; Crusafont-Pairó 1976; Santafé Llopis 1978a, b; Rotgers and Alba 2011; Alba et al. 2019), eulipotyphlans (Gibert 1974, 1975a, b; Gibert Clols 1975; Van den Hoek Ostende and Furió 2005), rodents (Aguilar et al. 1979; Agustí, 1981; Agustí et al. 1985; Casanovas-Vilar et al. 2016b; Alba et al. 2019), and lagomorphs (López Martínez 1989). Overall, the fauna from CB displays an interesting mixture of late Aragonian (MN7+8) and earliest Vallesian (MN9) elements (Alba et al. 2019), although it still needs revision to clarify the taxonomic identity of some of the present taxa at the genus or species rank, including some suids (see below).

CB is geographically located on the slopes of the left bank of the Ripoll River, near a homonymous country house (former medieval castle) and the old farmhouse of Ca n'Altimira (Fig. 1a), in the municipality of Barberà del Vallès (Catalonia, Spain)—UTM ETRS89 coordinates 31N 428314 E, 4596862 N (Alba et al. 2019). The site was excavated from the early 1950s until 1981 (most intensively during the late 1960s and the 1970s), and temporarily reopened in 2014 and 2015 (Fig. 1b), which showed that the main fossiliferous layer is exhausted (Alba et al. 2019). The outcrops, which are currently covered, mostly consisted of mudstones (mainly siltstones with some claystones) with interbedded sandstone layers (Santafé Llopis 1978a; Alba et al. 2019). Although the exact provenance of most of the fossils from CB is not recorded, many came from a single accumulation located at about mid-height of the short (~20 m deep) stratigraphic section (level CB-D of Alba et al. 2019). From a geological viewpoint, CB is found within the Vallès-Penedès Basin, an elongate half-graben located close to Barcelona and bounded between the Littoral and Prelittoral Coastal Ranges (Fig. 1c) that has delivered a rich continental fossil vertebrate record spanning from the Early to the Late Miocene (~20–7 Ma; Casanovas-Vilar et al. 2016a, 2022). In particular, CB is located on the distal facies of the Castellar del Vallès alluvial fan system (Alba et al. 2019), which belongs to the Middle to Late Miocene Upper Continental Units of the basin (Agustí et al. 1985; Casanovas-Vilar et al. 2016a).

The age of CB was controversial for many years. The site was initially considered either immediately pre-Vallesian (Crusafont Pairó and Truyols Santonja 1951; Golpe-Posse 1971, 1972, 1974; Crusafont-Pairó and Golpe 1972; Crusafont-Pairó and Golpe-Posse 1972, 1974; Crusafont-Pairó 1975b) or, more sporadically, earliest Vallesian (Crusafont-Pairó and Golpe-Posse 1971). The former view was initially based on the lack of

hipparionins, despite the subsequent find of surface-collected hipparionin remains (Crusafont-Pairó and Golpe-Posse 1974; see also Rotgers and Alba 2011), which were assumed to have originated from layers stratigraphically higher than the main fossiliferous horizon (see also Santafé Llopis 1978a). Indeed, Crusafont-Pairó and Golpe (1972) correlated the site with a local biozone that they had recently established based on the assumption that giraffids dispersed sometime before hipparionin equids (Crusafont Pairó and Golpe Posse 1971). This view, which was promoted further by Agustí et al. (1985, 1997, 2001), led most authors to continue accepting a latest Aragonian age (MN7+8, ~11.9–11.2 Ma) for CB (e.g., Agustí et al. 1997; Casanovas-Vilar et al. 2011; Robles et al. 2010, 2013; Alba and Moyà-Solà 2012), with very few exceptions (de Bruijn et al. 1992; Andrews et al. 1996). Nevertheless, the presence of hipparionins ultimately led Casanovas-Vilar et al. (2016a, b) to tentatively favor a correlation with the earliest Vallesian (MN9) and, more recently, Alba et al. (2022) confirmed that there is no accurately dated evidence of giraffids in the Vallès-Penedès Basin before the earliest Vallesian. Furthermore, an earliest Vallesian age for CB was confirmed by fieldwork and associated paleomagnetic samplings performed in 2014–2015 (Alba et al. 2019). These works confirmed the presence of *Hippotherium* in the main fossiliferous layer (CB-D) and enabled its magnetostratigraphic correlation with C5r.1n (11.188–11.146 Ma; boundaries after Ogg 2020). The first appearance datum of hipparionin equids in Western Europe—which marks the beginning of the Vallesian land mammal age (Crusafont Pairó 1950, 1951, 1953; Crusafont Pairó and Truyols Santonja 1960; Garcés et al. 1996; Agustí et al. 1997)—is correlated to the base of this chron in the Vallès-Penedès locality of Creu de Conill 20 (CCN20), with an interpolated age of 11.18 Ma (Garcés et al. 1996; Agustí et al. 1997; Casanovas-Vilar et al. 2016b). CB is thus securely correlated to the earliest Vallesian, with an estimated age of ~11.2 Ma that is roughly coeval to that of CCN20 (Alba et al. 2019).

The suids from Castell de Barberà

The suids from CB were originally studied by Golpe-Posse (1971, 1972), who reported the presence of *Listriodon splendens* von Meyer, 1846, *Hyotherium palaeochoerus* (Kaup, 1833), and *Hyotherium soemmeringi* [sic] von Meyer, 1834. Note that, according to the provisos of the Code (International Commission on Zoological Nomenclature 1999: Articles 32–33), the correct spelling for the latter species name is *H. soemmerringi*, as used by some authors (Hünermann 1968; contra Pickford 2016b). Unfortunately, more recent authors (e.g., Golpe-Posse 1971, 1972; Schmidt-Kittler 1971; Van der Made 1998, 2010; Pickford 2016b) have generally used this unjustified emendation. Crusafont-Pairó and Golpe (1972) first reported a faunal list of CB, which omitted the previous citation of *H. palaeochoerus* but added a small 'tayassuid' referred to as *Taucanamo pygmaeum* (Déperet, 1892)—currently classified in the chainochoerine suid genus *Albanohyus* Ginsburg, 1974. The omission of the former was apparently inadvertent, as it was later added in the updated list provided by Crusafont-Pairó and Golpe-Posse (1974) and Golpe-Posse (1974). Soon thereafter, Golpe-Posse (1975) provided a preliminary description of the small suid remains, which were ultimately employed to erect the genus and species *Barberahyus castellensis* Golpe-Posse, 1977.

During the following decades, Van der Made and Moyà-Solà (1989) reported from CB the presence of *Korynochoerus palaeochoerus* (Kaup, 1833), while Van der Made (1990a, 1990b) recognized the presence of *L. splendens*, *B. castellensis*, the tetraconodontines *Conohyus steinheimensis* (Fraas, 1870) and *Parachleuastochoerus huenermanni* (Heissig, 1989), and the suine *K. palaeochoerus*. Van der Made (1990b)

noted that the previous citations of *H. soemmeringi* by Golpe-Posse (1971, 1972) corresponded in fact to *C. steinheimensis*, but no clarification was provided regarding the distinction of a second tetraconodontine at CB. Subsequently, Van der Made (1996a) considered *Barberahyus* Golpe-Posse, 1977 to be a subjective junior synonym of the cainochoerine suid genus *Albanohyus* (see also Fortelius et al. 1996; Van der Made 1997) and Van der Made (1996b) described the remains of *L. splendens* from CB. Van der Made (1997) recognized from this site the same species previously reported by him (Van der Made 1990b) but updated their taxonomy following Fortelius et al. (1996). These updates included considering *Korynochoerus* Schmidt-Kittler, 1971 as a junior subjective synonym of *Propotamochoerus* Pilgrim, 1925 and including *C. steinheimensis* into *Parachleuastochoerus* Golpe-Posse, 1972.

During the last decade, the taxonomy of European tetraconodontines has been subject to various revisions (Pickford 2014, 2016a; Pickford and Laurent 2014), leading to various controversies (see Van der Made 2020) that are relevant for clarifying the taxonomic identity of the CB tetraconodontine remains. For decades, *C. steinheimensis* was considered either a subspecies (Thenius 1956) or just a junior subjective synonym (Hünermann 1968) of *Conohyus simorrensis* (Lartet, 1851), the type species of the genus *Conohyus* Pilgrim, 1925, until its distinct species status became generally accepted after Chan (1984). Fortelius et al (1996) transferred *C. steinheimensis* to *Parachleuastochoerus*—an opinion that was accepted by some (Van der Made 1997, 1999, 2020; Pickford 2012, 2013a; Van der Made et al. 2014) but not all (Bernor et al. 2004; Fortelius et al. 2005; Harris and Liu 2007; Pickford 2013b) researchers. More recently, the genus *Versoporcus* Pickford, 2014 was erected with *Versoporcus steinheimensis* (Fraas, 1870) as its type species. Pickford (2014) further resurrected *Versoporcus grivensis* (Gaillard, 1899) and included it in the genus newly erected by him (see also Pickford 2016a). These proposals have tentatively been accepted by some researchers (McKenzie et al. 2023a, 2023b) and rejected by others (Van der Made 2020; Iannucci and Begun 2022). In particular, Van der Made (2020) considered *Versoporcus* to be a junior subjective synonym of *Parachleuastochoerus* and *V. grivensis*, in turn, a junior subjective synonym of *Pa. steinheimensis*, while McKenzie et al. (2023a, b) preferred to tentatively keep both *Versoporcus* species separate until their distinctiveness or purported synonymy could be further ascertained based on additional material.

Regarding the distinction of the genus *Versoporcus* from *Parachleuastochoerus* proposed by Pickford (2014, 2016a), as remarked by Iannucci and Begun (2022) and McKenzie et al. (2023b), it largely relies on the inclusion of *Parachleuastochoerus valentini* (Filhol, 1882) in *Parachleuastochoerus*, which is in itself controversial. Following the lectotype designation for *C. simorrensis* and the proposal of an emended diagnosis of *Conohyus* by Pickford and Laurent (2014), the latter authors resurrected the long-forgotten nominal species *Sus valentini* Fihol, 1882 within *Parachleuastochoerus*, which was redescribed in greater detail by Pickford (2014, 2016a). Van der Made (2020) questioned the lectotype designation and considered *Pa. valentini* to be a junior subjective synonym of *C. simorrensis*. In contrast, McKenzie et al. (2023b) accepted the taxonomic validity of the species and its distinction from *C. simorrensis*, but considered that its referral to *Parachleuastochoerus* instead of *Conohyus* needed to be better substantiated. The latter authors also partially concurred with Van der Made (2020) that some of the material included in the *Pa. valentini* hypodigm by Pickford (2014, 2016a)—in particular, that originally used to describe *Conohyus melendezi* Golpe-Posse, 1972—belongs in fact to *C. simorrensis*. Finally, McKenzie et al. (2023b) further questioned the distinctiveness of *Conohyus doati* (Lartet, 1851), which was considered a junior subjective synonym of *C. simorrensis* by Van der

Made (2020), and concluded that some of the material assigned to the former species by Pickford (2016a) would be referable instead to *Pa. valentini* or of uncertain taxonomic attribution.

In summary, while McKenzie et al. (2023a, b) concurred with Pickford (2014, 2016a) that a large tetraconodontine different from *C. simorrensis* and *Versoporcus* spp. is recorded in the MN7+8 and MN9 of Europe, they remained skeptical about its inclusion in *Parachleuastochoerus* instead of *Conohyus*. As noted by Iannucci and Begun (2022), the cranial differences between *V. steinheimensis* and *Pa. valentini* used by Pickford (2014) to justify the distinction of *Versoporcus* could merely reflect that the latter species belongs to *Conohyus* instead of *Parachleuastochoerus*. Unfortunately, there is no cranial material of the type species of the latter genus (*Parachleuastochoerus crusafonti* Golpe-Posse, 1972) to compare with. Moreover, the unknown morphology of the *Pa. valentini* c1m (McKenzie et al. 2023b) further precludes to ascertain whether this species displays the characteristic band of cementum that is currently considered diagnostic of *Conohyus* (Pickford and Laurent 2014; Pickford 2016a).

Pickford (2014, 2016a) argued that previous citations of *P. palaeochoerus* from MN7+8 localities such as Sant Quirze, Saint-Gaudens, and Abocador de Can Mata (Van der Made 1990b, 1997; Alba et al. 2006) were incorrect and stemmed from a confusion with *Pa. valentini*, with the former species not being conclusively recorded before the earliest Vallesian (see also Alba et al. 2022; McKenzie et al. 2023b). This does not apply to CB, given its earliest Vallesian age (Alba et al. 2019). However, somewhat surprisingly in the light of previous work by Van der Made (1990b, 1997), most recently Pickford (2016a) only reported the presence of a single tetraconodontine (*V. steinheimensis*) in CB and did not signal the presence of *P. palaeochoerus* either. Pickford (2016b) reported the previous citations of *H. palaeochoerus* and *H. soemmeringi* from CB by Golpe-Posse (1972), but refrained from providing their current taxonomic attribution, merely implying that they are not hyotheriines. As such, it is currently uncertain whether Golpe-Posse's (1971, 1972) citations of *H. palaeochoerus* from CB correspond to *P. palaeochoerus* (as supported by Van der Made 1990b, 1997), *Pa. valentini*, or both. To make the situation even more confusing, McKenzie et al. (2023a) reassigned to *V. grivensis* the tetraconodontine material from the Vallès-Penedès site of Ca l'Almirall, previously assigned to *V. steinheimensis* by Pickford (2016a). The former authors remarked that the two *Versoporcus* species considerably overlap in stratigraphic range and that other previous reports of *V. steinheimensis* from the same basin are in need of revision. Therefore, it is also uncertain if the material from CB attributed to *H. soemmeringi* by Golpe-Posse (1971, 1972) represents one or the other species of *Versoporcus*, or whether some of the material might belong instead to *Pa. huenermanni* (cited from the site by Van der Made 1990b, 1997) and/or the larger *Pa. valentini*. The fact that neither Golpe-Posse (1971, 1972) nor Van der Made (1990b, 1997) figured or described in detail the tetraconodontine or suine material from CB makes it impossible to clarify further the composition of the suid assemblage without studying the fossil material.

With this aim in mind, here we describe and figure all the available (both published and unpublished) tetraconodontine and suine dental and dentognathic material from CB, and on the basis of detailed morphological and morphometric comparisons we justify their species attribution. The implications for tetraconodontine systematics are further discussed.

Materials and methods

Studied material

The described material includes 228 specimens, which consist of 207 isolated teeth and 21 dentognathic fragments, tooth series, or associated remains, representing in total up to 280 teeth (Appendix Table 1). All the specimens are housed in the ICP in Sabadell (Catalonia, Spain) and their catalog numbers are preceded by the acronym IPS (following the previous informal name of this institution, 'Institut de Paleontologia de Sabadell'). Dentognathic fragments are depicted in buccal, lingual, and occlusal views, and their socketed cheek teeth are also figured along with isolated specimens. In the latter illustrations, some third and all fourth permanent premolars, deciduous third and fourth premolars, and molars are depicted only in occlusal view, whereas the remaining premolars are further figured in buccal and lingual views. In turn, incisors and canines are depicted in lingual, mesial, labial, and distal views. In all occlusal views, mesial is located on top.

Part of the studied material from CB was already reported (but not figured or described in much detail) by Golpe-Posse (1971, 1972) using catalog numbers similarly preceded by the acronym 'IPS' but which do not correspond to the currently valid ones using the same acronym. We were able to establish the correspondence with most of the specimens reported by Golpe-Posse (1971, 1972), only in a few cases tentatively, thanks to the fact that they are usually written on the specimens. The old numbers are provided within brackets in Appendix Table 1, with uncertainties about the equivalences and/or locality provenance specified in footnotes, and the same convention is followed when old numbers are mentioned in the main text. Most of the specimens without old numbers (and some with old numbers not recorded in Golpe-Posse, 1971) must have been recovered after ca. 1970–1971, which is not surprising given that the site was excavated at least until 1981 (Alba et al. 2019) and that subsequent publications by the same author (Golpe-Posse 1975, 1977, 1978) evinced the discovery of additional suid remains. Indeed, based on museum records, some of the reported specimens were collected in 1977, 1978, and 1980 (see Appendix Table 1 for details). It is also noteworthy that, in the course of cross-checking Golpe-Posse's (1971) old numbers, we located several teeth of *Pa. crusafonti* from Can Llobateres 1 and *Pa. huenermanni* from Can Poncic 1 incorrectly cataloged during the 1980s as from CB. The provenance of these specimens is straightforward based on Golpe-Posse (1971, 1972), and hence they have been ignored in the present study. However, most likely they constitute the basis of Van der Made's (1990b, 1997) report of *Pa. huenermanni* from the site, as we were unable to find any specimens attributable to a small-sized tetraconodontine among the rest of the sample from CB.

Dental terminology and measurements

Uppercase and lowercase letters are used to denote tooth type for the upper and lower dentition, respectively: I/i, incisor; C/c, canine; P/p, premolar; M/m, molar. Deciduous teeth are preceded by D/d, while m/f indicate whether canines belong to male or female individuals, respectively. Tooth position for each tooth type is indicated by a number (e.g., m3 is the lower third molar while C1m refers to the male upper canine). Dental axes are termed following Smith and Dodson (2003: fig. 7), except that the use of 'labial' is restricted to the incisors and canines, whereas 'buccal' is used for the cheek teeth. Dental terminology is generally based on Van der Made (1996b: figs. 1–15), albeit with some modifications (Fujita et al. 2000: fig. 2; Thaung-Htike et al. 2006: fig. 2; for further details, see McKenzie et al. 2023a, b).

Dental measurements of crown maximum mesiodistal length (MD) and labiolingual/buccolingual breadth (BL) were taken for all tooth loci except c1m, in which case maximum labial (La), lingual (Li), and distal (Di)

breadths were measured. For molars, buccolingual breadth was taken separately at the mesial (BLm) and distal (BLd) lobes (or central, in the case of third molars), with the greatest value being taken as BL. All measurements were taken with a digital caliper to the nearest 0.1 mm. A breadth/length index (BLI = BL / MD × 100) was also computed to reflect overall crown proportions. Dental size and proportions are compared by means of bivariate plots of BL vs. MD for deciduous and permanent cheek teeth. The range of variation for the analyzed species in the comparative sample (see next subsection) are highlighted by means of convex hulls.

Comparative sample

Dental measurements for the comparative sample were taken from the literature. The selected species include the suine *P. palaeochoerus* and the tetraconodontines *Pa. valentini* (including most of the remains previously included in *C. doati* by Pickford 2013a, 2014, 2016a) and *V. steinheimensis* s.l. (i.e., including *V. steinheimensis* s.s. and *V.* '*grivensis*' sensu Pickford 2014).

The comparative sample of *P. palaeochoerus* (Mottl 1966; Hellmund 1995; Van der Made et al. 1999; Fortelius et al. 2005; Pickford 2013a, 2015; Iannucci and Begun 2022; McKenzie et al. 2023a) includes specimens from CCN20 in Spain; the Drôme Dept. in France; Eppelsheim, Esselborn, Gau-Weinheim, Melchingen, Münchener Flinz, Wallertsheim, Westhofen, and Wolfsheim in Germany; Brunn am Gebirge, Eichkogl (Guntramsdorf), Groß Mugl, Hennersdorf, Johnsdorf bei Feldbach, Laßnitzhöhe bei Graz (Schottergrube Grießl), Pyhra, Saaz bei Feldbach, Wien III/Belvedere, and Wien X/Wienerberg in Austria; Rudabánya and Alsótelekes in Hungary; and Grytsiv in Ukraine. Except for the recently described remains from the roughly coeval site of CCN20 (McKenzie et al. 2023a), other samples of *P. palaeochoerus* from the Vallès-Penedès Basin have not been included because they are pending revision, given that Golpe-Posse's (1971) identifications are not entirely reliable. Currently, there is consensus that *P. palaeochoerus* is restricted to the Vallesian, with most localities being correlated to MN9 and a few to MN10 (Pickford 2013a, 2016a; Alba et al. 2022; McKenzie et al. 2023a).

In turn, the comparative sample of *Pa. valentini* includes the material previously attributed to this species from the following localities (Pickford 2014, 2016a; McKenzie et al. 2023a): CCN20 and Sant Quirze in Spain; Charmoille, Valentine, and Saint-Gaudens in France; Gau-Weinheim, Hammerschmiede, Hinterauerbach bei Wartenberg, Kleineisenbach, Tutzing, and Wartenberg bei Erding in Germany; and Hollabrunn, Klein Hadersdorf, and Pitten in Austria. The comparative sample of this species thus includes material from two Vallès-Penedès sites attributed to *Pa. valentini* during the last decade (Pickford 2014; McKenzie et al. 2023a) but it is uncertain whether it is recorded among the material from other sites of the same basin that awaits (re)description. Even though the dating of some sites with *Pa. valentini* is uncertain, those more securely dated are correlated to either MN7+8 or MN9 (Pickford 2016a; McKenzie et al. 2023a). It is noteworthy that the much older sample from Mira (Spain), originally used to erect *Conohyus melendezi* Golpe-Posse, 1972 and attributed to *Pa. valentini* by Pickford (2014, 2016a), has been excluded from the comparative sample of this species because it is considered a junior synonym of *C. simorrensis* instead (Van der Made 2020; McKenzie et al. 2023a). In contrast, a P3 and an M3 from Hammerschmiede and three M3s and an m3 from Gau-Weinheim, attributed by Pickford (2013a, 2016a) to *C. doati*, are here included in *Pa. valentini* following McKenzie et al. (2023a), despite concurring with Van der Made (2020) that the nominal species *C. doati*—as defined by the holotype M3 from Bonnefond in France (Pickford and Laurent 2014; Pickford 2016a)—might be a junior

synonym of *C. simorrensis* (see the Discussion for further details). The type material of *Conohyus ebroensis* Azanza, 1986 from El Buste in Spain, as well as that from Fonte o Pinheiro in Portugal attributed by Van der Made (1989) to the same species—referred to *C. doati* by Pickford (2016a) and considered a junior synonym of *C. simorrensis* by Van der Made (2020)—is here also referred to *Pa. valentini*, along with the material from Gaiselberg near Zistersdorf in Austria. This possibility was already considered but not formalized by McKenzie et al. (2023a); however, we consider this as the most likely attribution, given the morphology of the p4 from El Buste (less inflated than in *C. simorrensis*) and the large size variation of *Pa. valentini* upper molars—suggesting that the large lower molars from the aforementioned sites merely correspond to large individuals of this species.

Finally, the comparative material of *Versoporcus* (Van der Made et al. 2014; Pickford 2016a; McKenzie et al. 2023b) is divided in two subsamples despite the fact that, for the reasons that will be exposed in the Discussion, we consider that *V. grivensis* is a junior subjective synonym of *V. steinheimensis*. Thus, those remains previously reported as *V. grivensis* in the literature (Pickford 2014, 2016a; McKenzie et al. 2023b) have been labeled as *V. 'grivensis*' (with the trivial name within quotes) in the dental plots and in the text, while *V. steinheimensis* s.s. has been employed for those samples assigned to this species by the same authors. The sample of the latter includes material from La Grive-Saint-Alban in France; and Steinheim (type locality) in Germany. In turn, the sample of *V.* '*grivensis*' comprises material from Ca l'Almirall in Spain; La Grive-Saint-Alban in France; Anwil in Germany; and Gratkorn in Austria. McKenzie et al. (2023b) reviewed the stratigraphic ranges of the two purported *Versoporcus* species and concluded that they substantially overlapped—from 13.8–13.5 to at least 12.4–11.9 Ma in the case of *V. steinheimensis* s.s. (up to 11.2 Ma if the material from CB, attributed by Pickford, 2016a to this species, is included) and from 13.3 to at least 11.9 Ma in that of *V.* '*grivensis*'. The older material from Lučane in Croatia (~15 Ma), attributed by Van der Made (2020) to *Parachleuastochoerus steinheimensis olujici* (Bernor et al. 2004), is here excluded from the *Versoporcus* sample as the former taxon is considered a junior subjective synonym of *Pa. huenermanni* following Pickford (2016a) and McKenzie et al. (2023a, b).

Data availability

All data generated during this study are included in this published article or in the supplementary information file. The dataset of published measurements analyzed during the current study is available from the corresponding author on request.

Abbreviations

Locality and institutional abbreviations: CB, Castell de Barberà; CCN20, Creu de Conill 20; ICP, Institut Català de Paleontologia Miquel Crusafont, Sabadell, Barcelona, Spain; IPS, acronym of the ICP collections (for the former 'Institut de Paleontologia de Sabadell').

Measurement abbreviations: BL, maximum labiolingual or buccolingual breadth; BLI, breadth/length index; BLm = BL at the mesial lobe (form molars); BLd = BL at the distal lobe (for molars; central lobe in M3s and m3s); L, left; Li = lingual breadth (for c1m); Li = labial breadth (for c1m); Di = distal breadth (for c1m).

Systematic paleontology

Order Artiodactyla Owen, 1848

Superfamily Suoidea Gray, 1821

Family Suidae Gray, 1821

Subfamily Suinae Gray, 1821

Tribe Dicoryphochoerini Schmidt-Kittler, 1971

Genus *Propotamochoerus* Pilgrim, 1925

Propotamochoerus palaeochoerus (Kaup, 1833)

Figures 2a–b, d–e, 3a–c, h, k–l, 4a–d, 5a–g, j–p, r–w, z–j', 6a–f, r–x, b'–k', 7a–f, 8a–d, f–i, 9a, d–e, 10a–c, k–l, q–s, u–y, 11a–c, k–m, s–u, 12a–b, g–o, u–z, m'–s', 13a–d, i, m–n, p, r, w–z.

Selected synonyms

1833 *Sus palaeochoerus* Kaup (original description).

1926 *Hyotherium palaeochoerus* (Kaup, 1833): Pilgrim (new combination).

1966 *Hyotherium palaeochoerus* (Kaup, 1833): Mottl.

1971 *Korynochoerus palaeochoerus* (Kaup, 1833): Schmidt-Kittler (new combination and designation of type species in the erection of the genus).

1972 *Hyotherium soemmeringi* von Meyer, 1834: Golpe-Posse, partim (based on specimens detailed in Golpe-Posse, 1971).

1972 *Hyotherium palaeochoerus* (Kaup, 1833): Golpe-Posse, partim (based on specimens detailed in Golpe-Posse, 1971).

1980 *Korynochoerus palaeochoerus* (Kaup, 1833): Ginsburg, partim.

1989 *Korynochoerus palaeochoerus* (Kaup, 1833): Van der Made and Moyà-Solà, partim.

1990a *Korynochoerus palaeochoerus* (Kaup, 1833): Van der Made, partim.

1992 *Propotamochoerus palaeochoerus* (Kaup, 1833): Van der Made et al. (new combination), partim.

1996 *Propotamochoerus palaeochoerus* (Kaup, 1833): Fortelius et al.

1999 *Propotamochoerus palaeochoerus* (Kaup, 1833): Van der Made et al., partim.

2022 *Propotamochoerus palaeochoerus* (Kaup, 1833): Iannucci and Begun.

2023a *Propotamochoerus palaeochoerus* (Kaup, 1833): McKenzie et al.

Referred material

See Appendix Table 1 for a list of the referred material and Appendix Table 2 for measurements.

Description

Upper permanent incisors: No socketed incisors are available from the maxillary specimens included in the studied sample (Fig. 2), but several isolated specimens are attributed to *P. palaeochoerus*. The following description of the I1 is based on a completely preserved and moderately worn specimen (Fig. 3a). The two remaining ones (Fig. 3b–c) display more advanced wear and are missing the tip of the root, but otherwise their preserved morphology conforms well with that of the former specimen. The crown is high and asymmetrical (tilted mesially), with a labiolingually compressed occlusal contour and a short incisal edge that displays a

slightly oblique wear facet. The crown walls are markedly convex except for its distolingual portion, which is concave above the marked cingulum. The latter is continuous with the precrista, which reaches the incisal edge and is flanked by a deep and narrow groove. The postcrista is less defined than the precrista and culminates toward the crown base in a distinct cuspule (the metacone of Van der Made, 1996b). The latter, which displays some dentine exposure, is separated from the cingulum by a sinuous deep groove that extends up to the cervix. Above the cingulum, there are two narrow and vertical cristae that fade away well before reaching the incisal edge. The cervix is markedly asymmetrical, with a deep and U-shaped preanticline mesiolabially and a marked endosyncline distolingually. The root is higher and more labiolingually compressed than the crown, being somewhat waisted at the cervix. It progressively tapers from cervix to apex and is rather straight in mesial and distal views, but markedly curved distally toward the apex in labial and lingual views.

The single I2 of *P. palaeochoerus* (Fig. 3h) displays a moderately advanced degree of wear. The crown is low and labiolingually elongate (i.e., very labiolingually compressed) and widest toward its mesial half, progressively tapering distally. Due to wear, occlusal details cannot be adequately ascertained, except that there is a distinct lingual cingulum along the distolingual margin of the crown. The cervix is not markedly asymmetrical, with a mildly developed mesiolingual preanticline and a similarly developed distal endosyncline. The root is comparatively much less developed than in the I1 and labiolingually compressed, being slightly curved lingually and markedly tilted distalward relative to the crown.

The two I3s of *P. palaeochoerus* (Fig. 3k–l) display an advanced degree of wear, which is more marked on the distal half of the crown, where an oblique wear facet has completely obliterated the cervix and eroded away the basal-most distal portion of the root. Nevertheless, one of the specimens (Fig. 3k) still displays the characteristic triangular labial and lingual profile of this tooth position in *P. palaeochoerus*, given the presence of a smaller oblique wear facet on the mesial portion of the crown, whereas in the other specimen (Fig. 3l) the mesial-most end of the crown remains unworn. The latter thus preserves a distinct mesial preconule, which is lingually flanked by a well-developed precrista—both structures being eroded by wear in the other specimen. Otherwise, the two I3s display similar size and shape regarding both the crown and the root. The crown is mesiodistally elongate, with its highest portion being more mesially located than crown mid-length along the main mesiodistal axis of the crown. The root is stout and very labiolingually compressed throughout most of its extension, and displays bulging mesial and distal profiles except at its apical-most portion, which is tilted lingually.

Upper permanent canines: The upper canines are represented by four C1fs, including two antimeres from a single individual that preserves other tooth loci (Fig. 4c–d), as well as by two isolated specimens (Fig. 4a–b) that, based on shape and wear stage similarities, might also represent the left and right antimeres of another individual. The former specimens, which are missing the root apices, only display some apical wear and a shorter mesial wear facet that does not reach the cervix, enabling us to ascertain the distal morphology of the crown. The other specimens are almost completely preserved (only the root apices are slightly damaged) but more worn, displaying two vertical wear facets (a narrow mesial one and a more extensive distal facet) that are confluent on the crown's apex and closely approach or reach the level of the cervix. Except for wear, the four available C1fs display a similar morphology. The crown is labiolingually compressed and displays a subtriangular profile in labial and lingual views. The labial crown wall displays a convex contour, whereas the mesiolingual one is straighter; there is no distinct precrista on the basal-most preserved portion of the crown. The

distolingual aspect of the crown, when unworn, is concave, being delimited by two vertical cristae that extend from the crown's apex to the cervix and are eroded in specimens with a more advanced degree of wear. The distolingual endocrista is more tenuous, whereas the distal postcrista is much sharper and better developed, labially flanked by a distinct vertical groove and forming a distinct distal protrusion above the cervix. The cervix displays a shallow ectoanticline and a slightly more marked preanticline. The root is moderately stout and higher than the crown, labiolingually compressed, and moderately curved distally (tapering from base to tip due to the more curved mesial than distal profile in labial and lingual views).

Upper permanent premolars: There P1s of *P. palaeochoerus* include two sets of antimeres (Fig. 5a–d) and additional isolated specimens (Fig. 5e–g). All of them preserve the crown, which is worn to some extent except in a single specimen (Fig. 5g), and most of them also have complete or partial roots. The crown displays a low relief and is very compressed buccolingually. Despite some variation in occlusal contour, in all instances, the crown is slightly constricted at about mid-length. There are two main cusps: the paracone, which is the highest and most extensive one, is centrally located slightly toward the mesial side of the crown; in turn, the metacone (eroded by wear in most specimens) is located close to the distal end of the crown and slightly more lingual than the paracone. Two mesiodistally aligned crests originate from the tip of the paracone: the precrista ends in a well-developed prestyle that is located at the mesial end of the crown and only slightly lower than the metacone; in turn, the slightly shorter postcrista is directed toward the metacone, albeit separated from the latter by a cleft. No distinct metacone postcrista can be ascertained. No continuous buccal or lingual cingula are present, although some remnants are present surrounding the prestyle and, in some specimens, at the level of the paracone postcrista and the metacone. There are two distinct and well-developed roots, both curved and/or tilted distally, the mesial one being generally stouter and slightly longer than the distal.

Almost all the P2s (Fig. 5j–p) are assigned to *P. palaeochoerus*, because despite some variation in size and occlusal contour they do not display the more trenchant morphology that would be expected for a tetraconodontine. The most complete specimen (Fig. 5j) preserves the moderately worn crown and most of the two roots, and, along with its antimere (Fig. 5m), is the largest P2 of the sample. These two specimens clearly display a figure-eight occlusal contour, with two distinct lobes showing very convex margins, the distal one being clearly broader than the mesial. As far as this can be ascertained due to preservation, this characteristic applies to most other specimens, although in some P2s (Fig. 5k, p) the buccolingual constriction and the difference in breadth between the two lobes are much less accentuated. The crown displays low relief, with the highest cusp (paracone) being located on the mesial half of the crown. The narrow but rather blunt paraprecrista connects the apex of this cusp with a moderately developed prestyle, which is located on the mesial end of the crown and flanked by well-developed cingula. A similarly developed but less steep parapostcrista terminates in a rather indistinct smaller and lower cusp (metacone), which is higher than the prestyle and slightly more buccal than the paracone. The apices of the two cusps, and sometimes also the parapostcrista, are worn in most specimens. A short metapostcrista is normally directed toward the distobuccal corner of the crown. All the specimens display a well-developed but discontinuous lingual cingulum, which is interrupted at about the level of the paracone and in some specimens becomes ledge-like on its distolingual aspect. The buccal cingulum is comparatively more inconspicuous, being only well developed along the distobuccal portion of the crown. The two roots are similarly developed and rather vertically oriented, being only fused at their basal-most portion.

The P3s display variable degrees of wear, from very advanced (most of the occlusal surface shows dentine exposure; Fig. 5r–s) to moderately advanced (two dentine exposures, one including the paracone and metacone, and the other corresponding to the paracone; Fig. 5u–v) or slight (only the apices of the paracone and metacone; Fig. 5t, w). The latter P3s, consequently, are the ones that display higher occlusal relief, which is more marked than in the P1 and P2. The occlusal contour Is subovoid (somewhat longer than wide and wider distally than mesially) but markedly asymmetrical—with a markedly convex mesial contour, a moderately convex to somewhat sinuous labial contour, a straight distal contour, and a lingual contour displaying a marked constriction at the level of the paracone, separating the convex mesiolingual crown portion from the bulging distolingual one, where the protocone is located. Despite the higher occlusal relief than in the preceding premolars, the crown does not appear particularly trenchant even when only slightly worn. The paracone is centrally located and linked to the generally well-developed mesial cingulum by a slightly mesiodistally oriented paraprecrista, without forming a conspicuous prestyle. In some (e.g., Fig. 5t) but not all (e.g., Fig. 5u) specimens, the mesial cingulum forms small basin-like structures at the sides of the precrista. The paracone would have originally been linked to a distinct metacone by means of a short parapostcrista, which is lower than and mesiodistally aligned with the former cusp, and linked to a moderately developed distal cingulum by a short metapostcrista. The buccal crown wall is convex except for a mild vertical cleft at the level of the parapostcrista, and shows no cingulum throughout most of its length. In contrast, most of the lingual side is surrounded by a strongly developed cingulum, which is partly (Fig. 5u) to completely (Fig. 5t, w) interrupted at the level of the paracone apex. The protocone is very low and peripherally located on the distolingual bulging crown portion, barely protruding from the cingulum. Nevertheless, it is separated from the bases of the paracone and metacone by a very deep and obliquely oriented groove, which sometimes even constitutes a narrow basin-like fossa (Fig. 5t) enclosed by the surrounding cusps and cingula. This premolar is triradiculate, with two distal roots and a somewhat stouter but similarly vertical mesial one (albeit the distolingual root is preserved in none of the CB specimens).

The P4 is the premolar most abundantly represented among the studied sample, being represented by 11 specimens (Fig. 5z–j'), including some antimeres. All specimens are worn to some extent. A partial crown only shows dentine exposures at the apices of the buccal cusps (Fig. 5e'), but most other specimens also show a dentine exposure at the apex of the protocone (Fig. 5z–d'); in specimens with a more advanced degree of wear (Fig. 5f'–j'), the buccal cusps have completely been eroded by wear and a single dentine lacuna occupies most of the buccal half of the crown. The occlusal contour is subtrapezoidal and lingually tapering, being somewhat broader than long and longer buccally than lingually. The mesial and distal contours are rather straight, while the lingual contour is convex to a variable degree, and the buccal one displays two convexities separated by a vertical groove that separates the buccal walls of the paracone and metacone. The protocone is somewhat more extensive, more centrally located along the mesiodistal axis of the crown, and less peripheral than the buccal cusps. The metacone is subequal in size to the paracone; both cusps are closely packed but well distinct from one another, and separated from the protocone by a deep protofossa. As far as it can be ascertained in some specimens, lingually from the paracone there is a moderately developed preconule that partly obliterates the protofossa and, in most specimens, is continued mesially by a precrista that interrupts the well-developed mesial cingulum. The distal cingulum is similarly well developed, and both cingula are buccally flanked by a well-developed prestyle and a lesser developed poststyle on the mesiobuccal an distobuccal corners of the crown,

respectively. There is no lingual cingulum, while the buccal one is generally restricted to small remnants next to the prestyle and poststyle (sometimes slightly more developed; Fig. 5d').

Upper molars. All the M1s (Fig. 6a–f) and M2s (Fig. 6r–x) of *P. palaeochoerus* from CB display quite an advanced degree of wear that does not enable to ascertain many occlusal details. They display a comparable occlusal morphology at a different size, with the M2 being larger than the M1. Both molars display a subrectangular occlusal outline longer than broad, with bilobed convex buccal and lingual sides. The mesial and distal lobes, separated by marked buccal and lingual constrictions, display a similar breadth but are slightly offset from one another, the distal one being slightly more lingually positioned (or, at least, more lingually protruding) than the mesial. There are four main cusps of similar size, the lingual ones being more distally located than the corresponding mesial cusps. A smaller hypopreconule can still be discerned despite wear in some M2s, at least partially blocking the transverse valley between the mesial and the distal lobes (although this is difficult to ascertain due to wear). The latter valley is usually open lingually, but buccally enclosed by a distinct metaectoconule. The mesial and distal cingula are well developed, the former being centrally interrupted by a protopreconule that, in all available specimens, is eroded by wear. In contrast, there is no lingual cingulum, whereas the buccal one is restricted to a variably developed distobuccal cingulum that is only present in some specimens and does not always become continuous with the distal cingulum.

The available M3s (Fig. 6b'–k') are less worn than the other upper molars and differ from them in size, proportions, and other occlusal details. In particular, the M3 is slightly broader and much longer than the M2, and displays an elongate and asymmetric subtriangular occlusal contour that is moderately convex mesially and markedly tapers distally, with the crown being longer lingually than buccally. Three distinct lobes are discernible, being separated by more or less marked constrictions, which tend to be more developed on the buccal side. The mesial lobe is the broadest, while the distal one is rather small and restricted to the lingual half of the crown. The least worn specimens display abundant remains of Fürchen and secondary crenulations of the enamel throughout the occlusal surface. There are five main cusps, the lingual ones (protocone and hypocone) being more distally located than the corresponding buccal ones (paracone and metacone)—more clearly so than in the M1 and M2. The mesial cusps are bulbous and similarly extensive, whereas the hypocone and metacone are smaller and more buccolingually compressed (especially the hypocone). The paracone and metacone are mesiodistally aligned, whereas the hypocone is more lingually situated than the protocone. The pentacone, which is the smallest main cusp, is slightly more centrally located than the protocone, being either distally directed or lingually tilted (depending on the specimen). The mesial cingulum is very well developed and displays a beaded appearance when unworn. It is constituted by two arched portions surrounding the protocone and paracone that merge toward the crown midline in a conspicuous protopreconule. As in the other upper molars, there is no lingual cingulum and no continuous buccal cingulum, although the latter can be variably developed around the paracone as a continuation of the mesial cingulum in some specimens. The hypopreconule is large, comparable to the protopreconule but smaller than the main cusps, and does not block the transverse valley separating the mesial and the distal lobes. As in the M1 and M2, there is a variably developed buccal metaectoconule. The M3 displays five roots, unlike the four-rooted M1 and M2.

Lower permanent incisors: Mandibular fragments (Fig. 7c–f) are scarce and not particularly informative, merely showing in some cases the association of some cheek teeth (Fig. 7c, e) but no incisors.

The three lower permanent incisors are represented by isolated specimens, including four i1s (Fig. 8a–d) and four i2s (Fig. 8f–i). The description of the i1 is based on the best-preserved crown (Fig. 8a), while the remaining specimens are more worn but nevertheless enable to ascertain the morphology of the root, which is vertically aligned with the crown without waisting at the cervix. The crown is tall and mesiodistally compressed at the base, being similarly long throughout its whole extension but progressively becoming labiolingually flatter toward the incisal edge. The labial crown wall is convex, whereas the lingual displays a broad and protruding endocristid (eroded by wear except in the least worn specimen; Fig. 8a), which originates from a basal bulge and is slightly tilted mesially, terminating before reaching the incisal edge. On its apical portion, the lingual side displays marked mesial and distal marginal ridges (precristid and postcristid) that enclose the prefossid and the similarly deep but mesiodistally narrower endofossid, respectively. The ectosynclinid extends slightly farther onto the rooth than the endosynclinid, while the pre- and postanticlinid display an inverted V-shape and are similarly developed. The root is taller and more mesiodistally compressed than the crown, progressively tapering from base to apex and curving lingually along its apical portion. In all the specimens that preserve the root, a broad and shallow apicobasal sulcus can be ascertained, extending from the tip throughout most of the distal side of the root without reaching the cervix.

The i2 is similarly represented by four specimens (Fig. 8f–i) that preserve both the crown and the root but which, with a single exception (Fig. 8g), are heavily worn. The crown is more asymmetrical than that of the i1, being tilted mesially and thus slightly higher mesially than distally, but similarly vertically aligned with the root without conspicuous waisting at the cervix. The crown is mesiodistally compressed at its base, with a markedly convex lingual wall and a more concave lingual portion, whose morphology cannot be adequately ascertained due to wear. A mesially tilted endocristid would have originally been present throughout most of the lingual side of the crown, but only its basal-most portion is still preserved in one of the specimens (Fig. 8g), which clearly shows that the endofossid extended farther basally toward the cervix than the prefossid. Unlike in the i1, the endosynclinid appears to extend farther onto the root than the ectosynclinid, while the pre- and postanticlinid are shallower and less pointed than in the i1. There are no i3s of *P. palaeochoerus* among the studied sample.

Lower permanent canines: An apical c1m fragment of 47 mm in length is assigned to *P. palaeochoerus* (Fig. 9a). The distal face is enamel-free and at the tip displays a wear facet against the upper canine that extends farther lingually than buccally. The cross section roughly resembles an equilateral triangle with mildly convex sides. The proportions are thus verrucosic, with the labial and lingual faces being approximately equally broad and only minimally narrower than the distal face.

Two c1fs also display the typical morphology of *P. palaeochoerus*: the best-preserved specimen (Fig. 9d) shows moderately advanced wear, whereas the other specimen (Fig. 9e) displays a similar morphology and degree of wear but is less well preserved, with enamel missing from both the labial and lingual sides due to wear and/or damage. Both specimens are missing the tip of the root. Their crowns display two (mesiolabial and distal) large wear facets, so that enamel is only preserved on the lingual and, to a lesser extent, labial sides of the crown. Both facets extend farther labially than lingually beyond the cervix and apically shape a sharp and oblique apical edge that is higher lingually than labially. Both the crown and the root are curved toward their apices and labiolingualy compressed, with the root displaying greater dimensions and slightly tapering toward its apex. The root displays a convex cross section except at the distal side, where a conspicuous sulcus located toward the lingual half of the crown extends in apicobasal direction throughout the root.

Lower permanent premolars: Three p1s of *P. palaeochoerus* are available: two of them (Fig. 10a–b) display very light wear and preserve the roots to some extent, whereas the remaining one (Fig. 10c) is much more worn (with abundant dentine exposure along the mesial half of the crown) and only preserves the basalmost portion of the root. The crown is low and buccolingually compressed, and displays a subelliptical occlusal contour that is slightly pointed mesially and more convex distally, with the crown somewhat expanded on its distolingual corner. The crown is highest at the protoconid, which is very mesially located along the crown mesiodistal axis. A sharp, short, and steep protoprecristid links the protoconid apex with a moderately developed prestylid—better developed in some specimens (Fig. 10a) than in others (Fig. 10b)—located on the mesial end of the crown. The protopostcristid is shorter and less steep than the protoprecristid, giving rise to a thickening of the enamel that may be interpreted as a rudimentary metaconid (only ascertainable in the unworn specimens). From the latter cuspid, a single cristid (metapostcristid) descends until ending at the distolabial corner of the crown. In one specimen (Fig. 10b), this cristid ends in a distinct cuspulid-like structure, which might be interpreted as the hypoconid. Together with the indistinct metaconid and metapostcristid, it separates the rather convex labial crown wall from a basin-like fovea located on the distolingual portion of the crown. In another specimen, in contrast, this metapostcristid appears more serrated and bears no distinct cuspulid at its end (Fig. 10a). In two of the specimens (Fig. 10a, c), there is no distinct distolingual fovea, this portion of the crown being partly occupied by cristid-like folds of the enamel that radiate from the lingual aspect of the metapostcristid. Although they do not merge with the cristid, together with the latter the distal-most enamel fold partly delimits a small and triangular, shallow fossid on the distal end of the crown. In one specimen, two (lingual and labial) narrow and deep grooves flank the aforementioned cristid of distolabial direction (Fig. 10a). There are no cingulids except for that corresponding to the mesiolingual aspect of the prestylid in one of the specimens (Fig. 10a). As far as it can be ascertained due to incomplete preservation, one of the specimens is uniradiculate (Fig. 10c), whereas in contrast the other two display two fused roots, the distal one being stouter than the mesial, and both being distally tilted (Fig. 10a–b).

There are two p2s of *P. palaeochoerus* (Fig. 10k–l), which preserve a moderately worn crown and at least part of the roots. This premolar is much larger than the p1. The crown displays a subelliptical and buccolingually compressed occlusal contour. The latter is mesially more convex (less pointed) than in the p1 but, as in the latter, it is somewhat asymmetrical, with a uniformly convex buccal contour and a distolingually expanded one. The crown displays low relief despite the moderate degree of wear that mostly affects the tip of the protoconid. The protoprecristid is short and narrow, ending in a well-developed mesial prestylid that is only somewhat lower than the protoconid. In one of the specimens (Fig. 10k), lingually from the prestylid there is a secondary cuspulid. The protopostcristid is similarly developed to the protoprecristid and at least a moderately developed hypoconid (largely worn away) was present far from the distal end of the crown. The crown walls are only slightly convex around the protoconid and otherwise rather concave, with moderately developed but discontinuous lingual and buccal cingula (more marked along the mesial half of the crown distally from the prestylid) that are interrupted at the level of the protoconid. The cervix displays very shallow labial and buccal anticlinids and there are two distinct vertical roots that are only fused at their basal-most portion, the mesial one being higher and slightly stouter than the distal.

Among the three p3s of *P. palaeochoerus*, only two completely preserve the crown and the basal portion of the roots. In both specimens, a single wear facet with dentine exposure extends from the protoconid along the

distal portion of the crown. One of the specimens (Fig. 10q) is less worn than the other (Fig. 10s), so that the presence of two distinct cuspids distally from the protoconid can still be ascertained. This is more clearly shown by the partial p3 (Fig. 10r), which preserves the distal portion of the tooth and is only slightly worn (without dentine exposure). The two complete crowns are longer than broad and broader distally than mesially, displaying a similar occlusal profile that is moderately convex and constricted at the level of the protoconid, both buccally and lingually. One of the specimens (Fig. 10q) appears relatively broader than the other due to the more markedly expanded distobuccal crown portion. The protoconid is moderately high and centrally located slightly toward the mesial half of the crown, connected to the distinct mesial prestylid by a blunt, thick, and moderately steep protoprecristid. The buccolingually compressed metaconid is mesiodistally aligned with the protoconid and located close to the latter, without a distinct intervening protopostcristid, in a slightly lower position. A short, blunt, and very thick metapostcristid links the metaconid with a much lower hypoconid close to the distal end of the crown. Besides the prestylid, the development of cingulids is variable in the distal portion of the crown: two specimens (Fig. 10r–s) display a distinct distobuccal cingulid and a lesser developed distolingual cingulid, whereas in the other (Fig. 10q) the distobuccal cingulid is more inconspicuous and the distolingual one is wider and ledge-like (forming a distinct fossid buccally from the metaconid and hypoconid). This premolar displays distinct buccal and lingual anticlinids at the cervix as well as two distinct roots, the mesial one being more mesially tilted than the distal.

The p4 of *P. palaeochoerus* is represented by five specimens (Fig. 10u–y), most of them preserving the whole crown at different wear stages and some further preserving part of the roots. The best-preserved specimen displays a very slight degree of wear (with minimal dentine exposure only at the apex of the metaconid; Fig. 10u), followed by two specimens that have a somewhat more advanced degree of wear (with a confluent dentine exposure affecting the protoconid and the metaconid, and a smaller one corresponding to the hypoconid; Fig. 10V–W). The two latter p4s also display very similar occlusal features, to the extent that they might represent antimeres from a single individual. In the remaining specimens (Fig. 10x–y), most of the occlusal surface has been worn away or is not completely preserved, so only a few details can be ascertained. The occlusal contour is longer than broad but variable, from suboval to subrectangular, with a convex to concave mesial contour and variously developed labial and lingual constrictions at the level of the protoconid. In all specimens, maximum breadth is attained at the distal half of the crown and the buccal crown wall appears more bulging than the lingual at the level of the metaconid. Occlusal relief is marked when the tooth in unworn but rapidly decreases toward more advanced wear stages. The protoconid is the most voluminous cuspid, being centrally located toward the mesial half of the crown. A distinct and smaller, but similarly high, metaconid can be discerned mesiolingually from the protoconid, the apices of the two cuspids being separated by an oblique groove. A blunt protoprecristid links the protoconid apex with a mesial prestylid. The latter basically consists in a mesial cingulid that becomes thickened (cuspulid-like) on the mesiolingual corner of the crown. The protopostcristid is similarly inclined to, but slightly shorter than, the protopostcristid, linking the apex of the protoconid with a well-develped hypoconid that is nevertheless smaller and lower than the former. The hypoconid is mesiodistally aligned with the protoconid and located close to the distal end of the crown. The crown walls are markedly concave distally from the protoconid, due to the presence of distinct vertical clefts on the buccal and the lingual side. There are no distinct cingulids except for the mesial one associated to the prestylid and a variable cingular development at the

distobuccal end of the crown. This premolar displays three roots, the mesial one more mesially tilted than the distal ones.

Lower molars: The m1 and m2 of *P. palaeochoerus* and those of similarly-sized tetraconodontines may be difficult to distinguish, particularly when they display substantial degree of wear and are not associated with an m3, as in the case of the mandibular fragment assigned to the former species (Figs. 7e and 11a, k, s). This specimen shows that the m1 and m2 display a similar occlusal contour at different sizes, the m2 being much larger than the m1. An isolated partial m1 (Fig. 11b) is similarly worn, whereas there is also an unfinished crown germ that displays the unworn occlusal morphology of the m1 (Fig. 11c), characterized not only by the presence of Fürchen but also abundant crenulations of the enamel. Remnants of Fürchen can also be ascertained in two lightly worn m2s (Fig. 11l–m). Both the m1 and the m2 display a subrectangular (longer than broad) occlusal profile with two distinct (mesial and distal) lobes separated by moderately developed constrictions. The distal lobe appears broader and mesiodistally more extensive than the mesial one (more markedly so in the m2). There are four similarly-sized and equally peripheral main cuspids, the buccal ones being higher than and transversely aligned with the corresponding lingual ones. A well-developed and centrally located hypopreconulid, lower than the main cuspids, blocks to a large extent the transverse valley separating the two lobes. This valley is lingually open, whereas buccally it displays a moderately developed hypoectoconulid. A similarly developed and centrally located pentaconid is present on the distal end of the crown. There are no distinct lingual or buccal cingulids, whereas a moderately developed mesial cingulid can still be discerned in a few specimens, being otherwise erased by interproximal wear. This mesial cigulid displays a beaded appearance when unworn and is better developed (with secondary enamel cuspulids) at the mesiolingual corner of the crown. A similarly developed but buccolingually narrower and distally projecting cingulid with secondary cuspulids can also be discerned at the distolingual and distobuccal corners of the crown, flanking the pentaconid, in the less worn specimens. In the m1 germ and the two less worn m2s, just distally from the mesial cingulid, there is a semicircular cristid, formed by the merged protoprecristid and metaectocristid. This continuous cristid mesially encloses the protofossid, which is lingually obliterated to a large extent by the thick metaprecristid. In the m1 germ (Fig. 11c), the proto- and metaendocristid merge in a distinct endoconulid, located mesially from the hypopreconulid. In contrast, in the m2s (Fig. 11l–m), these cristids appear to connect directly to the hypopreconulid.

The m3 of *P. palaeochoerus* is represented by two antimeres of a single individual (Fig. 11s–t) plus an isolated specimen (Fig. 11u). They display a similar degree of wear, with dentine exposure on all the main cuspids and associated cuspulids. The m3 differs from the m2 by displaying a more elongate occlusal contour (both in absolute and relative terms), with three distinct lobes. The mesial one resembles in width that of the m2, while the central lobe (bearing the hypoconid and entoconid) is slightly narrower, although less than the distal lobe of the m3 (which bears the pentaconulid). Unlike in the m1 and m2, the buccal cuspids of the m3 are more mesially located than the lingual ones (particularly the protoconid as compared with the metaconid). The hypoconid and entoconid are subequal in size to, as well as mesiodistally aligned with, the corresponding mesial cuspids. The pentaconid is well developed but smaller than the remaining main cuspids, being centrally located on the distal lobe, which is buccally tilted. The hypo- and pentapreconulid are well developed but smaller than the pentaconid, being similarly centrally located. In the isolated m3 (Fig. 11u), the transverse valley between the mesial and central lobes displays no ecto- or endoconulid, whereas the two antimeres (Fig. 11s–t) display a distinct hypoectoconulid. In contrast, the transverse valley between the central and the distal lobes displays

similarly developed pentaectoconulid and pentaendoconulid between the pentapreconulid and the pentaconid—the pentaendoconulid being slightly larger and more distally located than the pentaectoconulid, due to the distobuccal tilting of the pentaconid. No distinct cingulids can be discerned, except for remains of the mesial cingulid in one of the specimens (Fig. 11u), which has been largely eroded by interproximal wear.

Upper deciduous incisors: Two isolated DI1s (Fig. 12a–b), preserving the slightly worn crown and most of the root, are assigned to *P. palaeochoerus*. They are smaller and more labiolingually compressed than their permanent counterparts, with a relatively lower crown and a slenderer and less curved root. The two available specimens display a mesial contact facet affecting the moderately developed marginal ridge, as well as some dentine exposure along the oblique incisal edge and the curved distal marginal ridge of the crown. The crown is convex mesiolabially and concave distolingually above a mildly developed lingual cingulum, which centrally displays two vertical cristae that do not reach the incisal edge. There is a marked and V-shaped preanticline mesiolingually and a more rounded endosyncline distally. The root is moderately short, labiolingually compressed, and slightly curved distally. Judging from the orientation of the mesial contact facet and the incisal edge, the DI1 would have been more obliquely implanted than the I1, similarly to both the I2 and the DI2.

The DI2 is represented by four specimens (Fig. 12g–j), of which one preserves the root and displays a very slight degree of wear. Coupled with an unworn unfinished crown germ (Fig. 12j) and another lightly worn crown (Fig. 12g), this enables to ascertain occlusal morphology better than for the DI1. The crown of the DI2 is similar in size to that of the DI1 but more labiolingually compressed. The mesiolabial side is thus markedly convex and similarly displays a marked and V-shaped preanticline, while the distolingual side consists of a very deep and narrow (almost fissure-like) concavity, with a rounded distal endosyncline. The lingual cingulum is more marked than in the DI1 (almost cusp-like in some specimens). A single marked but short endocrista originates from the mesial portion of the lingual cingulum, being vertically aligned but not reaching the incisal edge. The precrista is thick, while the postcrista is sharper and serrated when unworn. The incisal edge displays distinct mamelons in the available germ. The root is labiolingually compressed and only slightly curved but at least as markedly tilted distally (if not more) relative to the crown than in the DI1.

Two upper incisors are smaller than the DI1 and DI2, being identified as DI3s based on some morphological differences relative to the former. One of them is completely preserved despite conspicuous corrosion of the crown and root (Fig. 12k), while the other includes the crown (not particularly well preserved either) and a small portion of the root (Fig. 12l). The crown is labiolingually compressed and displays an asymmetric subtriangular profile. The precrista is marked and curved but shorter than the sharper, more indistinct, and obliquely oriented postcrista, while the incisal edge appears rounded. The labial crown wall is moderately convex, while the lingual is mildly concave except for a blunt and rather indistinct vertical endocrista. The latter progressively fades away before reaching the distal portion of the incisal edge, separating the small prefossa from the similarly shallow but more extensive endofossa. The lingual cingulum is only slightly developed. The root is straight and less labiolingually compressed than the crown, progressively tapering toward its apex but tilted distally relative to the crown as in the other upper deciduous incisors.

Upper deciduous premolars: The DP2 is represented by two complete specimens (Fig. 12m–n) and a partial one (Fig. 12o). The crown displays a subelliptical and asymmetrical contour, clearly longer than broad and broadest at the distal half of the crown, which is longer lingually than buccally due to its markedly protruding distolingual corner. Otherwise, the occlusal contour is very convex mesially, straight to moderately sinuous

lingually, and variably convex distobuccally. The crown displays a low relief and a moderately trenchant profile in buccal and lingual views. The buccal crown wall is somewhat concave except at the level of the main cuspid (paracone), whereas the lingual concavity is more marked. The paracone is located slightly toward the mesial half of the crown. The paraprecrista is mesially directed and displays a sinuous profile in buccal and lingual views, terminating at a well-developed mesial prestyle that is slightly mesiolingually directed. The parapostcrista is denticulated when unworn but displays no distinct metacone. It is obliquely oriented, terminating at the distolingual corner of the crown. The buccal cingulum is poorly developed, being restricted to the distobuccal corner of the crown in two of three specimens. The lingual cingulum is variously developed along the mesial half of the crown distally from the prestyle but discontinuous in all specimens at the level of the paracone. In contrast, the lingual cingulum is markedly developed along the shelf-like distolingual extension of the crown, where it constitutes a low but moderately developed cuspule (which would correspond to the protocone) and is separated from the parapostcrista by a deep valley. The cervix displays moderately developed anticlines both buccally and lingually, and there are two roots, the distal one being stouter than the mesial.

Six DP3s (Fig. 12u–z), all of them slightly to very slightly worn, are preserved. They all preserve the complete crown except for a single distal half fragment. The crown displays a subtriangular occlusal contour that is longer than broad and more convex mesially than distally, with two moderately to slightly developed concavities at each side of the crown (more or less marked depending on the specimen). A moderately developed transverse groove further contributes to poorly delimiting the mesial from the distal lobe. The distolingual corner of the crown is generally more protruding than the distobuccal. The mesial lobe displays a single main cusp of pyramidal shape (paracone), from which three crests originate, whereas the distal lobe displays two lower but similarly developed cusps that are variably compressed buccolingually depending on the specimen. The development of the paracone crests is variable among specimens, sometimes being discontinuous, although the two distal crests (paraendocrista and parapostcrista) are in all instances longer and more marked than the mesial (paraprecrista). The latter is mesiolingually directed and generally merges with the junction of the mesial and the lingual cingula without forming a distinct prestyle. The paraendocrista and parapostcrista are distolingually and distobuccally directed, respectively, becoming continuous with the protoprecrista and metaectocrista, which are similarly developed. The generally shorter protoectocrista and metaprecrista can also be discerned in most specimens. A short metaendocrista of lingual direction and a longer protoendocrista of distobuccal direction (ending at the distal cingulum) can be discerned in most specimens, but the bases of the distal cusps are in all instances separated by a distinct groove of mesiodistal direction. None of the cusps is peripherally located and the crown is surrounded by a distinct cingulum of beaded appearance that becomes more marked mesiolingually and distobuccally.

None of the seven DP4s assigned to *P. palaeochoerus* (Fig. 12m'–s') is associated with other deciduous premolars or permanent molars of the same individual, but they are assigned to this species based on some similarities in occlusal contour and pattern with the M1 and M2 of this species. Except for a specimen where the enamel cap is poorly preserved (corroded and/or partly dissolved; Fig. 12q'), the specimens preserve the complete and unworn to slightly worn crown, thereby enabling to adequately ascertain their occlusal morphology. Fürchen are marked but partly disrupted by the abundant wrinkling of the enamel. The occlusal contour is subrectangular (longer than broad), with a straight but obliquely oriented mesial side (relative to the main mesiodistal axis of the crown) and a markedly convex distal one, as well as two distinct (mesial and distal)

lobes separated by well-marked buccal and lingual constrictions. The distal lobe is similarly broad to the mesial one, but appears more extended, as in the M1 and the M2 of the same taxon. The mesial and distal cusps are similarly extensive, with the apices of the lingual cusps slightly more distally located than those of the corresponding buccal cusps (particularly the hypocone compared with that of the metacone). The mesial cingulum is very marked and partly interrupted by a distinct (albeit variously developed) protopreconule, which is centrally located at the end of the protoprecrista. The latter is better developed (longer and/or thicker) than the protoectocrista. There is no distinct paraprecrista originating from the paracone apex; in contrast, a curved and distinct crista extends along the mesiobuccal aspect of the paracone base, approximately between the ends of the paraectocrista and the paraendocrista. The transverse valley between the mesial and distal lobes is not blocked by the moderately well-developed hypopreconule, which is centrally located and similarly developed to the protopreconule. A variably developed hypoectoconule is present in all specimens at the end of the hypoectocrista. There is no lingual cingulum, while the distal cingulum is very distinct (albeit slightly less developed than the mesial one), similarly displaying profuse enamel folds and continuing along the distobuccal portion of the crown. In a few specimens, there is a small metaectoconule at the end of the distobuccal cingulum.

Lower deciduous incisors: Two lower incisors from a single individual (Fig. 13a–b), preserving most of the root as well as the crown with a moderate degree of apical wear, can be confidently identified as di1s of *P. palaeochoerus* given similarities with the permanent i1s of this species at a much smaller size. Two additional specimens that display more advanced wear and only preserve the basal portion of the root are also tentatively attributed to this species (Fig. 13c–d). The crown appears high and mesiodistally compressed at the base, progressively becoming labiolingually narrower toward the apex, which displays an inclined incisal edge. The crown is labially convex and lingually concave, with a distinct (narrow but sharp) vertical endocristid that is slightly tilted mesially. This endocristid originates in a moderately developed basal bulge located above the cervix and fades away just before reaching the incisal edge, separating the prefossid from the similarly shallow and slightly less extensive endofossid. These fossids are further delimited mesially and distally, respectively, by mildly developed precristid and postcristid. These cristids become continuous with the lingual cingulid, which is poorly developed and barely discernible at both sides of the basal bulge. The crown is vertically aligned with the root with only minimal waisting at the cervix. The rootward extension of the ectosynclinid is greater than that of the endosynclinid. The pre- and postanticylinids are deep and V-shaped. The root is much higher and mesiodistally compressed than the crown, reaching its maximum mesiodistal length at about its basal third, and progressively tapering toward its apex, with a convex labial profile and a concave lingual one in mesial and distal views. Unlike for the i1 of the same species, no conspicuous sulcus can be discerned along the distal side of the root.

A single di2 (Fig. 13i), preserving the basal portion of the crown and the root, is tentatively assigned to *P. palaeochoerus* based on similarities with the permanent i2. The crown is not worn but apically broken, which hinders a more secure taxonomic attribution, but its basal portion appears vertically aligned with the root, being more mesially tilted toward the apex. The crown is mesiodistally compressed at the base and progressively tapers labiolingually toward the apex. The precristid and postcristid are relatively marked but the endocristid is clearly more developed. The endosynclinid displays a greater extension onto the root than the ectosynclinid, and the preanticlinid is deeper than the postanticlinid. The root is mesiodistally compressed and only minimally curved mesially toward its apex.

In turn, two completely preserved and slightly worn di3s of this species are available (Fig. 13m–n). The crown is elongate (very labiolingually compressed) and low relative to length, and in labial and lingual views it displays a markedly asymmetrical profile that is much higher mesially than distally. The incisal edge, which is slightly worn, is limited to the mesial half of the crown and appears slightly convex, although distinct mamelons might have been originally present. A moderately deep prefossid is present at the mesiolingual end of the crown, being mesially delimited by a short and curved precristid. Distally from it, the crown displays a diffuse and vertical bulging portion. A sharp endocristid originates from the distal end of the incisal edge and descends toward the distolingual corner of the crown, paralleling the course of the postcristid at a lower crown height. Together, the postcristid and endocristid enclose a distolingually oriented, long, and deep endofossid. The mesial end of the crown is mesially protruding but follows the same curvature as the mesial aspect of the root in labial and lingual views. In contrast, the distal end of the crown bulges relative to the cervix level. The cervix is horizontal both labially and lingually, and the root is labiolingually compressed and tilted distally but recurved mesially along its apical half, ending in a pointed apex.

Lower deciduous premolars: A lower premolar is tentatively identified as a dp2 of *P. palaeochoerus* (Fig. 13p). It is completely preserved, but displays a steep wear facet on the distal portion of the crown, which hinders a complete assessment of its occlusal morphology. The crown displays a subtriangular occlusal contour that is longer than broad and broader distally than mesially, with a pointed and mesiolingually directed mesial end. The crown is low and displays a single main cuspid (protoconid) located toward the mesial half of the crown. From the protoconid apex, the protoprecristid progressively descends and curves in mesiolingual direction until reaching a poorly developed and mesiolingually tilted prestylid. Due to wear, it cannot be ascertained whether a metaconid or hypoconid were originally present. At the cervix, very shallow anticlinids are present at the lingual and buccal sides. This premolar displays two distinct and diverging roots that only merge at their basal-most portion: the mesial one is mesially tilted and slender, whereas the distal is somewhat shorter, much stouter, and more vertically implanted.

The sample further includes a dp3 that unambiguously belongs to *P. palaeochoerus* (Fig. 13r). It preserves the complete crown with moderate wear restricted to its distal half. The crown displays a subelliptical occlusal contour that is broadest toward the distal half of the crown. Mesially, the crown displays straight to mildly concave mesiolingual and mesiobuccal contours, with a rounded mesial end. The crown becomes slightly bulging distally from the protoconid and then it is slightly constricted close to the distal end, where the crown walls display moderately developed clefts. The crown is low and the main cuspid (protoconid) is located slightly toward the mesial half of the crown. The long and steeply inclined protoprecristid ends in a low, centrally located, and well-developed prestylid at the mesial end of the crown. The presence of metaconid cannot be ascertained due to wear, but a low hypoconid seems to have been originally present at the distal end of the crown. The lingual and distal roots appear divergent and well distinct.

A complete dp4 with an advanced degree of wear (Fig. 13y), a partial germ missing the distal-most portion (Fig. 13w), and two distal crown fragments of the same tooth locus (Fig. 13x, z) are assigned to *P. palaeochoerus*. The complete specimen displays a mesially tapering and elongate occlusal profile, with three lobes that are convex both lingually and buccally, and distinguished from one another by moderately marked constrictions. Each lobe displays a large dentine lacuna, communicated to the adjacent one at the level of preconulids, so that most occlusal details have been eroded by wear. The distal portion of the crown appears

projecting and would have originally displayed a distinct and centrally located pentaconid. The partial germ and the much less worn dp4 distal fragments enable to ascertain better the occlusal morphology. The cristids are thick and display abundant crenulations of the enamel. One of the distal fragments preserves a moderately developed hypopreconulid. The hypoconid and entoconid are transversely aligned. The distal margin moderately projects distally and bears a centrally located pentaconid, which is well developed but smaller than the other cuspids and surrounded by short cingulids. The pentaconid contacts the end of the hypoendocristid, which is particularly thick and separated from the ends of the entopostcristid, entoendocristid, and hypopostcristid by deep grooves.

Subfamily Tetraconodontinae Lydekker, 1876

Genus *Parachleuastochoerus* Golpe-Posse, 1972

Parachleuastochoerus valentini (Filhol, 1882)

Figures 3d–g, i–j, 4e–f, 5h–i, x–y, k'–m', 6g–o, y–a', l'–u', 8j–m, 8o–t, 9f–g, 10d–h, z–a', 11d–e, n, v, 12c–f, p–q, a'–g', t'–v', 13e–f, j, o, s, a'.

Selected synonyms

1851 *Sus*? *Doati* Lartet: partim—not including the lectotype.

1882 *Sus Valentini* Filhol (description of the species).

1899 *Hyotherium simorrense* var. *Doati* (Lartet, 1851): Stehlin (new combination), partim.

1899 *Hyotherium simorrense* var. *Valentini* (Filhol, 1882): Stehlin (new rank and combination).

1907 *Hyotherium simorrense* var. *Doati* (Lartet, 1851): Roman.

1868 *Conohyus simorrensis* (Lartet, 1851): Hünermann, partim.

1972 *Hyotherium soemmeringi* von Meyer, 1834: Golpe-Posse, partim (based on specimens detailed in Golpe-Posse, 1971).

1972 *Hyotherium palaeochoerus* (Kaup, 1833): Golpe-Posse, partim (based on specimens detailed in Golpe-Posse, 1971).

1986 *Conohyus ebroensis* Azanza (original description).

1989 *Conohyus ebroensis* Azanza, 1986: Van der Made.

1990a *Conohyus steinheimensis* (Fraas, 1870): Van der Made, partim.

2014 *Parachleuastochoerus valentini* (Filhol, 1882): Pickford and Laurent (new combination), partim—excluding *Conohyus melendezi* Golpe-Posse, 1972.

2014 *Conohyus doati* (Lartet, 1851): Pickford and Laurent, partim—excluding the lectotype.

2014 *Parachleuastochoerus valentini* (Filhol, 1882): Pickford, partim—excluding *Conohyus melendezi* Golpe-Posse, 1972.

2014 *Conohyus doati* (Lartet, 1851): Pickford, partim—excluding the lectotype.

2016a *Parachleuastochoerus valentini* (Filhol, 1882): Pickford, partim—excluding *Conohyus melendezi* Golpe-Posse, 1972.

2016a *Conohyus doati* (Lartet, 1851): Pickford, partim—excluding the lectotype.

2020 *Conohyus simorrensis* (Lartet, 1851): Van der Made, partim.

2023a *Parachleuastochoerus valentini* (Filhol, 1882): McKenzie et al.

Referred material

See Appendix Table 1 for a list of the referred material and Appendix Table 2 for measurements.

Description

Upper permanent incisors: Four I1s are assigned to *Pa. valentini*. One of them (Fig. 3f) is completely preserved but displays an advanced degree of wear, similar to another (Fig. 3e) that is only missing the tip of the root. Occlusal morphology can thus be better ascertained in a third specimen (Fig. 3d) that preserves the unworn crown and the basal-most portion of the root, as well as in a partially preserved crown germ (Fig. 3g). The crown is high, markedly compressed labiolingually, and slightly tilted mesially, with convex walls except at the distolingual side, which is markedly concave. The lingual cingulum is well distinct but markedly inclined, forming an abrupt angle with the precrista, whereas on the distal side there is a bulbous but rather indistinct cuspule (metacone), which together with the cingulum conforms an inverted V-shape. One of the specimens (Fig. 3g) displays a faint endocrista that does not reach the incisal edge and is located toward the distal side of the crown, whereas in another I1 (Fig. 3d) the endocrista appears more centrally located but is even more indistinct and bifurcates basally. The postcrista is moderately curved, sharp, and serrated when unworn, whereas the precrista is shorter, blunter, and more markedly curved, confluent with the former in the pointed crown apex. The cervix displays moderately shallow preanticline and endosyncline, and is only minimally waisted. The root is robust, labiolingually compressed, and only moderately high. Its mesial profile is somewhat more curved than the distal, and tapers from base toward the apex only slightly, until ending abruptly in a lingually tilted apex.

Two upper incisors (Fig. 3i–j) are considered I2s of *Pa. valentini*. One of the specimens (Fig. 3j) is damaged and corroded, but in overall size and shape resembles the better-preserved specimen (Fig. 3i). They are similar to the I1s of the same species except for their smaller size and slenderer morphology, the less mesially tilted crown, and the less bulbous metacone. Furthermore, the lingual cingulum is less marked and less obliquely oriented, more gently merging with the precrista. From their junction, a distinct but narrow endocrista originates, being somewhat obliquely oriented and fading away well before the crown apex, thus only partly separating the small prefossa from the much more extensive endofossa. The postcrista is longer than, but as curved as, the precrista, further being minimally serrated on its basal-most portion. The cervix displays moderately developed preanticline and endosyncline, and the root is labiolingually compressed and moderately curved distally. No I3s are identified among the sample, although it should be considered that this tooth position is unknown for this species (see comparisons below for further discussion in this regard).

Upper permanent canines: Two C1fs are attributed to *Pa. valentini* (Fig. 4e–f). Both specimens are completely preserved, but one of them (Fig. 4f) displays a much more advanced degree of wear, so that only part of the labial and lingual crown walls are preserved. In contrast, the least worn specimen (Fig. 4e) only shows a small vertical wear facet that does not reach the cervix or the crown's apex on the mesial side. The crown is labiolingually compressed and slightly higher than mesiodistally long, with a trenchant triangular profile in labial and lingual views. The labial crown wall is moderately convex, whereas the mesiolingual aspect is flatter and the distolingual one is markedly convex, being delimited by a rather indistinct endocrista and a sharper postcrista that distally bulges just above the cervix. The latter displays relatively well-developed ectoanticline

and endosyncline. The root is robust, being curved distally and also labially on its apical half, and terminating quite abruptly.

Upper permanent premolars: Two very slightly worn P1s are attributed to *Pa. valentini* (Fig. 5h–i). One of them only preserves the crown (slightly damaged distally), while the other also includes part of the distal root. The crown is buccolingually compressed (slightly wider distally than mesially), displays marked occlusal relief and has a trenchant appearance in buccal and lingual views. The occlusal contour is markedly convex distally and, especially, mesially, with the lingual and buccal sides being mildly sinuous. The high and pointed main cusp (paracone) is mesially tilted and clearly located on the mesial half of the crown. A sharp and steep precrista descends from the paracone apex down to distinct prestyle located at the mesial end of the crown. A shorter and slightly less inclined postcrista connects the paracone apex with a mildly developed cuspule (metacone). A long metapostcrista progressively curves and descends until reaching the distolingual corner of the crown; in labial and lingual views, this crest displays an irregularly convex profile. There are no distinct cingula. The ectoanticline and endoanticline are quite marked, with enamel extending much more extensively onto the root on the distal than on the mesial half of the crown, and the distal-most end of the crown markedly protruding from the cervix level. The mesial and distal roots appear to have been distinct except at their basal-most portion, but their morphology cannot be adequately ascertained.

There is no P2 attributable to *Pa. valentini*, whereas two P3s are assigned to this species. Both are extensively worn and somewhat damaged: one of them (Fig. 5x) is missing the distobuccal end of the crown but enables to estimate the occlusal dimensions, while the other (Fig. 5y) is missing the distolingual crown wall and hence does not enable to readily measure buccal dimensions or the development of the protocone. The crown displays straight to moderately convex buccal and lingual sides and a markedly convex mesial end. The occlusal contour only slightly tapers mesially, being much longer than wide and wider distally than mesially. The distolingual corner of the crown is not markedly protruding. The mesial end of the paraprecrista is preserved, but the development of the prestyle and mesial cingulum cannot be adequately ascertained due to wear or incomplete preservation. However, marked cingular developments can be ascertained on both sides of the preserved portion of the paraprecrista (better developed on the buccal side). There is no well-developed cingulum along the rest of the buccal wall, whereas the lingual cingulum appears discontinuous at the level of paracone but becomes much more strongly developed distally from it, constituting a small and poorly developed protocone close to the distoligual corner of the crown (only ascertainable in one of the specimens; Fig. 5x). The P3 is three-rooted but only the mesial root can be adequately described, being stout and slightly curved mesially.

Three P4s are assigned to *Pa. valentini* (Fig. 5k'–m'). They display a subtriangular and lingually very tapering contour that is much broader than long. The protocone is centrally located along the mesiodistal axis of the crown on its lingual side, being less peripheral and more extensive than the two buccal cusps. The latter are worn to some extent, with the paracone displaying a smaller dentine exposure than the metacone. These two cusps are very closely packed to one another and not well individualized, although a short vertical groove separates their apices on the buccal crown wall. As far as it can be ascertained due to damage in the various specimens, the mesial and distal cingula, as well as associated prestyle and poststyle, are moderately developed. These cingula continue along the mesiobuccal and distobuccal aspects of the crown, becoming fainter or disappearing buccally. The protofossa separating the protocone from the buccal cusps is mostly obliterated by a well-developed protopreconule (located between the protocone and paracone apices) mesially and by a long

postcrista of the protopreconule distally, thus being restricted to a deep and narrow groove distobuccally from the protocone.

Upper molars: The M1s (Fig. 6g–o) and M2s (Fig. 6y–a') assigned to *Pa. valentini* are similar in size and overall proportions to those of *P. palaeochoerus*, displaying a subrectangular to subsquare occlusal contour with two distinct lobes. The lingual constriction between the two lobes is more marked than the buccal. Some of the specimens are less worn than those of *P. palaeochoerus*, preserving the Fürchen and showing some degree of enamel wrinkling (but not to the extent present in suines). There are four main cusps, the lingual ones being only slightly more distally positioned than the corresponding buccal ones. The mesial and distal cingula are relatively well developed, although the distal is more restricted buccolingually and displays some development of secondary cuspules. A buccal cingulum is also present, even if discontinuous in some specimens. A small but indistinct buccal ectoconule is generally present. The protopreconule and hypopreconule are well developed but do not appear particularly well defined, probably due to wear.

The M3s of *Pa. valentini* (Fig. 6l'–u') include several lightly worn specimens with no dentine exposure at all, clearly displaying the Fürchen but displaying a limited amount of enamel wrinkling. There is marked variation in size and some variation in occlusal contour, although all the specimens display a subtriangular outline that tapers distally. The mesial contour is clearly convex and the mesial and central lobes are separated by marked buccal and lingual constrictions. The central lobe is narrower than the mesial one, but not very markedly so, the occlusal contour of the crown more abruptly tapering distally along its distal-most portion. There are five main cusps, the mesial ones being slightly larger. Unlike in the M1 and M2 of the same species, the lingual cusps are clearly more distally situated than the corresponding buccal ones. The main cusps are conical and well individualized, the distal ones (especially the metacone) slightly more buccally compressed than the mesial. The pentacone is much smaller than the remaining cusps but generally well developed, except in a single specimen (Fig. 6n'), where it is represented by a tiny cuspule that is located on the lingual distal-most end of the crown and is even smaller than the pentapreconule—which, in the remaining specimens (if present at all), is clearly smaller than the pentacone. In all but the aforementioned specimen, the pentacone is centrally located on the distal-most end of the crown, either being distally directed or, more frequently, tilted buccally to some extent. The protoprecone and hypoprecone are large and similar in size to one another. The mesial cingulum is well developed, while the presence of a narrow buccal cingulum appears variable, and there are no lingual or distal cingula. The presence and development of buccal and labial ectoconules is variable among specimens. Originally the M3s displayed five roots, although only the lingual ones are partly preserved in some specimens.

Lower permanent incisors: No i1 of *Pa. valentini* has been found among the CB incisor sample, whereas in contrast there are four lower incisors that we identify as i2s of this species (Fig. 8j–m). The best-preserved specimen (Fig. 8k) includes the unworn crown and the root's basal portion, while another i2 (Fig. 8j) seemingly preserves the intact crown. Another i2 crown with a more advanced degree of wear (Fig. 8l) displays an occlusal morphology entirely consistent with that of the two unworn specimens, while a senile specimen (Fig. 8m) only enables to ascertain the morphology of the root. The unworn crown is tall and markedly asymmetrical, with an almost straight mesial profile and a markedly curved distal profile in lingual view. The incisal edge is curved and bears two or three poorly developed mamelons (Fig. 8j). The crown is mesiodistally compressed toward the base, progressively tapering labiolingually toward its apex. Mesiodistal length is greatest on the lower third of the crown, which progressively tapers apically due to the marked curvature of the postcristid. The labial wall is

markedly convex, whereas the lingual is concave except for a sharp, straight, and lingually protruding endocristid of vertical orientation (only slightly tilted mesially). This endocristid originates from a basal moderate swelling located above the cervix and extends until merging (Fig. 8j) or almost reaching (Fig. 8k) the junction between the incisal edge and the postcristid. The precristid is not marked and restricted to the apical third of the crown, enclosing a very restricted prefossid mesially from the apical portion of the endocristid. In contrast, the postcristid is very marked and curves along the whole distal margin of the crown—delimiting, together with the endocristid, a much more extensive endofossid that, on its basal portion, ends above the basal swelling close to the cervix. The ecto- and endosynclinid similarly extend onto the root, whereas the preanticlinid is much deeper than the postanticlinid. The root is not vertically aligned with the crown, but rather follows the same curvature of the latter throughout the cervix. The root is long and mesiodistally compressed at its base, progressively tapering in all directions toward its apex, and further curving in mesial and lingual directions.

Multiple i3s are attributed to *Pa. valentini* (Fig. 8o–t) but only a single specimen (Fig. 8o) preserves both the crown (which is slightly worn) and the root. The remaining specimens correspond to isolated unworn germs or slightly to moderately worn crowns, which except for very minor differences agree well with the occlusal morphology of the most complete i3. The crown is much lower than in the other incisors, mesiodistally compressed, and asymmetrical, with a markedly convex mesiolabial aspect and a concave distolingual one. The crown is tilted mesially and higher distally than mesially. The moderately developed precristid is curved but vertically oriented, whereas the postcristid is more marked, convex, and obliquely oriented, displaying a more markedly serrated appearance when unworn. Both cristids become continuous with the incisal edge, which is markedly curved when unworn. There is no well-developed lingual cingulid; instead, the pre- and postcristid converge toward a distinct swelling located at the lingual base of the crown. There is a very well-developed and lingually protruding endocristid, which originates from the junction of the precristid and the basal swelling, being quite vertically oriented. The endocristid ends close to the upper third of the postcristid, thus separating a vertical and narrow endofossid from the more extensive prefossid. In some specimens, a fainter and shorter, but similarly vertically oriented cristid, originates midway from the precristid and fades away shortly before reaching the incisal edge, dividing the prefossid. The crown is somewhat waisted at the cervix, particularly on the distal side. The cervix conforms no distinct postanticlinid, contrasting with the marked and wide mesiolabial preanticlinid. The root is very mesiodistally compressed and triangular in mesial and distal views, markedly tapering and slightly curving mesially toward its apex.

Lower permanent canines: There is no c1m attributed to *Pa. valentini* among the sample, whereas in contrast two c1fs (Fig. 9f–g), completely preserved except for the tip of the root, are assigned to this species. One of specimens is more heavily worn, to the extent that only a small basal portion of the lingual crown wall is preserved (Fig. 9f). This specimen displays a long distal wear facet and an oblique mesiolabial facet, confluent at the obliquely oriented apical margin. The other specimen (Fig. 9g) is larger and displays a different wear pattern, with a single distal wear facet that has eroded about half of the crown and extends farther labially (down to the cervix level) than lingually. As a result, the base and a large portion of the mesial half of the crown are preserved, displaying a convex and labiolingually compressed contour. The basal portion of the root is also labiolingually compressed and displays larger dimensions than the crown, markedly tapering and slightly curving distally toward the apex. The cross section of the root is convex, becoming somewhat flatter on the distal

side, where no longitudinal sulcus can be discerned. The tips of the roots are missing in both specimens and might have not been originally closed.

Lower permanent premolars: Of the seven p1s that display a tetraconodontine morphology, five are assigned to *Pa. valentini* (Fig. 10d–h). The best-preserved specimen (Fig. 10d) only shows minimal wear at the apex of the main cuspid and almost completely preserves the two roots. The remaining specimens also preserve the unworn or slightly worn crown, and in a couple of them the distal root is also preserved. The crown is very elongate (buccolingually compressed) and only moderately high, with the main cuspid (protoconid) located slightly toward the mesial half of the crown. The occlusal contour is subelliptical, with a more marked convexity on the distobuccal aspect of the protoconid. The crown walls are slightly more convex around the protoconid and become slightly concave distally from it. A sharp, steep, and straight to moderately mesiobucally curved protoprecristid links the protoconid with a low and moderately developed prestylid at the mesial end of the crown. When unworn, the protoprecristid displays a sinuous profile in buccal and lingual views, being convex close to the protoconid and becoming concave toward the prestylid. A less steep and serrated protopostcristid runs in distal direction from the protoconid apex, until terminating into a cuspulid-like thickening of the enamel (hypoconid) before reaching the distal-most end of the crown. A steep cristid abruptly descends from the hypoconid toward the distal end of the crown, which bulges distally from the cervix level. There are no distinct cingulids. The cervix displays marked lingual and buccal anticlinids between the two roots and extends farther rootward on the distal than on the mesial half of the crown, particularly on the buccal side. The two roots are well separated from one another: the distal one is vertically oriented, while the mesial is slightly longer and mesially tilted.

None of the tetraconodontine p2 or p3 are assigned to *Pa. valentini*, although it should be considered that the former tooth locus is yet unknown for this species. In contrast, two p4s are assigned to *Pa. valentini*, including a moderately worn crown with the basal-most portion of the root (Fig. 10z) and a partial germ missing the distal portion of the crown (Fig. 10a'). The occlusal contour is subelliptical and quite symmetrical, and the protoconid is relatively high but occlusal relief is not very marked. A thick and sharp protoprecristid steeply descends from the protoconid apex down to the mesial prestylid, which is very well developed and about as high as the hypoconid (resulting in a relatively short protoprecristid). The mesiolingual and mesiobuccal cingulids associated with the prestylid are very developed and almost ledge-like, but do not extend distally forming conspicuous cingulids, except on the lingual side of one specimen (Fig. 10a'), where a narrow and poorly defined cingulid is present (albeit interrupted at the level of the protoconid). The protopostcristid is similarly developed to the protoprecristid, ending in a poorly developed and very inconspicuous cuspulid that would correspond to the metaconid. From the latter, two short and thick cristids diverge, preceding a more distinct hypoconid located at the distal end of the crown (only observable in one of the specimens; Fig. 10a'). The hypoconid is lower than the protoconid but quite high, being located at about two-thirds of crown height. The crown walls are inflated along the mesial half of the crown, whereas distally from the protoconid they become concave, forming two well-developed vertical clefts flanking the protopostcristid—the distolingual one being more marked than the distobuccal and further displaying a moderately developed cingulid at its base.

Lower molars: Two m1s (Fig. 11d–e) and a single m2 (Fig. 11n) are attributed to *Pa. valentini*. Such attribution is somewhat tentative because the specimens are isolated (i.e., not associated with more diagnostic tooth positions), being based instead on minor differences compared with those assigned to *Versoporcus*—some of

which can be confidently attributed to the latter genus (see below)—generally paralleling those between the respective m3s of these taxa. These molars display a subrectangular (longer than broad) occlusal contour that is straighter lingually than buccally and two (mesial and distal) moderately distinct lobes (with a more marked buccal than lingual constriction). The m2 displays the same occlusal pattern as the m1 at a larger size. Fürchen and some degree of enamel crenulations can be clearly discerned in the least worn specimen (Fig. 11d), but are also still observed in the remaining ones, which despite their greater degree of wear show very limited dentine exposure. The cuspids are pyramidal and somewhat inflated. The mesial and distal pairs of main cuspids are transversely aligned to one another. At the mesial lobe of the m1s, a curved and long protoprecristid is directed toward the end of the much shorter metaectocristid and metaprecristid, but does not merge with either of them, being separated by an oblique groove that runs from the mesial cingulid toward the protofossid. The protoprecristid is thicker in one specimen (Fig. 11e) and double in another one (Fig. 11d); in the latter, the protoprecristid s.s. originates from the protoconid apex, running in parallel to a more lingual cristid that originates from the mesial aspect of the short and cuspulid-like protoendocristid. The protofossid is partly obliterated lingually by the first portion of the metaprecristid and buccally by the protoendocristid. The m2 shows a similar pattern except for the more buccally curved metaectocristid and metaprotocristid. The protofossid is distally closed by a well-developed metaendoconulid that is located toward the lingual side of the crown. The transverse valley between the mesial and distal lobes displays a well-developed, centrally located, and buccolingually elongate hypopreconulid, which is slightly larger than the more lingually positioned metaendoconulid. There is no distinct entoendoconulid, while the hypoectoconulid is constituted by multiple enamel thickenings in the m1s and a slightly better developed single cuspulid in the m2. The main cuspulids of the distal lobe are mesiodistally aligned with those of the mesial lobe and similarly extensive. The distal end of the crown displays a moderately (m1s) to well-developed (m2) and centrally located pentaconid. There are no buccal or lingual cingulids. Instead, there is a continuous and moderately developed mesial cingulid that displays some development of secondary cuspulids, and a continuous, curved, and distally protruding cingulid. The latter displays some development of secondary cuspulids and is more protruding distolingually in the m2.

The m3 of *Pa. valentini* is represented by an isolated specimen (Fig. 11v) that displays an elongate occlusal contour that moderately tapers distally and displays three lobes separated by moderately marked constrictions. Despite wear, the cuspids show almost no dentine exposure and appear inflated. Some remnants of Fürchen can still be discerned on the main cuspids. The protoconid is transversely aligned with the metaconid. A very thick and cuspulid-like protoprecristid stands out mesiolingually from the protoconid, contrasting with the poorly developed metaectocristid but resembling the very thick and cuspulid-like metaprecristid, which occupies most of the protofossid. The transverse valley separating the mesial from the central lobe is lingually open but closed buccally by a well-developed hypoectoconulid, and otherwise obliterated by the centrally located and much larger hypopreconulid (distally) and a similarly developed metaendoconulid (mesially). On the central lobe, the hypoconid and entoconid are somewhat lower but similarly extensive to the mesial cuspids. The third lobe is distally oriented and displays a small and distally located pentaconid (comparable in size to the ecto- and endoconulids). The pentaconid is preceded mesially by a much more extensive pentapreconulid (even slightly larger than the hypopreconulid and metaendoconulid). Well-developed and transversely aligned pentaectoconulid and pentaendoconulid are peripherally located between the levels of the pentapreconulid and the pentaconid. The latter is also flanked by cuspulid-like cingular remnants on either side. There are no

discernible cingulids except by a strongly developed mesial one that has been largely eroded by interproximal wear but apparently constituted well-developed stylids on the mesiobuccal and mesiolingual corners of the crown.

Upper deciduous incisors: Four upper incisors, three of them preserving the complete crown and most of the root, are identified as DI1s of *Pa. valentini* (Fig. 12c–f) because they are similar in size and shape to one another and consistently differ from those assigned to *P. palaeochoerus* in several features. Nevertheless, such an attribution must be tentative, given the presence of a second tetraconodontine at the site. In the four specimens, the crown is labiolingually compressed and displays a convex mesiolabial wall and a slightly concave distolingual one. The lingual cingulum is moderately developed but higher toward its central portion, where it originates a vertical and distinct endocrista that weakens toward the incisal edge, partially separating the prefossa from the endofossa. The pre- and postcrista are moderately marked and the slightly worn incisal edge appears rounded. The mesiolingual preanticline is moderately deep, while the distal endosyncline is more indistinct. There are no DI2s or DI3s assigned to this taxon among the studied sample but one of the specimens (Fig. 12f) shows slightly smaller dimensions and is more labiolingually compressed than the others, so that it might alternatively be interpreted as a DI2.

Upper deciduous premolars: Two slightly worn DP2 crowns are assigned to *Pa. valentini* (Fig. 12p–q). The crown is very low and elongate (buccolingually compressed) but displays a markedly asymmetric occlusal contour, being distolingually tilted. The mesial contour is rounded and the distal one is markedly convex but slightly more pointed. The crown walls and basal contour are only convex at the level of the main cusps and concave otherwise. The highest cusp is the paracone, which is very buccolingually compressed and clearly located on the mesial half of the crown. It is linked by means of a long, sharp, and moderately steep paraprecrista to a well-developed prestyle. The parapostcrista is much shorter and links the paracone with a well-developed and buccolingually compressed metacone that is slightly higher than the prestyle. A longer metapostcrista curves toward the distolingual end of the crown, where a poorly developed cuspule (protocone) might have originally been present. There is no buccal cingulum, whereas the lingual one is moderately developed except at the distolingual aspect of the crown and discontinuous at the level of the paracone. At the cervix, the buccal and lingual anticlines are shallow. There were two (mesial and distal) distinct roots, whose relative development cannot be ascertained due to incomplete preservation.

The DP3 of *Pa. valentini* is represented by three complete and four partial crowns (Fig. 12a'–g'). The occlusal contour is vaguely 8-shaped to subtriangular, longer than broad, with a markedly convex mesial lobe that is much narrower than the distal one, which appears more protruding distolingually. The two lobes are separated by marked buccal and lingual constrictions. The main cusps are pyramidal in shape and the occlusal surface displays abundant grooves and crenuations. The mesiolingually oriented paraprecrista is not very well defined, contrasting with the more marked paraendocristid and parapostcristid, which display a beaded appearance when unworn and become more or less continuous with the mesial crests of the protocone and metacone. There is marked and beaded distal cingulum that continues along the distolingual portion of the crown. The mesial cingulum is similarly developed, continuing along the lingual side of the mesial lobe.

The DP4s assigned to *Pa. valentini* (Fig. 12t'–v') include a complete (albeit slightly damaged) crown that is slightly worn and shows some development of enamel wrinkling, as well as two partial crowns that show a more advanced degree of wear. As far as it can be ascertained, they display a similar occlusal pattern to those of *P.*

palaeochoerus (see above), being assigned to *Pa. valentini* based on the less marked enamel wrinkling and some other minor details. The crown displays a subrectangular contour longer than broad, with two distinct lobes; the mesial margin is straight and obliquely oriented. The lingual cusps appear slightly more distal than the buccal ones, whereas the distal cusps appear closer to one another than the mesial. There is a well-developed hypopreconule and a smaller but distinct hypoendoconule, whereas in contrast no protopreconule can be distinguished. The mesial and distal cingula are relatively well developed and display secondary folds of the enamel, whereas there is also a narrower distobuccal cingulum.

Lower deciduous incisors: Two partial lower incisors are identified as di1s of *Pa. valentini*, one preserving a slightly worn crown (Fig. 13e) and the other the apical portion of an unworn germ (Fig. 13f). The incisal edge is inclined and, when unworn, displays two mamelons, the mesial one being much apically protruding than the distal. The crown is mesiodistally compressed at the base, progressively becoming longer and more labiolingually compressed toward the apex. The labial crown wall is convex except for a few vertical grooves located close to the apex in the unworn germ, whereas the lingual wall is concave but occupied to a large extent by a very thick (pillar-like) endocristid. The latter is slightly tilted mesially, lingually protruding, and very broad in its basal portion, which is continuous with the basal bulge and progressively tapers apically without reaching the apical edge. The endocristid separates the V-shaped prefossid and endofossid, which are similarly deep and extensive, except that the former extends slightly more than the latter toward the cervix. The precristid and postcristid are similarly marked. The ectosynclinid appears only slightly more extended onto the root than the endosynclinid, and the pre- and postanticlinid are V-shaped and very marked (the former more so). The crown appears waisted at the cervix, but root morphology cannot be evaluated.

The di2 of *Pa. valentini* is represented by a relatively complete specimen that displays slight wear and is only missing the apical portion of the root (Fig. 13j). The crown is mesiodistally compressed at the base, progressively becoming more labiolingually compressed toward the apex. It is very tilted mesially, expanding slightly toward mesial at about crown mid-height but showing a more uniform curvature on the distal side, thus progressively tapering apically on the upper half of the crown. The preserved (worn) incisal edge is moderately inclined. The precristid and postcristid are moderately marked, separating the convex labial wall from the concave lingual side, which displays a sharp endocristid. The latter originates from a moderately developed basal swelling and fades away close to the incisal edge. The endocristid separates the moderately shallow prefossid from the narrower (almost groove-like) endofossid. The ectosynclinid and the endosynclinid appear similarly developed, while the postanticlinid and the preanticlinid are quite deep. The root is mesiodistally compressed and curved mesially from base to apex.

A tetraconodontine di3 is assigned to *Pa. valentini* (Fig. 13o). It consists of an unworn crown germ that displays a very similar lingual morphology to the i3 of the same taxon but is somewhat lower-crowned relative to mesiodistal length and slightly labiolingually instead of markedly mesiodistally compressed. The crown is mesially tilted and broadest at the base, progressively becoming more labiolingually compressed toward the apex. The labial crown wall is convex, while the lingual one is concave. The unworn incisal edge is markedly curved without mamelons, distally becoming continuous with the long, mesially inclined, and moderately marked postcristid. Mesially, in contrast, the incisal edge constitutes a marked angle with the precristid, which is roughly parallel and slightly more marked than the postcristid. A vertical and distinct endocristid originates from the distolingual end of the crown and progressively tapers apically, ending close to the apical portion of the

poscristid shortly before reaching the distal portion of the incisal edge. Because the cervix is not lingually preserved, it cannot be ascertained whether a distinct basal lingual swelling was present as in the i3 of the same taxon. A groove-like vertical endofossid can be discerned between the endocristid and the postcristid, contrasting with the much more extensive and moderately shallow prefossid. The latter is subdivided into two distinct portions by a poorly defined vertical secondary cristid that originates in a cuspulid-like enamel thickening midway along the precristid and almost reaches the incisal edge. The cervix is only preserved at the mesial side, where a relatively well-developed and U-shaped preanticlinid can be observed.

Lower deciduous premolars: Three partial dp3s from CB display tetraconodontine affinities, one of them (Fig. 13s) being here tentatively assigned to *Pa. valentini*. It only preserves the distal portion of the crown and the distal root. The preserved crown portion appears only moderately high but displays abundant wear along the distal aspect of the protoconid. A distinct metaconid seems to have been originally present just distally from the protoconid, but this cannot be adequately ascertained due to wear. The crown appears longer on the lingual side due to the greater distal protrusion of the distolingual corner. There are no conspicuous cingulids, but the preserved lingual wall is very convex, displaying a very marked cleft at the level of the metapostcristid, whereas in contrast the buccal wall appears uniformly convex. Despite wear, it can still be ascertained that the metapostcristid bifurcated into two distinct cristids of mesiolingual direction, apparently delimiting a small and distolingually directed fossid.

A single dp4 crown displaying slight wear is identified as *Pa. valentini* (Fig. 13a'). It displays an elongate and mesially tapering subrectangular contour with three lobes. The lingual crown wall is straighter than the buccal, where the lobes display a more convex profile and are separated by moderately developed constrictions, while the distal portion of the crown is centrally projecting (shaping a more marked convexity than the mesial margin). Each lobe displays two main cuspids that are quite transversely aligned with one another. The main cuspids are pyramidal in shape and display sharp cristids and marked Fürchen. The centrally located protopreconid and hypopreconid are moderately developed, slightly more so than the pentaconid, which is distally surrounded by a well-developed cingulid.

Genus *Versoporcus* Pickford, 2014

Versoporcus steinheimensis (Fraas, 1870)

Figures 2c, 5q, n'–o', 6p–q, v'–a", 7g–h, 8e, n, u, 9b–c, 10i–j, m–p, t, b'–d', 11f–j, o–r, w–z, 12r–t, h'–l', w'–y', 13g–h, k–l, q, t–v, b'–e'.

Selected synonyms

1870 *Chaeropotamus Steinheimensis* Fraas, partim.

1892 *Hyotherium soemmeringi* race *Grivense* Depéret (erection of new species-group taxon), partim—excluding the lectotype according to Pickford (2014).

1899 *Sus grivensis* Gaillard (erection of new species—not a junior synonym but a homonym of the nominal taxon *Hyotherium soemmeringi grivense*).

1899 *Hyotherium simorrense* (Lartet, 1851): Stehlin, partim.

1926 *Conohyus simorrensis* (Lartet, 1851): Pilgrim (new combination), partim.

1956 *Conohyus simorrensis steinheimensis* (Fraas, 1870): Thenius (new rank).
1968 *Conohyus simorrensis* (Lartet, 1851): Hünermann, partim.
1972 *Hyotherium soemmeringi* von Meyer, 1834: Golpe-Posse, partim (based on specimens detailed in Golpe-Posse, 1971).
1972 *Hyotherium palaeochoerus* (Kaup, 1833): Golpe-Posse, partim (based on specimens detailed in Golpe-Posse, 1971).
1984 *Conohyus steinheimensis* (Fraas, 1870): Chen (new rank and lectotype designation).
1990a *Conohyus steinheimensis* (Fraas, 1870): Van der Made, partim.
1996 *Parachleuastochoerus steinheimensis* (Fraas, 1870): Fortelius et al. (new combination).
1999 *Parachleuastochoerus steinheimensis* (Fraas, 1870): Van der Made.
2004 *Conohyus steinheimensis* (Fraas, 1870): Bernor et al.
2014 *Parachleuastochoerus steinheimensis* (Fraas, 1870): Van der Made et al., partim.
2014 *Versoporcus steinheimensis* (Fraas, 1870): Pickford (new combination and designation as type species in the description of the genus).
2014 *Versoporcus grivensis* (Gaillard, 1899): Pickford (new combination in the description of the genus).
2016a *Versoporcus steinheimensis* (Fraas, 1870): Pickford.
2016a *Versoporcus grivensis* (Gaillard, 1899): Pickford.
2020 *Parachleuastochoerus steinheimensis* (Fraas, 1870): Van der Made, partim.
2023b *Versoporcus grivensis* (Gaillard, 1899): Mckenzie et al.

Referred material

See Appendix Table 1 for a list of the referred material and Appendix Table 2 for measurements.

Description

Upper permanent premolars: No upper permanent incisors of *Versoporcus* are identified in the studied sample, whereas premolars are restricted to a partial P2 (Fig. 5q) and two P4s (Fig. 5n'–o') that display an advanced degree of wear but allow one to discern some occlusal details. The partial P2 preserves the slightly worn distal portion of the crown and the distal root. The crown is only moderately high, with a pointed paracone and a distinct but lower and more buccally located metacone. The buccal and lingual crown walls are concave distally from the paracone, with a poorly developed buccal cingulum and a much better-developed distolingual cingulum. The P4s are three-rooted and their crown displays a suboval occlusal contour that is broader than long, with moderately convex mesial and distal profiles that converge on a markedly convex lingual contour. Nevertheless, the lingual half of the crown is not strongly tapering. Despite wear, it can be ascertained that the buccal cusps were distinct but closely packed with one another, with no appreciable groove separating their apices on the preserved portion of the buccal wall. The mesial and distal cingula appear well developed, with marked protoprestyle and protopoststyle, and even better developed mesiobuccal and distolingual cingula that do not merge with one another.

Upper permanent molars: Only two M1s, both very lightly worn, are assigned to *Versoporcus* (Fig. 6p–q). One specimen belongs to a maxillary fragment that further includes the DP2–DP4 series (Fig. 2g–i), whose morphology supports an assignment to *Versoporcus*. In turn, the attribution of another specimen (Fig. 6q),

associated with a lower molar of the same individual (Fig. 11f; see later), is based on its closest similarities to the M1 of the maxillary fragment (Fig. 6p). Both M1s display a subrectangular occlusal contour clearly longer than broad, with two lobes separated by mildly developed buccal and lingual constrictions, and four main cusps that are quite transversely aligned and similar in size. Fürchen can be clearly discerned but there is no secondary wrinkling of the enamel. The mesial and distal cingula are well developed, whereas there are not lingual or buccal cingula. The mesial cingulum displays a distinct and centrally located protopreconule that is continuous with the protoprecrista. The hypopreconule is very well developed but does not block the transverse valley separating the mesial and distal lobes, being smaller than the four main cusps but about twice as large as the protopreconule. There is a poorly developed ectoconule enclosing the transverse valley buccally, whereas on the lingual side there is a more distally located and variably developed ectoconule at the end of the hypoectocrista. The distal cingulum displays some development of secondary cuspules.

In turn, up to six M3s are attributed to *Versoporcus* (Fig. 6v'–a"), some of them unworn or with very slight wear. They display considerable variation in size and proportions, but consistently differ from those of the other two species described above (see comparisons below). The crown displays a slightly asymmetrical suboval contour, which is longer than broad and broadest mesially, tapering distally in a rather uniform fashion. The buccal constriction between the mesial and the central lobes is in most specimens much more accentuated than the corresponding lingual one. There are five main cusps not completely transversely aligned, i.e., the protocone and hypocone are more distally located than the paracone and metacone, respectively. The mesial cusps are larger and slightly more peripheral than those of the central lobe. The pentacone, which is centrally located and much smaller than the remaining main cusps, does not protrude distally from the rest of the crown. Instead, it is largely surrounded by secondary cuspules and/or cingular developments both distobuccally and distolingually. In most specimens, a distinct (albeit small) pentapreconule is present between the pentacone and the metacone, next to the hypocone. The mesial cingulum is very well developed and bears a distinct protopreconule, which appears somewhat smaller than the hypoprecone. There is a very well-developed lingual ectoconule mesiolingually from the metacone, while a smaller ectoconule is present on the buccal side in the largest specimen.

Lower permanent incisors: A single i1 is assigned to *Versoporcus* (Fig. 8e). Occlusal morphology cannot be adequately ascertained due to the rather advanced degree of wear, with dentine exposed along most of the lingual surface. The crown is mesiodistally compressed and appears to have been moderately tall, being slightly widest below the preserved incisal edge and becoming labiolingually broadest toward the cervix. The root is vertically aligned with the crown, which displays some waisting at the cervix except at the labial side. The ectosynclinid extends much farther onto the root than the endosynclinid, resulting in asymmetrically V-shaped anticlinids, with the preanticlinid being slightly deeper and more pointed than the postanticlinid. The root is more mesiodistally compressed than the crown and becomes slightly more so toward the apex, whereas in contrast there is almost no apical labiolingual tapering.

There is also a single i2 of *Versoporcus* (Fig. 8n), whose crown displays an advanced degree of wear, so that most occlusal details cannot be ascertained, while the root is completely preserved. The crown appears tilted mesially relative to the root's apicobasal axis. A groove seemingly corresponding to the basal-most end of the endofossid can still be ascertained on the lingual side, distally from a mild basal lingual swelling, indicating that the prefossid did not extend as much down to the crown base. The ectosynclinid extends further onto the root than the endosynclinid, at least on its distal portion, while the preanticlinid is much more marked than the very

shallow postanticlinid. There is little waisting at the cervix and the root is markedly compressed mesiodistally and rather straight, progressively tapering toward its apex in mesiodistal direction but preserving its basal labiolingual breadth throughout most of its extension (only tapering labiolingually and being slightly curved in lingual direction in its apical-most portion).

An i3 assigned to *Versoporcus* (IPS93077; Fig. 8u) is completely preserved except for some damage on the base of the root and a missing lingual portion close to its apex. The crown is only moderately worn apically, with no marked dentine exposure on the lingual surface, although its basal-most lingual portion is missing a chip of enamel. The crown is low, mesiodistally compressed, and mesially tilted, with a markedly convex prestylid, an almost straight but inclined poststylid, and a straight and slightly tilted incisal edge. The mesiolabial aspect of the crown is convex, whereas the distolingual aspect is concave and displays a very thick and protruding endocristid that is obliquely oriented, diagonally crossing most of the crown's lingual aspect and thus separating the moderately developed prefossid from the deeper and somewhat more extensive endofossid. A shorter and diffuse cristid, parallel to the endocristid, seemingly fills most of the prefossid. The crown is basally bulging, resulting in appreciable waisting at the cervix. The preanticlinid is shallow and there is no postanticlinid. The root is verticalized, mesiodistally compressed, and quite robust, only markedly tapering in labiolingual direction in its apical-most portion.

Lower permanent canines: A complete (Fig. 9b) and a partial (Fig. 9c) c1m are attributed to *Versoporcus*. The former is 81 mm in length and displays a clearly scrofic morphology, with the labial face being much narrower than the lingual and distal faces, and the lingual being the broadest. The distal face displays a flattish contour in cross section and is devoid of enamel, displaying a wear facet against the upper canine in its apical-most third. The tooth is markedly curved in labial and lingual views, and more moderately curved towards labial in distal and mesial views. The cross-sectional contour of the lingual aspect of the crown is convex, whereas the labial is somewhat concave, displaying a broad and shallow sulcus that extends from base to tip. In mesial view, the keel formed by the confluence of the labial and lingual sides appears rather blunt. The c1m fragment, in turn, measures 43 mm and also shows a scrofic cross section with similar dimensions, merely being slightly narrower labiolingually. This is probably because the fragment corresponds to the canine portion close to the tip, thus being attributable to the same taxon. No female lower canines from CB are assigned to this species.

Lower permanent premolars: Besides isolated teeth, two mandibular fragments (Fig. 7g–h) are assigned to *Versoporcus*. The most complete one allows us to relate the morphology of the molars to that of the premolars (except for the p1; Fig. 7g).

The two smallest tetraconodontine p1s among the sample (Fig. 10i–j) are attributed to *Versoporcus*. They preserved very lightly worn crowns and, in one of the specimens, the basal portion of the roots. The crown displays a subelliptical and very buccolingually compressed occlusal contour. The protoconid is located on the mesial half of the crown, giving rise to a very steep protoprecristid and a longer and somewhat less inclined protopostcristid. The former is rather blunt and ends in a low but marked prestylid at the mesial end of the crown. In turn, the protopostcristid is thicker and denticulated, but bears no distinct metaconid. The latter cristid ends close to the distal end of the crown, which is distally protruding and displays a moderately developed hypoconid. The latter is as low as the prestylid but less marked. There are no cingulids, but the crown walls are only slightly bulging at the level of the protoconid, otherwise becoming convex (more markedly so distally from the protoconid, almost developing a cingulid on the distal half of the crown). There are marked labial and lingual

anticlinids at the cervix, which extends much farther rootward distally than mesially. The two roots are well separated and, as far as it can be ascertained due to incomplete preservation, the mesial one might have been more mesially tilted than the distal.

The four tetraconodontine p2s from CB are attributed to *Versoporcus*. They include a lightly worn isolated specimen (Fig. 10m), another slightly worn and complete p2 (Fig. 10o) that unambiguously belongs to this tooth locus because it is socketed in the IPS1713 mandible (Fig. 7s–u), and two partial isolated specimens that are missing the mesial portion of the crown as well as the mesial root (Fig. 10n, p). The two complete crowns display a similar occlusal pattern but strikingly differ in proportions and occlusal relief. The isolated specimen (Fig. 10m) displays a subelliptical contour that is only moderately buccolingually compressed as well as marked occlusal relief with a trenchant appearance and a centrally located protoconid along the mesiodistal axis, being reminiscent of a p3 (although it appears too small to belong to this tooth locus). In contrast, the p2 from the mandible (Fig. 10o) is longer and displays a very elongate (buccolingually compressed) occlusal contour, a less marked occlusal relief, and a somewhat mesially located protoconid, being more reminiscent of the morphology of the p1 at a much greater size. In both specimens, the protoprecristid ends in a low and moderately developed prestylid at the mesial end of the crown; however, given the higher protoconid, the protoprecristid is longer and steeper in the isolated specimen, whereas it is sharper and slightly tilted mesiobuccally in the socketed p2. In both specimens, the metaconid appears slightly more buccally positioned than the protoconid. However, the protopostcristid is longer in the socketed specimen, linking the protoconid with the poorly developed and buccolingually compressed metaconid, whereas in the isolated p2 the metaconid is located very close to the protoconid. In both specimens, there is a short metapostcristid that bifurcates into two distinct cristids that define a restricted triangular fossid close to the distal end of the crown, distally from a variously developed hypoconid. The two incomplete p2s attributed to the same species, as far as it can be ascertained, display in the distal half of the crown a similar occlusal morphology and proportions to the isolated specimen. However, while in one of them (Fig. 10n) the distal fossid is likewise centrally located, in the other (Fig. 10p) it appears to have been distobuccally situated, as in the socketed specimen. None of the p2s displays distinct cingulids except around the mesial prestylid. The buccal and lingual crown walls are convex around the protoconid, but otherwise concave, particularly distally from the protoconid, with the isolated complete specimen displaying marked vertical clefts flanking the metapostcristid. In all the p2s, the cervix shows moderately developed buccal and lingual anticlinids and extends farther rootward distally than mesially. There are two distinct roots only fused at their basal-most portion, the mesial one being apparently slenderer and more mesially tilted than the distal, as far as it can be ascertained in the socketed specimen.

A single p3, displaying a slight degree of wear and belonging to the aforementioned mandible (Fig. 10t), is assigned to *Versoporcus*. It displays a subrectangular occlusal contour, only minimally longer but relatively much broader than the p2 of the same individual, further displaying more pronounced occlusal relief. In the latter regard, the p3 of IPS1713 is more similar in occlusal shape to the smaller premolar IPS92720 (Fig. 10m)—here interpreted as a p2 (see above). The protoconid is centrally located at about crown mid-length and buccolingually compressed, with the crown displaying a trenchant appearance. The protoprecristid is sharp, steeply inclined, and slightly tilted mesiolingually, terminating in a low but very well-developed prestylid located slightly toward the lingual side of the crown. Despite wear, a distinct metaconid, lower but similarly developed to the protoconid, can still be discerned just distally from the latter. A very thick and barely distinct metapostcristid bifurcates close

to the distal end of the crown, defining a triangular and steeply inclined distal fossid. The buccal side of the latter is partly obliterated by a bulbous thickening of the enamel that corresponds to the hypoconid, which is thus located slightly more buccally than the protoconid and metaconid. This premolar displays two roots, whose morphology cannot be adequately ascertained because the single available specimen is socketed.

The p4s attributed to *Versoporcus* include the specimen socketed in the aforementioned mandible (Fig. 10b'), which displays a moderate degree of wear, an isolated specimen (Fig. 10c') that preserves the lightly worn crown and a large portion of the distolingual root, and a partial p4 (Fig. 10d') that includes the mesial portion of the crown and the mesial root. These specimens display a similar occlusal pattern with only minor differences. The crown is suboval, longer than broad as well as broader distally than mesially, with variously protruding distobuccal and distolingual corners. There is some variation among the available specimens in occlusal contour, with the specimen from the mandible (Fig. 10b') having straighter edges and a more distobuccaly protruding contour than the other specimen (Fig. 10c'–d'), which display a more marked lingual (instead of buccal) constriction and a more distolingually protruding crown corner. There is also variation in occlusal relief, which appears less pronounced in the specimen from the mandible than in the remaining ones—such differences can be only partly attributed to wear, since dentine exposure is still restricted in the socketed specimen. The presence of a distinct metaconid close to the protoconid can be ascertained in the three available specimens irrespective of wear, although in the least worn specimen the former appears rather indistinct (Fig. 10c'), being connected to the protoconid by a slightly obliquely oriented protopostcristid. The sharp protoprecristid that originates at the protoconid apex is steeply inclined and more or less mesiodistally aligned, ending in a generally well-developed and relatively high prestylid at the mesial end of the crown. A shorter metapostcristid originates from the distal aspect of the metaconid, being mesiodistally aligned but more lingually located than the protoprecristid. The metapostcristid bifurcates into two short, thick, and blunt (cuspulid-like) cristids that terminate close to the distal margin of the crown, which displays one or more secondary cuspulids without a distinct hypoconid. The metapostcristid is flanked by deep vertical clefts both buccally and lingually and there are no well-developed cingulids except for those associated with the mesial prestylid and the distal aspect of the aforementioned clefts. The crown displays a mesial and two distal roots, which appear fused at their basal-most portion.

Lower molars Several tetraconodontine m1s (Fig. 11f–j) and m2s (Fig. 11o–r) are attributed to *Versoporcus* instead of *Pa. valentini*, although such an attribution is more secure for some specimens than for others. Thus, the assignment of the lower molars of the IPS1713 mandible (Fig. 11i, q) to *Versoporcus* is based on the more diagnostic morphology of the premolars (particularly the p4, see above), whereas the assignment of the lower molars (Fig. 11j, r) of another mandibular fragment without premolars (Fig. 7h) to the same genus is based on similarities between the respective m3s. In turn, one of the m1s (Fig. 11f) is associated with an M1 of the same individual (Fig. 6q), which more clearly shows differences relative to the upper molars of *Pa. valentini*. The attribution of the two remaining m1s (Fig. 11g–h) and m2s (Fig. 11o–p) is more tentative but supported by minor occlusal details. The m1 and m2 display a similar occlusal contour and pattern, characterized by a subrectangular shape longer than broad and rather straight margins with two moderately distinct lobes. The socketed m1s are only moderately smaller (narrower and shorter) than the m2s of the same individuals. Unworn and lightly worn specimens show marked Fürchen and a moderate degree of enamel wrinkling, which can still be observed in slightly more worn molars. The four main cuspids are pyramidal in size and somewhat buccolingually compressed. The protoconid is slightly more mesially located than the metaconid, while the hypoconid and

endoconid are transversely aligned. There is a narrow but distinct mesial cingulid. Distally from it, the protoprecristid merges with the shorter metaectocristid, while the metaprecristid is directed toward the protofossid. There is generally a moderately developed metaendoconulid, as well as a well-developed hypopreconulid at about the center of the transverse valley and a small hypoectoconulid on the buccal side. On the distal end of the crown there is a small and centrally located pentaconid (larger in the m2 than in the m1). The pentaconid interrupts the distally protruding cingulid, which displays more or less developed secondary enamel folds and grooves.

The m3 of *Versoporcus* is represented by two socketed specimens from the aforementioned mandibles (Fig. 11y–z), plus two isolated partial specimens (Fig. 11w–x). As noted above for the m1 and m2, the m3 of IPS1713 can be securely assigned to this species because the mandible further preserves the p2–p4 series, with the p4 being particularly diagnostic of the genus. The remaining specimens are attributed to the same taxon given similarities in occlusal contour and pattern, which are ascertainable despite differences in wear. The m3 of IPS1713 displays a slight degree of wear with no dentine exposure that enables to adequately describe occlusal details, as well as to ascertain the presence of marked Fürchen but only a limited amount of enamel wrinkling. This tooth displays a subtriangular occlusal contour longer than broad, with three lobes separated from one another by only moderately developed constrictions and five main cuspids. The mesial lobe is the broadest and the crown contour progressively tapers distally, more markedly so along the buccal side except at the distal lobe, which is distally to buccally tilted depending on the specimen. At the mesial lobe, the protoconid is slightly more mesially located than the metaconid and the protoprecristid forms a continuous curved and transversely aligned crest with the similarly developed metaectocristid. The metaprecristid is transversely directed toward the protoconid but only moderately developed, so that there is a spacious protofossid between the bases of the protoconid and the metaconid. The obliquely oriented metaendocristid terminates in a distinct and moderately developed metaendoconulid. The transverse valley between the mesial and central lobes is centrally interrupted by a relatively well developed hypopreconulid but displays no entoendoconulid, while the hypoectoconulid is absent to very poorly developed depending on the specimen. At the central lobe, the hypoconid is transversely aligned with or slightly more distally located than the entoconid. Both cuspids are lower but only slightly less extensive than the mesial ones. The distal lobe bears a centrally to distobuccally located hypoconid that is much smaller than the remaining main cuspids and is surrounded by two (buccal and lingual) very small secondary cuspulids. The transverse valley between the central and distal lobes displays moderately developed pentaectoconulid and pentaendoconulid, as well as a centrally located and very well-developed pentapreconulid (similar in size to the hypopreconulid and somewhat larger than the pentaconid). There are no cingulids except for a moderately developed and continuous mesial cingulid.

Upper deciduous premolars: Three DP2s are attributed to *Versoporcus* (Fig. 12r–t). They preserve the slightly worn crown and two of them also include part of the roots. One of the specimens (Fig. 12r) belongs to a maxillary fragment that further preserves the DP3–M1 series (Fig. 2g–i). The occlusal contour is much longer than broad and distolingually tilted, and the crown displays a marked occlusal relief despite being low in height, with convex buccal and lingual walls except around the main cusps. The paraprotocrista is long and sharp, ending in a moderately developed mesial prestyle. The short parapostcrista links the paracone with an elongate and distolingually oriented metacone, which is very protruding (only slightly lower than the paracone and much higher than the mesial prestyle). There is no buccal cingulum except at the mesiobuccal portion of the crown,

while the lingual one is better developed (particularly distolingually) but discontinuous at the paracone level. The cervix displays marked buccal and especially lingual anticlines, and the mesial root appears more mesially tilted than the distal.

Four complete and one partial DP3s (Fig. 12h'–l') display tetraconodontine affinities but are assigned to *Versoporcus* instead of *Pa. valentini* based on their smaller size and some minor occlusal differences. One of them belongs to the aforementioned maxillary fragment (Fig. 2g–i) that further displays a DP2 more consistent in morphology with *Versoporcus*. The general occlusal pattern is basically the same already described above for the other taxa, with three main cusps and two distinct lobes, the mesial one being narrower than the distal, and a vaguely subtriangular occlusal contour. The mesial and distal lobes are separated by moderately developed buccal and lingual constrictions, and the distal one is particularly asymmetrical (distolingually more protruding). The subtle paraprecrista is mesiolingually oriented, and the distal cristae of the paracone are confluent with but more marked than the mesial cristae of the protocone and metacone. The cingula are variably developed, more marked in the largest specimens, particularly along the mesiolingual and distobuccal portions of the crown.

The DP4s attributed to *Versoporcus* (Fig. 12w'–y') display some differences relative to the other two taxa described above. One of the specimens (Fig. 12w') belongs to the IPS1712 maxillary fragment (Fig. 2g–i) that further preserves the DP2 and DP3. The attribution of the other (isolated) specimens is based on similarities to the former. The crown displays a vaguely subrectangular occlusal profile (longer than broad), with two distinct lobes that appear lingually convergent to one another, because they combine a marked lingual protrusion of the mesial lobe with a mesial contour that is straight lingually but curved buccally. The mesial and distal cingula are marked and display secondary enamel folds and grooves, while the distobuccal cingulum is poorly developed. The protopreconule is only moderately developed, while the hypoprecone is larger and generally more distinct. There is also a moderately developed hypoendoconule and a more or less distinct metaectoconule.

Lower deciduous incisors: Two di1 germs are attributed to *Versoporcus* (Fig. 13g–h). The unworn incisal edge is inclined and constituted by two poorly distinguished mamelons. The crown is compressed mesiodistally at the base, progressively becoming longer toward its apex. The basal half of the crown is labiolingually wide and lingually bulging, whereas the upper half is very compressed. Indeed, the labial crown wall is not uniformly convex, but displays a broad and deep depression on its upper half. The lingual wall, in turn, displays a pillar-like and mesially tilted endocristid that is very wide basally and progressively tapers apically without reaching the incisal edge. The prefossid and endofossid display similar depth and extension, except that the former extends slightly farther toward the crown base. Both the precristid and postcristid are well developed. Neither the extension of the synclinids nor the degree of crown waisting at the cervix can be evaluated, but the preanticlinid appears moderately marked.

Two di2s are attributed to *Versoporcus* (Fig. 13k–l), given their overall morphology that displays some differences relative to those assigned to *Pa. valentini* coupled with some similarities to the di1 of *Versoporcus*. One of the specimens is completely preserved (despite some damage at the crown) and shows a slight degree of wear (Fig. 13k). The other is a partially preserved crown with somewhat more advanced apical wear (Fig. 13l), which is assigned to the same taxon given similarities in crown shape (including the development of the endocristid). The crown is mesiodistally compressed and mesially tilted, but conforms a continuous curvature with the root through the cervix. Furthermore, the crown maintains a similar mesiodistal length throughout most of its height (due to the straight postcristid, parallel to the precristid), only tapering distally very close to the

incisal edge. The endocristid is very broad and lingually protruding, progressively tapering apically, almost reaching the incisal edge. As a result, the prefossid is very narrow, being restricted to the apical half of the crown. The endofossid is slightly broader and much higher, progressively becoming groove-like down to the cervix level. The crown appears labiolingually compressed in its upper half, particularly in the most complete specimen, where the labial wall appears depressed close to the apex. The endo- and ectosynclinid are similarly developed, while the preanticlinid is much deeper than the postanticlinid. The root is longer than the crown, mesiodistally compressed, and quite slender, progressively tapering and curving mesially toward the apex. No di3 of *Versoporcus* has been identified among the CB sample.

Lower deciduous premolars: An isolated dp2 (Fig. 13q), damaged on its mesial-most portion, is attributed to *Versoporcus.* The crown, which displays a moderate degree of wear, is damaged mesially, and only the distal root is partially preserved. The crown is low and elongate, with rather straight buccal and lingual contours, and markedly convex mesial and distal ones (the latter being slightly distolingually protruding). The protoconid is buccolingually compressed and located toward the mesial half of the crown. A long and sharp protoprecristid links the apex of the protoconid with the mesial prestylid, which is lingually tilted but whose development cannot be ascertained due to incomplete preservation. The protopostcristid is obliquely oriented toward the distobuccal corner of the crown. Due to wear, it is unclear whether a poorly developed hypoconid was originally present, but the distal cristid bifurcates, enclosing a small distobuccal fossid. Some secondary cuspulids are present on the cingular extension at the distolingual corner of the crown.

Three tetraconodontine dp3s are also assigned to *Versoporcus* (Fig. 13t–v). One of them is only slightly worn but partially preserved (Fig. 13u), missing the mesial end of the crown, the mesial root, and the tip of the distal root. There is also a partial crown germ (Fig. 13v) that neither preserves the mesial end of the crown, but which more adequately enables to ascertain its unworn morphology. The remaining dp3 (Fig. 13t) is missing the mesial portion of the crown and displays a more unusual morphology than the other specimens, its identification being much more tentative. The crown is moderately high and displays a subelliptical contour that is longer than broad and broadest distally. The development of the prestylid, mesially from the protoprecristid, cannot be evaluated due to incomplete preservation. The protoconid is the highest cuspid. In two specimens, an elongate and buccolingually compressed metaconid, slightly lower than the protoconid, is located just distally from the apex of the latter (Fig. 13u–v), whereas in the remaining specimen the metaconid is distobuccally positioned relative to the protoconid (Fig. 13t). In all the specimens, the metapostcristid bifurcates into two diverging and moderately developed cristids than configure a subtriangular distal fossid. The latter is moderately extensive except in the specimen displaying a differently located metaconid, in which it is much more extensive and flanked by more marked distobuccal and distolingual cingulids (Fig. 13t). Two roots were originally present, being fused at their basal-most portion.

Finally, four dp4s are assigned to *Versoporcus*, including two complete crowns with slight wear (Fig. 13b'–c') and two distal fragments (Fig. d'–e'). The crown displays a subrectangular occlusal contour that is longer than broad but only slightly tapers mesially and displays three distinct lobes. The occlusal contour is very straight lingually and only moderately convex at the level of each lobe buccally. The six main cuspids are pyramidal in shape and the cristids are sharp, with marked Fürchen but limited wrinkling of the enamel. The mesial cuspids are transversely aligned to one another, but the remaining buccal cuspids (protoconid and hypoconid) appear more mesially located than the corresponding lingual ones (metaconid and entoconid,

respectively). The two preconulids and the pentaconid are only moderately developed and mesiodistally aligned. The paraprecristid is continuous with a narrow but mesially projecting mesial cingulid. The distal cingulid is only moderately developed along the rounded (not projecting) distal margin of the crown.

Comparisons

Upper permanent teeth

Upper permanent incisors: The I1s of *P. palaeochoerus* from CB (Fig. 3a–c) display similar dimensions and proportions (MD = 15.2–15.4 mm, BL = 10.0–10.5 mm, BLI = 66–69%, n = 3) to those from Gau-Weinheim (MD = 15.0–20.0 mm, BL = 8.0–10.2 mm, BLI = 42–64%, n = 5; Pickford 2013a) and their morphology agrees with previously published descriptions and iconography (Hünermann 1968: pl. I, figs. 8–9; Fortelius et al. 2005). The I1s from CB assigned to *Pa. valentini* (Fig. 3d–g) have very similar dimensions and proportions (MD = 15.0–16.4 mm, BL = 10.0–10.5 mm, BLI = 64–67%, n = 4) to those of *P. palaeochoerus* but display several morphological differences: less mesially tilted crown; more concave and smoother lingual surface; more inclined lingual cingulum that shapes a marked angle with the more curved precrista as well as with the less distinct metacone; less asymmetrical cervix (shallower preanticline and less marked endosyncline); and stouter, straighter, and shorter root. Furthermore, the best-preserved I1 crown of *Pa. valentini* from CB (Fig. 3d) resembles that of the somewhat more worn specimen IPS96058 [VP1013] of *Pa. valentini* from Sant Quirze (Pickford 2014: fig. 13A), supporting an attribution to the same species.

In turn, the single I2 of *P. palaeochoerus* from CB (Fig. 3h) displays the elongate and low crown with a well-developed lingual cingulum that is characteristic of the species (Hünermann 1968: pl. I, fig. 10; Van der Made and Moyà-Solà 1989: pl. 1, fig. 11; McKenzie et al. 2023a: fig. 3a). The CB specimen is less elongate (MD = 13.3 mm, BL = 8.1 mm, BLI = 61%) than those of the same species reported from CCN20 (MD = 15.7 mm, BL = 6.9 mm, BLI = 44%; McKenzie et al. 2023a) and Gau-Weiheim (MD = 16.0–18.0 mm, BL = 6.2–8.7 mm, BLI = 39–50%, n = 5; Pickford 2013a). However, its morphology is more consistent with this identification than an alternative attribution to an I3, which displays a more triangular crown (Hünermann 1968: pl. I, Fig. 11). Van der Made and Moyà-Solà (1989: pl. 1, fig. 10) figured an unworn I3 crown of *P. palaeochoerus* from CB that we have been unable to find among the ICP collections, but the two i3s reported here (MD = 10.8–11.1 mm, BL = 6.5–6.7 mm, BLI = 59–62%; Fig. 3k–l) roughly agree in proportions with, despite being smaller than, those from Gau-Weinheim (MD = 13.0–15.0 mm, BL = 6.5–8.9 mm, BLI = 49–60%, n = 3; Pickford 2013a). Two additional upper incisors from CB (Fig. 3i–j) resemble the I1s attributed to *Pa. valentini* in shape (displaying a high and shovel-like crown with a marked distolingual concavity and an obliquely oriented endocrista) as well as proportions, but are smaller and slenderer (MD = 8.6–10.2 mm, BL = 6.6–7.0 mm, BLI = 69–77%), being interpreted as I2s of the same taxon. The morphology of these incisors differs markedly from that of *P. palaeochoerus* (see above) and also from that of *Versoporcus*, which displays a more elongate I2 crown (Van der Made et al. 2014: fig. 8b), albeit without the well-developed lingual cingulum present in *P. palaeochoerus*. As the I2 had not been previously reported for *Pa. valentini*, these specimens from CB might be alternatively interpreted as I3s, whose morphology is similarly unknown. Pickford (2014) reported measurements for a purported I3 of this species from Sant Quirze. However, upon close inspection, we interpret it as an i3 (see below for further discussion). In any case, a similar I1 and I2/I3 morphology had previously been described for

C. simorrensis (Pickford 2013b: fig. 7A–B), contrasting with that of *Versoporcus* (Van der Made et al. 2014: fig. 8b–d) already discussed above.

Upper permanent canines: The C1fs from CB assigned to *P. palaeochoerus* (MD = 13.7–14.7 mm, BL = 8.1–10.0 mm, BLI = 58–68%, n = 4) fit relatively well in size and proportions with those previously reported for this species from CCN20 (MD = 12.8–14.1 mm, BL = 9.9–9.5 mm, BLI = 67–70%, n = 2; McKenzie et al. 2023a) and Grytsiv (MD = 12.4 mm, BL = 7.4 mm, BLI = 60%, n = 1; Van der Made et al. 1999), being larger than those from Rudabánya (MD = 9.2–12.4 mm, BL = 4.5–7.4 mm, BLI = 49–66%, n = 5; Fortelius et al. 2005). The CB specimens (Fig. 4a–d) quite closely resemble those previously reported (Van der Made et al. 1999: pl. 2, fig. 4; McKenzie et al. 2023a: fig. 3b–c). The C1fs from CB attributed to *Pa. valentini* (MD = 14.6–15.3 mm, BL = 9.9–10.4 mm, BLI = 65–71%, n = 2; Fig. 4e–f) are only minimally larger and relatively broader than those of *P. palaeochoerus* from the same site, but differ from them in the higher crown (at comparable wear stages), the stouter root, the blunter postcrista, the less distinct endocrista, and apparently the lack of apical wear at early wear stages—compare IPS93150 (Fig. 4e) with IPS1718 (Fig. 4a), although this might vary among individuals. The most worn specimen from CB (Fig. 4f) resembles a similarly worn specimen from CCN20 (McKenzie et al. 2023a: fig. 3d) attributed to *Pa. valentini*, which also displays very similar size and proportions (MD = 15.0 mm, BL = 10.2 mm, BLI = 68%).

Upper permanent premolars: The P1s of *P. palaeochoerus* from CB (BLI = 38–41%, n = 10) fit well with the metrical variation (Fig. 14d) and proportions (BLI = 33–52%, n = 10) previously documented for the species (Hellmund 1995; Fortelius et al. 2005; Pickford 2013a; McKenzie et al. 2023a). The specimens from CB (Fig. 5a–g) show some variation in occlusal contour, in agreement with variation evinced by previously published specimens (Stromer 1928: pl. II, fig. 20; Hünermann 1968: pl. 1, fig. 2; Schmidt-Kittler 1971: fig. 4; Mottl 1966: pl. IV; Fortelius et al. 2005; McKenzie et al. 2023a: fig. 4a–b). The P1s from CB (Fig. 5h–i) attributed to the tetraconodontine *Pa. valentini* overlap in proportions (BLI = 33–38%) with those of *P. palaeochoerus* (see above) but are slightly longer in absolute terms, and more clearly differ in terms of occlusal shape by displaying a more trenchant appearance, coupled with a much greater extension of the enamel onto the root on the distal half of the crown as well as a protrusion of the distal end of the crown as compared with the cervix. The P1s from CB assigned to *Pa. valentini* are somewhat shorter than the two previously reported specimens of this species and overlap instead with the variation displayed by the larger sample of *Versoporcus* P1s (Fig. 14d). Their proportions overlap with both *Pa. valentini* from Sant Quirze (BLI = 35–37%, n = 2; Pickford 2014: fig. 14G, I)—another specimen identified by Pickford (2014: fig. 14A) as a P1 (current catalog number: IPS96082) is here reinterpreted as a DP2 (see below)—and *Versoporcus* (BLI = 35–43%, n = 6; Pickford 2014, 2016a). However, the CB tetraconodontine P1s more closely resemble the former taxon in terms of occlusal morphology, differing from those of *Versoporcus* (Chen 1984: pl. 1, fig. 10; Pickford 2014: fig. 30A–B, 2016a: fig. 15) in the higher occlusal relief and less buccolingually compressed crown walls both mesially and distally from the paracone.

The P2s of *P. palaeochoerus* from CB (Fig. 5j–p), despite some variation in occlusal contour, agree well in proportions (BLI = 47–57, n = 6) and occlusal morphology (Stromer 1928: pl. II, fig. 20; Mottl 1966: pl. IV; McKenzie et al. 2023a: fig. 4c–d) with those previously reported in the literature (BLI = 39–59, n = 9; Hellmund 1995; Fortelius et al. 2005; McKenzie et al. 2023a), only slightly exceeding the previously recorded range of size variation (Fig. 14E). The CB specimens further overlap in proportions with the single complete P2 thus far

reported for *Pa. valentini* (BLI = 54%; McKenzie et al. 2023a: fig. 4e), which nevertheless differs by displaying a higher occlusal relief with a more trenchant morphology. The P2s of *Versoporcus* are generally longer in absolute terms (Fig. 14e) and display narrower proportions (BLI = 38–46, n = 9; Pickford 2014, 2016a; McKenzie et al. 2023a), as well as a distinct occlusal morphology (Chen 1984: pl. 1, fig. 10; Pickford 2014: fig. 30A–B, 2016a: fig. 15; McKenzie et al. 2023b: fig. 1b) that only fits with a partial P2 from CB (Fig. 5q).

Three of the six P3s from CB assigned to *P. palaeochoerus* (Fig. 5r–w) are longer than previously recorded for the species and approach the metrical variation of tetraconodontines (Fig. 14f). Nevertheless, the proportions of the specimens (BLI = 74–83, n = 5) agree with those previously recorded for *P. palaeochoerus* (BLI = 73–94, n = 26; Mottl 1966; Hellmund 1995; Fortelius et al. 2005; Pickford 2013a; Iannucci and Begun 2022; McKenzie et al. 2023a), and the same applies to their occlusal morphology, which is quite variable in the species regarding occlusal contour (Stromer 1928: pl. II, fig. 20; Mottl 1966: pl. IV; Hünermann 1968: pl. 1, fig. 2; Fortelius et al. 2005: fig. 5; Iannucci and Begun, 2022: fig. 2A; McKenzie et al. 2023: fig. 4f–g). The two P3s from CB attributed to *Pa. valentini* (Fig. 5x–y) display a different (more symmetrical and less distolingually protruding) occlusal contour. The only specimen for which both breadth and length can be estimated (Fig. 5x) only overlaps in length with *Pa. valentini* (Fig. 14f) and its occlusal proportions (BLI = 67%) fit with those previously reported for *Pa. valentini* (BLI = 66–85, n = 6; Pickford 2014, 2016a; McKenzie et al. 2023a) but not *Versoporcus* (BLI = 74–92, n = 10; Pickford 2014, 2016a). The morphology of the two P3s of *Pa. valentini* from CB, as far as in can be ascertained given their advanced degree of wear, differs from that of *Versoporcus* (Chen 1984: pl. 1, fig. 10; Pickford 2014: fig. 30A–B, 2016a: fig. 15) in the seemingly lesser developed prestyle and less mesially tapering occlusal contour. This morphology resembles that of some P3s previously attributed to *Pa. valentini* by Pickford (2014: fig. 9A, 2016a: fig. 7A–B), although admittedly this tooth locus displays considerable variation in occlusal contour, with other specimens being more asymmetrical and displaying a more protruding distolingual crown portion (Pickford 2014: figs. 9A, 11A, 2016a: figs. 7A–B, 13B; McKenzie et al. 2023a: 4h).

The sample of P4s of *P. palaeochoerus* from CB is quite extensive (Fig. 5z–j'). They generally overlap in size with the previously documented metrical variation of the species except for a couple specimens that are slightly longer (Fig. 14g), whereas their proportions (BLI = 113–133%, n = 11) also fit well (BLI = 102–136%, n= 47; Hellmund 1995; Van der Made et al. 1999; Fortelius et al. 2005; Pickford 2013a; Iannucci and Begun 2022; McKenzie et al. 2023a). In terms of occlusal shape, no relevant differences can be noticed, with the CB sample evidencing the same variation in occlusal profile as previously documented for the species—from subsquare to somewhat lingually tapering (Stromer 1928: pl. II, fig. 20; Mottl 1966: pl. IV; Hünermann 1968: pl. 1, figs. 2–3; Van der Made et al. 1999: pl. 1, fig. 2 and pl. 2, fig. 1; Fortelius et al. 2005: fig. 5; Iannucci and Begun 2022: fig. 2A; McKenzie et al. 2023a: fig. 4i–k). The three P4s from CB attributed to *Pa. valentini* (Fig. 5k'–m') fall within or close to the distribution of the species but in the overlap zone with both *Versoporcus* and *P. palaeochoerus* (Fig. 14g), while their proportions (BLI = 131–140%, n = 3) are consistent with those previously recorded for the former species (BLI = 123–140%, n = 9; Pickford 2014, 2016a; McKenzie et al. 2023a) as well as for *Versoporcus* (see below), and tend to be relatively broader than those of *P. palaeochoerus*. The P4s of *Pa. valentini* from CB differ from those of *P. palaeochoerus* in their more subtriangular (lingually tapering) contour and their more peripheral and indistinct buccal cusps (albeit with distinct apices), the less marked prestyle and poststyle, and the less developed mesial and distal cingula and better-developed lingual cingulum, more closely resembling the specimens previously attributed to *Pa. valentini* (Pickford 2014: figs. 9A,

14C, 2016a: fig. 7A–B; McKenzie et al. 2023a: fig. 4m). It is noteworthy that, as noted by McKenzie et al. (2023a), the P4 from Nuri Yamut (Van der Made and Tuna 1999: fig. 3), assigned to *C. doati* by Pickford (2016a), displays several differences compared with those of *Pa. valentini* and is thus not included here in the latter species. Finally, the two P4s from CB assigned to *Versoporcus* (Fig. 5n'–o') fall close to the *V.* '*grivensis*' range of size variation, in the overlap zone with *P. palaeochoerus* and *Pa. valentini*. Their proportions (BLI = 127–129%, n = 2) also fit well with those previously reported for this genus (BLI = 122–140%, n = 14; Pickford 2014, 2016a; McKenzie et al. 2023b), which nevertheless overlap extensively with those of the two other taxa recorded at CB (see above). Their attribution to *Versoporcus* is thus based on a few differences in occlusal shape, more closely resembling previously reported specimens of this genus (Chen 1984: pl. 1, fig. 10; Pickford 2014: fig. 30A–B, 2016a: figs. 15, 24B; McKenzie et al. 2023b: fig. 1c). In particular, they differ from those of *P. palaeochoerus* in the more oval occlusal contour and apparently the more closely packed buccal cusps, and from those *Pa. valentini* in the less peripheral buccal cusps, better-developed cingula, and more mesially located protocone (more transversely aligned with the paracone).

Upper molars: The upper molars from CB assigned to *P. palaeochoerus* fall within or very close to the respective convex hulls of this species based on the comparative sample (Fig. 14h–j), while their proportions (M1 BLI = 95–104%, n = 5; M2 BLI = 83–100%, n = 6; M3 BLI = 63–85%, n = 10) agree with those previously recorded for the species (Mottl 1966; Hellmund 1995; Van der Made et al. 1999; Fortelius et al. 2005; Pickford 2013a, 2015; Iannucci and Begun 2022; McKenzie et al. 2023a): M1 BLI = 79–104%, n = 54; M2 BLI = 79–102%, n = 72; M3 BLI = 58–87%, n = 71. Their occlusal shape (Fig. 6a–f, r–x, b'–k') is in accordance with that previously documented for the species (Stromer 1928: pl. II, fig. 20; Mottl 1955: fig. 1, 1966: pl. IV; Hünermann 1968: pl. 1, figs. 2–3; Van der Made et al. 1999: pl. 2, figs. 1–2; Fortelius et al. 2005: fig. 5; Iannucci and Begun 2022: fig. 2A; McKenzie et al. 2023a: fig. 4n–t, v–w, y–a', c'–h'). This includes the variation in the M3 occlusal pattern of the M3s of *P. palaeochoerus* from CB (Fig. 6b'–k'), which display a more or less well-developed distal lobe with a distinct pentacone that is distally to lingually directed, as in previously described M3s of this species (Stromer 1928: pl. II, fig. 2; Mottl 1955: fig. 1, 1966: pl. IV; Hünermann 1968: pl. 1, fig. 2; Van der Made et al. 1999: pl. 2, fig. 2; Fortelius et al. 2005; McKenzie et al. 2023a: fig. 4f'–h').

The upper molars from CB attributed to *Pa. valentini* (Fig. 6g–o, y–a', l'–u') also fall within or very close to the convex hulls of metrical variation for this species based on the comparative sample (except for a single M1 that appears particularly small), but nevertheless overlap extensively with both *P. palaeochoerus* and, to a lesser extent (especially regarding the M2), *Versoporcus* (Fig. 14h–j). In terms of occlusal proportions, the upper molars of *Pa. valentini* from CB (M1 BLI = 90–97%, n = 6; M2 BLI = 91–101%, n = 2; M3 BLI = 71–79%, n = 8) entirely overlap with the ranges of variation previously documented for the species (Pickford 2013a, 2014, 2016a; McKenzie et al. 2023a): M1 BLI = 89–106%, n = 10; M2 BLI = 88–105%, n = 11; M3 BLI = 62–83%, n = 16. It is noteworthy that the M3s from Hammerschmiede and Gau-Weinheim attributed by Pickford (2013a, 2016a) to *C. doati* are here included in the comparative sample of *P. valentini* for the reasons explained below, even though the lectotype of the former from Bonnefond (Pickford 2016a: fig. 19A), which displays slightly broader proportions (BLI = 86%; Van der Made 2020), clearly does not belong to *Pa. valentini* based on occlusal shape. The M1s and M2s of *Pa. valentini* from CB (Fig. 6g–o, y–a') differ from those of *P. palaeochoerus* in the more symmetrical occlusal profile, the more transversely aligned main cusps, the lesser developed buccal ectoconule, and the better-developed buccal cingulum, generally resembling those previously attributed to the

former species from elsewhere (Pickford 2014: figs. 9, 14, 15B, 2016a: figs. 7A, 22C–E, 26C; McKenzie et al. 2023: fig. 4u, b') as well as the M2 from Gaiselberg previously assigned to *C. doati* (see Pickford 2016a: fig. 4E). The M3s of *Pa. valentini* from CB (Fig. 6l'–u') are more distinctive, differing from those of *P. palaeochoerus* in the broader central lobe relative to the mesial one, as well as in the more abruptly distally tapering third lobe, with the pentacone being more centrally located and generally buccally tilted. In these regards, the M3s of *Pa. valentini* from CB resemble those of *Pa. valentini* from elsewhere (Pickford 2014: figs. 9, 14, 15B, 19D, 2016a: figs. 7A, C, 13C, 22F; McKenzie et al. 2023a: fig. 4j') and parallel the range of variation displayed by the latter. Thus, some specimens from CB display a well-developed pentacone with the distal lobe directed distally or only slightly buccally (Fig. 6l'–m', o'), resembling one of the specimens from Hollabrunn (Pickford 2016a: fig. 7C), that from Sant Quirze (Pickford 2014: fig. 14H), and especially two broader and larger specimens from Gau-Weinheim previously assigned to *C. doati* by Pickford (2013a: fig. 7A–B) and to *Pa. valentini* by McKenzie et al. (2023a). The latter authors argued that these specimens had probably been misclassified by Pickford (2013a), but it is here considered that *C. doati* is not a taxonomically valid species, with most of the material attributed to it by Pickford (2013a, 2016a) belonging to *Pa. valentini*, except for the M3 lectotype from Bonnefond (see below for further comparisons). Other M3s from CB attributed to *Pa. valentini*, in contrast, display a similarly well-developed pentacone with the distal lobe clearly oriented toward the buccal side (Fig. 6p'–r', u'), as in the holotype from Saint-Gaudens (Pickford 2014: fig. 9A) and two M3s from Hollabrunn (Pickford 2016a: fig. 7A–B), as well as another M3 from Gau-Weinheim previously assigned to *C. doati* by Pickford (2013a: fig. 6D). Finally, other M3s of *Pa. valentini* from CB display a much smaller pentacone and a poorly developed distal lobe (Fig. 6n'), similarly to (but even lesser developed than) the M3 of the same species from CCN20 (McKenzie et al. 2023a: fig. 4j').

In our opinion, the variation in the development of the distal lobe of the M3 described above for *Pa. valentini*, like variation in M3 size and proportions (Fig. 14j), is compatible with a single species and does not substantiate the distinction of *C. doati* based on the purportedly broader proportions of the former (contra Pickford 2013a, 2016a). Only two M3s from Kleineisenbach and Wartenberg bei Erding, previously attributed by Pickford (2016a: figs. 13C, 22F) to *Pa. valentini*, do not fit well and appear attributable to different taxon. It is noteworthy that these two specimens are the smallest in the *Pa. valentini* M3 sample, and the only ones overlapping with *Versoporcus* except for two of the new M3s from CB assigned to the former. Pickford (2016a) already recognized that the M3 from Kleineisenbach more closely resembled those of *Versoporcus* in proportions, but nevertheless attributed it to *Pa. valentini*, as the species is well documented at the site based on other tooth positions. While such an attribution is not impossible, based on the CB specimens assigned to *Versoporcus* (see below) we consider that an attribution to the latter genus is as (if not more) likely. On the same basis, the presence of *Versoporcus* cannot be either discounted for Wartenberg bei Erding, although the remaining M3s conclusively attest to the presence of *Pa. valentini* at the site. On the other hand, it is noteworthy that the M3 from Mira (Pickford 2014: fig. 18E), attributed by the latter author to *Pa. valentini*, also displays a well-developed but less distinct distal lobe that is oriented lingually instead of buccally, thereby contradicting Pickford's (2014, 2016a) attribution and supporting its alternative assignment to *C. simorrensis* (Van der Made 2020; McKenzie et al. 2023a).

The upper molars from CB attributed to *Versoporcus*, finally, are represented by two M1s (Fig. 6p–q) and six M3s (Fig. 6v'–a"), which largely overlap in size with previously known specimens of this genus but also overlap

to some extent with *Pa. valentini* and, in the case of the M3, extend the range of variation previously known for the former (Fig. 14f, h). The occlusal proportions for these two molar loci at CB (M1 BLI = 83–89%, n = 2; M3 BLI = 67–78%, n = 6) further overlap to a large extent with the comparative sample of *Versoporcus* (M1 BLI = 84–103%, n = 17; M3 BLI = 72–87%, n = 13; Pickford 2014, 2016a; McKenzie et al. 2023b). The two M1s from CB differ from those of both *P. palaeochoerus* and *Pa. valentini* from the same site in their smaller size and narrower proportions. When the comparative samples available for these species are considered, differences in proportions only hold for *Pa. valentini*, while the M1s of *Versoporcus* further differ from those of *P. palaeochoerus* in their more symmetrical occlusal profile. They are similar in shape to those previously figured for *Versoporcus* (Chen 1984: pl. 1, fig. 10; Pickford 2014: fig. 14A–B, 2016a: figs. 15, 24C–D) but, like the M1 and M2 of *Pa. valentini*, appear less distinctive than the M3. The M3s from CB attributed to *Versoporcus* differ from those of both *P. palaeochoerus* and *Pa. valentini* in the relatively narrower and less distally tapering occlusal profile, with a much lesser developed pentacone that does not protrude distally from the crown and which bears a distinct pentapreconule, as well as in the straighter lingual profile. As for *P. palaeochoerus* and *Pa. valentini*, the M3 sample of *Versoporcus* from CB displays considerable size and shape variation, which nevertheless is not at odds with that evinced by previously figured specimens of this genus (Chen 1984: pl. 1, fig. 10; Pickford 2014: figs. 14B, 19F, 2016a: figs. 15, 24G).

As for many other tooth positions, the comparative sample of M3s attributed to *V. steinheimensis* s.s. shows smaller dimensions than that of *V.* '*grivensis*' (Fig. 14j). Interestingly, however, the sample of *Versoporcus* M3 from CB encompasses (and surpasses) the whole metrical variation of *V. steinheimensis* s.s. and *V. 'grivensis*' combined (Fig. 14j), thus failing to support the distinction between the two species. Regarding occlusal contour and pattern, some M3s of *Versoporcus* from CB (Fig. 6v'–w') display a centrally located pentacone and broader proportions, resembling *V. steinheimensis* s.s. from Steinheim (Chen 1984: pl. 1, fig. 10; Pickford 2014: fig. 14B, 2016a: fig. 15). Another M3 from CB (Fig. 6x') is similar to the two previously mentioned in occlusal contour but displays a more lingually directed pentacone, similar to the figured M3 of *V.* '*grivensis*' from Anwil (Pickford 2016a: fig. 24G). Finally, the remaining M3s from CB assigned to *Versoporcus* (Fig. 6y'–a") display a more lingually located pentacone and a more elongate (relatively narrow) contour, more similar to the *V.* '*grivensis*' holotype and another M3 from La Grive (Pickford 2014: figs. 14B, 19F). Therefore, the sample of *Versoporcus* M3s from CB, even if somewhat restricted, encompasses the range of M3 shape variation accommodated by Pickford (2014, 2016a) into two distinct species, further supporting the view that such differences merely represent intraspecific variation. It is also noteworthy that one of the M3s from CB attributed to *Versoporcus* (Fig. 6v') is not so different from the lectotype of *C. doati* from Bonnefond (Stehlin 1900: pl. I, fig. 7; Pickford 2014: fig. 19A; Pickford and Laurent 2014: fig. 6). Peculiar as the latter might appear at first sight compared with some other *Versoporcus* M3s, the CB specimen is larger and agrees to a large extent in the position and development of the main cusps and cuspules—the Bonnefond specimen merely differing by displaying a more lingually protruding end of the mesial cingulum and hypoectoconule, a continuous distal cingulum around the pentacone, and a slightly less developed mesiobuccal cingulum. Similarities are certainly greater than those between the M3 lectotype of *C. doati* and specimens previously attributed to the latter species and here reassigned to *Pa. valentini* (see above). These considerations lead us to consider that the nominal species *C. doati* might potentially be a junior synonym of a *Versoporcus* species, instead of *C. simorrensis* as previously argued (Van der Made 2020; McKenzie et al. 2023a).

Lower permanent teeth

Lower incisors: The four i1s from CB attributed to *P. palaeochoerus* (Fig. 8a–d) agree in morphology with those previously figured from other localities (Hünermann 1968: pl. 1, fig. 13; Van der Made et al. 1999: pl. 2, fig. 7; Fortelius et al. 2005; Iannuci and Begun 2022: fig. 2D; McKenzie et al. 2023a: fig. 7a–d). In terms of size and proportions (MD = 7.4–7.9 mm, BL = 11.1–12.0 mm, BLI = 150–153%, n = 4), they also fit with previously published data for this species (MD = 5.8–7.1 mm, BL = 9.6–12.0 mm, BLI = 139–187%, n = 15; Van der Made et al. 1999; Pickford 2013a; Iannucci and Begun 2022), merely being slightly longer, thus resembling in this regard the incomplete and larger specimens from CCN20 (MD = 7.5–7.9 mm, n = 5; McKenzie et al. 2023a). The four i2s of *P. palaeochoerus* from CB (Fig. 8f–i) also agree well with those previously figured (Hünermann 1968: pl. 1, fig. 14; Van der Made et al. 1999: pl. 2, fig. 8; Fortelius et al. 2005; Iannucci and Begun 2022: fig. 2D; McKenzie et al. 2023a: fig. 7g–l), at least as far as crown morphology can be ascertained in the quite worn specimens from CB. Their dimensions and proportions (MD = 8.7–9.8 mm, BL = 12.9–13.7 mm, BLI = 132–158%, n = 3) also fit well with those previously reported for *P. palaeochoerus* i2s (MD = 6.9–9.7 mm, BL = 9.5–13.8 mm, BLI = 120–149%, n = 23; Van der Made et al. 1999; Pickford 2013a; Iannucci and Begun 2022; McKenzie et al. 2023a). Finally, no i3 of *P. palaeochoerus* has been identified in CB. The mesiodistally elongate and asymmetrical crown profile of this tooth position (Van der Made et al. 1999: pl. 2, fig. 6; McKenzie et al. 2023a: fig. 7p–t) enables to readily distinguish it from tetraconodontine i3s, which like other lower incisors are mesiodistally shorter (see discussion below for further details).

No i1 of *Pa. valentini* is represented at CB, at least following McKenzie et al.'s (2023a) proposal that the lower incisor from Sant Quirze figured by Pickford (2014: fig. 13B) is not an i2, as argued by the latter author, but an i1. In contrast, four i2s (Fig. 8j–m) and six i3s (Fig. 8o–t) of this species have been found. The i2s (MD = 7.8–8.4 mm, BL = 12.7–13.8 mm, BLI = 163–170%, n = 3) resemble in size and proportions the aforementioned probable i1 from Sant Quirze (MD = 8.5 mm, BL = 12.0 mm, BLI = 172%) and appear labiolingually broader than the CCN20 i2 (MD = 8.3 mm, BL = 10.7 mm, BLI = 129%; McKenzie et al. 2023a: fig. 7m) and another purported i2 partial crown from Wartenberg bei Erding (MD = 8.5 mm, BL = 9.6 mm, BLI = 113%) attributed to the same species by Pickford (2016a: fig. 21A)—although the basal portion of the crown of the latter specimen is damaged and would have originally been probably broader. Despite differences in basal proportions, the i2s of *Pa. valentini* from CB resemble the three aforementioned specimens, especially that from CCN20, as far as it can be ascertained based on the more advanced degree of the latter. In contrast, the i2s from CB differ from the Sant Quirze specimen by displaying a less verticalized crown, root, and enocristids, as well as a more curved postcristid, and an endofossid that is not widest at the base. These differences further support McKenzie et al.'s (2023a) previous assessment that the Sant Quirze specimen is best interpreted as an i1 despite its markedly tilted postcristid. The i2s of *Pa. valentini* from CB (and CCN20) differ from those of *P. palaeochoerus* in displaying a more asymmetrical crown (due to the very curved postcristid) and more mesially tilted root that shapes a continuous curvature with the crown throughout the cervix. In contrast, *P. palaeochoerus* displays a mesially tilted i2 crown with an angulated poststylid and a straighter root (e.g., Van der Made et al. 1999: pl. 2, fig. 8; Iannucci and Begun 2022: fig. 2D; McKenzie et al. 2023a: fig. 7i–j). In turn, the i3s of *Pa. valentini* from CB (MD = 6.0–7.4 mm, BL = 10.7–13.2 mm, BLI = 178–216%, n = 6 for MD and BL and n = 4 for BLI) do not fit with the measurements published for a single i3 of this species from Sant Quirze (IPS96087 [VP1004]), which

according to Pickford (2014) would be labiolingually compressed. However, our inspection of the actual specimen indicates that the dental axes are reversed, and that the specimen is mesiodistally compressed, like those from CB. We also found that IPS31060 [VP1003], reported but not figured by Pickford (2014) as a right I3 of *Pa. valentini* from Sant Quirze, is indeed a left i3, and discovered yet another left i3 of *Pa. valentini* (IPS95966 [Villalta's collection 5456]: MD = 7.0, BL = 10.8) among the collections from this site. When the three i3s are considered, the CB specimen resembles but somewhat exceeds the i3 size and proportions of *Pa. valentini* from Sant Quirze (MD = 6.1–7.0 mm, BL = 10.0–11.6 mm, BLI = 154–190%, n = 3; Pickford 2014; authors' own data). The i3s of *Pa. valentini* from CB further resemble the aforementioned specimens from Sant Quirze and differ instead from those of *P. palaeochoerus* from elsewhere (Van der Made et al. 1999: pl. 2, fig. 6; McKenzie et al. 2023: fig. 7p–s) in being mesiodistally compressed (instead of elongate) and displaying a less asymmetrical crown with a more centrally located (instead of listolingually situated) endocristid, a distinct prefossid, and a more extensive endofossid.

Finally, a single i1 (Fig. 8e), i2 (Fig. 8n), and i3 (Fig. 8u) of *Versoporcus* are identified among the CB sample. The i1 (MD = 6.3 mm, BL = 9.7 mm, BLI = 154%) fits well in size and proportions with specimens of both *V. steinheimensis* s.s. (MD = 5.6–7.0 mm, BL = 9.4–10.6 mm, BLI = 144–173%, n = 9) and *V.* '*grivensis*' (MD = 5.9–7.6 mm, BL = 9.3–11.9 mm, BLI = 147–190%, n = 9; Pickford 2014, 2016a), while in terms of shape it closely resembles the similarly worn specimen from Gratkorn figured by Van der Made et al. (2014: fig. 4b) and the less worn specimen from La Grive figure by Pickford (2014: fig. 32), albeit the CB specimen appears somewhat slenderer. The i1 of *Versoporcus* from CB differs from those of *P. palaeochoerus* in the presence of some waisting at the cervix, the greater extension of the ectosynclinid as compared with the endosynclinid, and the morphology of the root, which lacks an apicobasal distal sulcus and does not conspicuously taper or curve in labiolingual direction. In turn, the i1 of *Versoporcus* can be clearly distinguished from that of *Pa. valentini* from Sant Quirze (see discussion above) in the mesiodistally tapering crown from base to apex due to the markedly tilted postcristid. In turn, the i2 of *Versoporcus* from CB (MD = 7.9 mm, BL = 11.1 mm, BLI = 141%) fits in size with the metrical variation previously reported for both *V. steinheimensis* s.s. (MD = 5.0–7.9 mm, BL = 7.4–12.5 mm, BLI = 148–185%, n = 6) and *V.* '*grivensis*' (MD = 7.5–8.3 mm, BL = 10.8–13.0 mm, BLI = 140–163%, n = 7; Pickford 2014, 2016a). It is consistent with the morphology displayed by figured i2s of the same genus (Pickford 2014: fig. 32; Van der Made et al. 2014: fig. 4b) when the more advanced wear of the former is considered, merely differing (like the CB i1 of the same taxon) by being slightly less robust. However, an alternative identification as an i1 is precluded by the mesial tilt of the crown, and in any case the i2 of *Versoporcus* from CB appears more robust than the i1 of the same taxon from the same site. Compared with *Pa. valentini*, the crown appears less distally curved and the root less mesially tilted and less apically tapering in mesial and distal views than those of *P. palaeochoerus* i2s. Finally, the i3 of *Versoporcus* from CB (MD = 6.4 mm, BL = 10.1 mm, BLI = 158%) does not fit with measurements of *V.* '*grivensis*' published by Pickford (2014, 2016a), which would indicate that the tooth is labiolingually compressed. However, we suspect that Pickford (2014, 2016a) just reversed the dental axes (as for the i3 of *Pa. valentini*, see above), as further confirmed by the i3 from Gratkorn figured by Van der Made et al. (2014: fig. 4c), which is clearly mesiolingually compressed. When this caveat is considered, the CB specimen fits well with i3 size and proportions of *V.* '*grivensis*' (MD = 5.5–7.5 mm, BL = 9.4–10.6 mm, BLI = 125–193%, n = 4). The i3 of *Versoporcus* from CB differs from those of *P. palaeochoerus* in the same regards as those of *Pa. valentini* (see above), and generally resemble the latter in

occlusal pattern, despite some differences that support an attribution to a different taxon (the more marked endocristid and more extensive and deeper endofossid, the basally bulging crown waisted at the cervix, and the stouter and less apically tapering root). The i3 from CB assigned to *Versoporcus* closely resembles that from Gratkorn figured by Van der Made et al. (2014: fig. 4c), except that the latter displays a more extensive prefossid with a more distinct secondary cristid parallel to the endocristid.

Lower permanent canines: The c1m apical fragment from CB attributed to *P. palaeochoerus* (Fig. 9a) agrees well in shape with previously described c1ms of this species (Hünermann 1968: figs. 48–49, 51; Van der Made et al. 1999: pl. 2, fig. 5; Fortelius et al. 2005; McKenzie et al. 2023a: fig. 8f–h), in which the labial and lingual sides are similarly broad and resemble the breadth of the distal face, and they all display a mildly convex contour. The CB specimen (Li = 12.7 mm, La = 12.8 mm, Di = 13.1 mm) is intermediate in size between that from Grytsyv (Li = 11.0 mm, La = 10.5 mm, Di = 10.1 mm; Van der Made et al. 1999) and those from CCN20 (Li = 14.3–16.1 mm, La = 13.5–14.0 mm, Di = 13.1–13.8 mm, n = 3; McKenzie et al. 2023a), thereby further supporting an attribution to *P. palaeochoerus*. The other c1ms from CB (Fig. 9b–c) are consistent in morphology with those of *Versoporcus* (Pickford 2016a: fig. 19; Van der Made et al. 2014: fig. 8a) and at odds with an alternative attribution to *Conohyus*, which is similarly characterized by a scrofic morphology but displays a cementum band throughout the distal face (Pickford 2013b: fig. 6E, 2014, 2016a; Pickford and Laurent 2014). The cross-sectional dimensions of the complete specimen of *Versoporcus* from CB (Li = 16.7 mm, La = 9.4 mm, Di = 14.2 mm) fit well within the ranges of variation of *V. steinheimensis* s.s. from La Grive (Li = 12.5–17.0 mm, La = 7.0–10.0 mm, Di = 8.5–14.9 mm, n = 8; Pickford, 2014), being slightly smaller than those attributed to *V.* '*grivensis*' from the same site (Li = 19.3–20.0 mm, La = 9.5–12.4 mm, Di = 15.2–17.0 mm, n = 2; Pickford 2014). The fragmentary specimen from CB displays similar dimensions and scrofic proportions, thus being similarly attributable to *Versoporcus*.

The c1fs from CB attributed to *P. palaeochoerus* (Fig. 9d–e) resemble, as far as it can be ascertained given their advanced degree of wear, those previously described in the literature (Fortelius et al. 2005; Iannucci and Begun 2022: fig. 2D; McKenzie et al. 2023a: fig. 8a–c). Their crown proportions (BLI = 61–62%, n = 2) fall in the lower range of variation of the species based on published data (BLI = 62–94%, n = 9; Hellmund 1995; Pickford, 2013a; Iannucci and Begun 2022; McKenzie et al. 2023a), but this is probably because basal crown dimensions are not adequately preserved because of wear. In contrast, the c1fs from CB assigned to *Pa. valentini* (Fig. 9f–g) differ from those of *P. palaeochoerus* from CB and elsewhere (see references above) in their larger dimensions and stouter root without a distolingual longitudinal sulcus. In these regards, the CB specimens of *Pa. valentini* most closely resemble those previously assigned to this species by McKenzie et al. (2023a: fig. 8d–e).

Lower permanent premolars: The extensive sample of p1s from CB includes three specimens attributed to *P. palaeochoerus* (Fig. 10a–c), which fall within or very close to the size variation of this species from elsewhere (Fig. 15d). They also fit well in proportions (BLI = 44–48%, n = 3) with those previously described in the literature (BLI = 42–52%, n = 8; Fortelius et al. 2005; Iannucci and Begun 2022; McKenzie et al. 2023a). Their occlusal morphology is also similar to previously described specimens of this species (Fortelius et al. 2005; Iannucci and Begun 2022: fig. 2D; McKenzie et al. 2023a: fig. 9a–d)—excluding that from Grytsiv figured by Van der Made et al. (1999: pl. 1, fig. 3), which is likely tetraconodontine (McKenzie et al. 2023a). Taken together with the samples from Rudabánya (Fortelius et al. 2005) and CCN20 (McKenzie et al. 2023a), the CB specimens further illustrate the *P. palaeochoerus* variation in p1 occlusal contour and shape, including the more

or less pointed mesial end, as well as the development of the metaconid, the bifurcation of the protopostcristid, and the development of two (distal and distolingual) fossids displaying multiple minor variations even within a single site. Finally, the CB specimens confirm that the p1 of *P. palaeochoerus* variably presents a single fused (McKenzie et al. 2023a: fig. 9a; see our Fig. 10c) or two distinct but closely packed roots (Fortelius et al. 2005; Iannucci and Begun 2022: fig. 2D; McKenzie et al. 2023a: fig. 9d; see our Fig. 10a–b).

The tetraconodontine p1s from CB differ from those of *P. palaeochoerus* in multiple features, including the narrower crown with a somewhat more trenchant appearance, the less distinct metaconid, the lack of secondary cristids or cuspulid-like developments on the distal half of the crown, the more marked anticlinids, the greater rootward extension of the enamel on the distobuccal side of the crown, and the presence of two distinct and differently oriented roots. The p1s of *Pa. valentini* from CB (Fig. 10d–h) are consistent in proportions (BLI = 30–35%, n = 4) and occlusal shape with the previously described specimen from Sant Quirze (BLI = 31%; Pickford 2014: fig. 14D) as well as the partial p1 germ from CCN20 (McKenzie et al. 2023a: fig. 9e), and only slightly smaller than the former (Fig. 15d). In contrast, the p1s from CB attributed to *Versoporcus* (Fig. 10i–j) are smaller than those of *Pa. valentini* and more similar in length to those previously recorded of *Versoporcus*, albeit more buccolingually compressed on average (BLI = 31–37%, n = 2) than both *V.* '*grivensis*' (BLI = 35–42%, n = 2) and *V. steinheimensis* s.s. (BLI = 36–41%, n = 7; Pickford 2014, 2016a). They further resemble previously figured p1s of *Versoporcus* (Chen, 1984: pl. 2, fig. 2; Pickford 2016a: figs. 16–17) and differ from those assigned to *Pa. valentini* in minor occlusal differences, including a more mesially located protoconid, more steeply inclined protoprecristid and protopostcristid in buccal and lingual views (resulting in a more trenchant appearance), a comparatively more conspicuous prestylid, and more markedly concave crown walls distally from the protoconid. It is remarkable that the two p1s of *Versoporcus* from CB, like the two of *V.* '*grivensis*' included in the comparative sample, encompass almost the whole range of variation of *V. steinheimensis* s.s. (Fig. 15d).

The two p2s of *P. palaeochoerus* from CB (Fig. 10k–l), except for differences in preservation (one displaying a greater degree of corrosion), are remarkably similar to one another and display a similar degree of wear, raising the possibility that they are antimeres of a single individual. This seems even more likely given the degree of variation displayed by this tooth position in other samples, such as that from CCN20 (McKenzie et al. 2023a: fig. 9f–i), regarding the more or less marked occlusal relief, crown proportions and occlusal contour, the degree of lingual tilting of the prestylid, the development of the cingulids and the distal cuspids (metaconid and hypoconid), and the inclination of the mesial root. The CB ps2 of *P. palaeochoerus* differ from those of CCN20 in some minor details (the lower occlusal relief, more marked cingula, and the more verticalized mesial root), but otherwise agree well with the morphology of this tooth position when other samples of the same species are considered (Hünermann 1968: pl. 1, fig. 6; Van der Made et al. 1999: pl. 1, figs. 1, 4–5 and pl. 2, fig. 3; Fortelius et al. 2005; Iannucci and Begun 2022: fig. 2D). In terms of size, the p2s of *P. palaeochoerus* from CB overlap with the upper range of variation of *P. palaeochoerus* from elsewhere (Fig. 15e) and in terms of proportions (BLI = 43–45%, n = 2) they agree well with the variability displayed at CCN20 (BLI = 41–51%, n = 4; McKenzie et al. 2023a) and elsewhere (BLI = 42–50%, n = 16; Van der Made et al. 1999; Fortelius et al. 2005; Pickford 2013a; Iannucci and Begun 2022).

The tetraconodontine p2s from CB, here assigned to *Versoporcus*, differ from those of *P. palaeochoerus* by being longer (Fig. 15e) and displaying a more trenchant appearance—even if the degree of occlusal relief appears very variable among the available specimens—with lesser developed cingulids, more marked labial and

lingual anticlinids, and the cervix extending farther rootward on the distal half of the crown. One of the p2s attributed to *Versoporcus* (IPS1713; Fig. 10o) differs from the remaining ones (Fig. 10m–n, p) in the more elongate occlusal contour (BLI = 35%, being longer than previously recorded for this genus), the lower occlusal relief, and the lack of conspicuous buccal and lingual clefts at the distal half of the crown. However, this p2 belongs to a mandible (Fig. 7g) that further preserves the molars and the posterior premolars, whose morphology supports an attribution to *Versoporcus* rather than *Pa. valentini*. Given that the p2 of the latter species remains thus far undescribed, it cannot be entirely ruled out that some of the remaining p2s from CB—particularly IPS92720 (Fig. 10m), which is much higher-crowned and not very elongate (BLI = 47%), representing the broadest p2 of *Versoporcus* recorded so far—might belong to this species. However, we consider this alternate attribution unlikely because, except for the slightly broader dimensions and proportions, it fits relatively well with the morphology previously reported for both *V.* '*grivensis*' (Pickford 2014: fig. 30B; Van der Made et al. 2014: fig. 3b) and *V. steinheimensis* s.s. (Pickford 2016a: figs. 16–17), which appears somewhat intermediate between the two aforementioned specimens from CB in terms of occlusal relief and crown elongation (BLI = 35–42% and 34–39%, respectively, n = 5 in both cases; Pickford 2014, 2016a). The two specimens from CB more closely resemble in size the specimens previously assigned to *V.* '*grivensis*', while those of *V. steinheimensis* s.s. display a considerably smaller size with no overlap (Fig. 15e). This is, however, one of the few instances in which the convex hulls for the two putatively distinct species of *Versoporcus* do not overlap, and in any case their joint range of variation does not exceed that recorded for the same tooth locus in the more abundantly represented sample of *P. palaeochoerus*—thus being compatible with a single species.

The p3s of *P. palaeochoerus* from CB (BLI = 43–60%, n = 3; Fig. 10q–s) fit well with the variation in size (Fig. 15f) and proportions (BLI = 44–61%, n = 31; Hellmund 1995; Van der Made et al. 1999; Fortelius et al. 2005; Pickford 2013a; Iannucci and Begun 2022; McKenzie et al. 2023a) previously documented for this taxon. Their occlusal pattern also agrees well with that of *P. palaeochoerus* from other sites across Europe (Hünermann 1968: pl. 1, figs. 1, 7; Van der Made et al. 1999: pl. 1, figs. 1, 4 and pl. 2, fig. 3; Fortelius et al. 2005; Iannucci and Begun 2022: fig. 2D; McKenzie et al. 2023a: fig. 9j–m), including the presence of hypoconid as well as of metaconid at early wear stages, and particularly when variation in occlusal contour shape, proportions, and relief (particularly the height of the hypoconid), as well as in the distal development of cingulids and the degree of distobuccal bulging of the crown—as exemplified by the CCN20 sample (McKenzie et al. 2023a)—is considered.

The single p3 of *Versoporcus* from CB (Fig. 10t) differs from those of *P. palaeochoerus* in being more elongate (buccolingually narrower) and displaying a slightly more pronounced occlusal relief and trenchant appearance, with a more steeply inclined protoprecristid, a more protruding mesial prestylid, a more indistinct hypoconid, and lesser developed cingulids. This p3, which belongs to the IPS1713 mandible (Fig. 7g), is the longest p3 of *Versoporcus* recorded so far (Fig. 15f), overlapping in length with *Pa. valentini* but being more comparable in breadth to *Versoporcus*. As a result, the elongate tetraconodontine p3 from CB (BLI = 43%) is slenderer than those assigned to *Pa. valentini* (BLI = 53–59%, n = 5)—including the p3s attributed to this species by Pickford (2016a), as well as p3 from Fonte do Pinheiro previously assigned to *C. ebroensis* by Van der Made (1989) and to *C. doati* by Pickford (2016a). The proportions of the IPS1713 p3 are also narrower than in both *V.* '*grivensis*' (BLI = 52–55%, n = 4; Pickford 2014; McKenzie et al. 2023b) and *V. steinheimensis* s.s. (BLI = 51–56%, n = 9; Pickford 2014, 2016a). In this sense, the p3 of IPS1713 resembles the p2 of the same

individual, which appears particularly elongate. In any case, the p3 from CB more clearly differs from those of *Pa. valentini* reported by Pickford (2016a: figs. 9A–B, 13A) in the better-developed prestylid and more distinct metaconid, more closely resembling the specimens of *Versoporcus* figured in the literature, including both *V.* '*grivensis*' (Pickford 2014: figs. 30B–31, 33; Van der Made et al. 2014: fig. 3c: McKenzie et al. 2023b: fig. 1f–g) and *V. steinheimensis* s.s. (Chen 1984: pl. 2, fig. 1 and pl. 4, fig. 2; Pickford 2016: figs. 16–18). In terms of size, as mentioned above, the CB p3 falls outside the variation in length of the two putatively distinct *Versoporcus* species, whose convex hulls are close to one another and partly overlapping (with *V.* '*grivensis*' being minimally larger on average). Nevertheless, it is noteworthy that even when the CB specimen is included, the overall variation in dental dimensions of all the *Versoporcus* p3 sample does not exceed that displayed by *P. palaeochoerus* or *Pa. valentini*, thus being compatible with a single species.

The p4s of *P. palaeochoerus* from CB display similar size (Fig. 15g) and proportions (BLI = 67–80, n = 4) to those previously reported in the literature (BLI = 62–85, n = 44; Hellmund 1995; Van der Made et al. 1999; Fortelius et al. 2005; Pickford 2013a; Iannucci and Begun 2022; McKenzie et al. 2023a). They also fit well in terms of occlusal shape (Fig. 10u–y)—including the characteristic possession of a very well-developed metaconid—with published specimens of *P. palaeochoerus* (Hünermann 1968, pl. 1, fig. 1; Van der Made et al. 1999: pl. 1, figs. 1, 4 and pl. 2, fig. 3; Fortelius et al. 2005; Iannucci and Begun 2022: fig. 2D; McKenzie et al. 2023a: fig. 9n–p), despite variation in the size of the metaconid relative to the protoconid, the development of the distolingual and distobuccal cingulids, and the distal expansion of the crown.

The tetraconodontine p4s from CB largely overlap in dimensions with those of *P. palaeochoerus* (Fig. 15g), but nevertheless differ from them in terms of occlusal shape (slightly higher occlusal relief, generally better-developed and higher prestylid, and lesser developed metaconid). Otherwise, the p4s of the two tetraconodontine species recorded at CB are markedly different from one another. Those attributed to *Pa. valentini* (Fig. 10z–a') display a more symmetrical and elliptical occlusal contour, with a more inflated mesial half of the crown, and further lack a distinct metaconid and metapostcristid, displaying instead a longer protopostcristid and a more conspicuous hypoconid. The CB p4s attributed to this species closely resemble in shape those attributed to *Pa. valentini* by Pickford (2014: fig. 11B–C, 2016a: fig. 21C). They further fit in terms of proportions (BLI = 64%, n = 1) with those recorded for *Pa. valentini* (BLI = 62–79%, n = 6)—including not only the specimens attributed to it by Pickford (2014, 2016a) but also those assigned by him to *C. doati* and previously considered to belong to *C. ebroensis* (see Azanza 1986: pl. 2, fig. 1; Van der Made 1989). In contrast, the p4s from CB attributed to *Versoporcus* (Fig. 10b'–d') display a suboval occlusal contour that is somewhat contricted at the level of the protoconid, a metaconid that is distinct but closely packed to the protoconid with no protopostristid, and a metapostcristid that distally bifurcates and is surrounded by secondary enamel cuspulids without a distinct hypoconid. This morphology more closely resembles that of the p4s of both *V.* '*grivensis*' (Van der Made et al. 2014: fig. 4a; Pickford 2014: figs. 30–31, 33, 2016a: fig. 6; McKenzie et al. 2023b: fig. 1f) and *V. steinheimensis* s.s. (Chen 1984: pl. 1, fig. 11 and pl. 4, fig. 2; Pickford 2016a: figs. 16–18), even if they generally display a better-developed hypoconid than the CB specimens and in spite of the fact that the presence of a metaconid distinct from the protoconid is difficult to ascertain in most specimens due to wear. The CB p4s attributed to *Versoporcus* also agree relatively well in proportions (BLI = 64–72%, n = 2) with this genus, including both *V.* '*grivensis*' (BLI = 66–72%, n = 6; Pickford 2014; McKenzie et al. 2023b) and *V. steinheimensis* s.s. (BLI = 66–75%, n = 13; Pickford 2014, 2016a)—although the slightly narrower proportions of the IPS1713 p4 (BLI =

64%), which is the longest p4 of *Versoporcus* recorded so far (Fig. 15g), stand out as for the p2 and the p3 of the same individual (Fig. 7g; see above). It is also remarkable that, with only two complete specimens, the p4s of *Versoporcus* from CB almost encompass the whole range of variation of the two *Versoporcus* species, whose respective convex hulls only partially overlap based on the specimens included in the comparative sample. The range of variation recorded at CB for *Versoporcus*, thus, does not favor the distinction of these species and suggests instead that they represent the opposite ends of intraspecific variation for a single species.

Lower permanent molars: The m1s (Fig. 11a–c) and m2s (Fig. 11k–m) of *P. palaeochoerus* from CB agree well in occlusal morphology with those previously described in the literature for this species (Hünermann 1968, pl. 1, fig. 1; Van der Made et al. 1999: pl. 1, figs. 1 and 4; Fortelius et al. 2005; Iannucci and Begun 2022: fig. 2D; McKenzie et al. 2023a: fig. 9r–b')—characterized by a distal lobe mesiodistally and, to some extent, also buccolingually expanded relative to the mesial one, as well as the presence of abundant enamel wrinkling in unworn to slightly worn specimens. In terms of size and proportions, both the m1s (Fig. 15h; BLI = 68–74%, n = 2, excluding the unfinished germ) and the m2s (Fig. 15i; BLI = 73–78%, n = 3) of *P. palaeochoerus* from CB fit well with the size variation of the species as recorded in the comparative sample (Hellmund 1995; Van der Made et al. 1999; Fortelius et al. 2005; Pickford, 2013a; Iannucci and Begun 2022; McKenzie et al. 2023a): m1 BLI = 60–82%, n = 58 and m2 BLI = 65–82%, n = 82.

The tetraconodontine m1s and m2s from CB differ from those of *P. palaeochoerus* in displaying a less corrugated enamel in unworn to slightly worn specimens (contrasting with the similarly marked Fürchen), as well as straighter lingual walls with a less marked constriction separating the two lobes and, particularly, a less expanded distal lobe as compared to the mesial one. Those assigned to *Pa. valentini* (Fig. 11d–e, n) display a less straight lingual contour, more inflated cuspids and better-developed cuspulids, and a somewhat more projecting distal contour. They closely resemble the m1s and m2s of *Pa. valentini* from Gaiselberg, previously assigned to *C. doati* (Pickford 2016a: figs. 3A, 4A–B), those from other sites such as Saint-Gaudens, Sant Quirze, and Hinterauerbach bei Wartenberg (Pickford 2014: figs. 12A–B and 16E–F, 2016a: fig. 11), and, to a lesser extent, those from other sites (Pickford 2014: fig. 10A, 2016a: figs. 9C and 21D), including the holotype of *C. ebroensis* (Azanza 1986: pl. II, fig. 1). The proportions of the two m1s (BLI = 73%) and the single m2 (BLI = 76%) of *Pa. valentini* from CB overlap with those of specimens from the same site assigned to *Versoporcus* (m1 BLI = 70–77%, n = 4 and m2 BLI = 71–76, n = 3). However, this is not surprising given that the lower molars of *Pa. valentini* from elsewhere (m1 BLI = 68–80%, n= 7 and m2 BLI = 68–83, n= 11; Pickford 2014, 2016a; McKenzie et al. 2023a)—including specimens previously assigned to *C. ebroensis* by Van der Made (1989) and *C. doati* by Pickford (2016a)—also largely overlap in proportions with those of *Versoporcus*, including both *V.* '*grivensis*' (m1 BLI 66–82, n = 9 and m2 BLI = 70–82, n = 10) and *V. steinheimensis* s.s. (m1 BLI 63–76, n = 20 and m2 BLI = 69–80, n = 16; Pickford 2014, 2016a; McKenzie et al. 2023b).

The m1s and m2s from CB assigned to *Versoporcus* (Fig. 11f–j, o–r) appear compatible in occlusal morphology with those previously assigned to this genus (Chen 1984: pl. 1, fig. 11, pl. 2, fig. 1, pl. 4, fig. 2; Pickford 2014: fig. 31, 2016a: figs. 6, 16–18, 20B–C, 24F; Van der Made et al. 2014: figs. 3a and 4a; McKenzie et al. 2023b: fig. 9f), but are not particularly diagnostic and easy to conflate with those of similarly sized tetraconodontines such as *Pa. valentini*. Previously reported specimens of the latter species as well as *Versoporcus* indicated only a slight overlap in m1 size (Fig. 15h) and a more extensive overlap in m2

dimensions (Fig. 15i). However, the larger dimensions of the m1 and m2 of IPS1713 (Fig. 11i, q), whose premolar and m3 morphology supports an assignment to *Versoporcus* instead of *Pa. valentini*, indicates a much greater overlap in size than previously recorded between these taxa. It is noteworthy that, in the case of the m1, the range of variation displayed by *Versoporcus* from CB even surpasses that of the two species of the genus together as recorded in the comparative sample (Fig. 15h), further supporting the view that there is a single and variable species of *Versoporcus* rather than two distinct species that partly overlap in size. The m2s of *Versoporcus* from CB only overlap with those previously included in *V.* '*grivensis*' (Fig. 15i), but considerably expand their range of variation toward larger dimensions and overall indicates a range of metrical variation for the m2 of *Versoporcus* similar to that of the m1.

The CB m3s of *P. palaeochoerus* (Fig. 11s–u), like the m1s and m2s, agree well in size—albeit toward the upper range of the species (Fig. 15j)—and proportions (BLI = 48–52%, n = 4) with those available from the literature (BLI = 47–62%, n = 90; Hellmund 1995; Van der Made et al. 1999; Fortelius et al. 2005; Pickford 2013a; Iannucci and Begun 2022; McKenzie et al. 2023a). They also fit well in terms of occlusal morphology once the usual variation of the species is taken into account (Hünermann 1968, pl. 1, fig. 1; Van der Made et al. 1999: pl. 1, figs. 1, 4 and pl. 2, fig. 9; Fortelius et al. 2005; Iannucci and Begun 2022: fig. 2D; McKenzie et al. 2023a: fig. 9c'–h'). In the m3s from CB the third lobe is very long, distinct, and buccally tilted, as in those from CCN20 (McKenzie et al. 2023: fig. 9c'–e'), whereas the lectotype (Hünermann 1968: pl. 1, fig. 1) and some other figured specimens from elsewhere (Van der Made et al. 1999: pl. 1, figs. 1, 4 and pl. 2, fig. 9; Iannucci and Begun 2022: fig. 2D) display a somewhat shorter, less distinct, and distally oriented third lobe.

The tetraconodontine m3s from CB differ from those of *P. palaeochoerus* in the generally less elongate proportions, as well as in the comparatively less developed and more indistinct dital lobe. The m3 from CB attributed to *Pa. valentini* (Fig. 11v) displays an overall degree of elongation (BLI = 52%) comparable to that *P. palaeochoerus* (see above) and on the lower range both previously reported specimens of *Pa. valentini* (BLI = 52–59%, n = 6; Pickford 2013a, 2014, 2016a)—including the specimen attributed to *C. ebroensis* by Van der Made (1989) and to *C. doati* by Pickford (2016a)—as well as *Versoporcus* (see below). The occlusal contour of this specimen differs from that of the *P. palaeochoerus* m3s from CB in the distally instead of distobuccally oriented third lobe. However, such morphology is not incompatible with the variation displayed by the m3s of *P. palaeochoerus* as a whole, as shown for example by the specimens from Grytsyv (BLI = 53–55, n = 3; Van der Made et al. 1999: pl. 1, figs. 1, 4 and pl. 2, fig. 9). Nevertheless, the CB m3 assigned to *Pa. valentini* displays several additional differences relative to *P. palaeochoerus* that support an assignment to the former species, including the more inflated cuspids and comparatively larger cuspulids, the protoconid more transversely aligned with the metaconid, the presence of a well-developed metaendoconulid mesially from the hypopreconulid (although this is variably present also in *P. palaeochoerus*), and the much less developed pentaconid (which is even smaller than the pentapreconulid). In these regards, IPS33254 further differs from the m3s assigned to *Versoporcus* and more closely resembles some of the specimens assigned to *Pa. valentini* from Charmoille (Pickford 2016a: fig. 26B) or Gaiselberg (Pickford 2016: fig. 3A), the latter originally attributed to *P. palaeochoerus* (Zapfe 1949; Van der Made et al. 2014) and subsequently to *C. doati* by Pickford (2016a).

The m3s from CB attributed to *Versoporcus* (Fig. 11w–z), in turn, display similar dimensions to those included in the comparative sample except for being slightly broader in some cases (Fig. 15j). Their proportions (BLI = 52–63%, n = 3) further resemble but slightly surpass the range of both *V.* '*grivensis*' (BLI = 55–61%, n =

9; Pickford, 2014, 2016a; McKenzie et al. 2023b) and *V. steinheinmensis* s.s. (BLI = 53–60%, n = 9; Pickford 2014, 2016a), besides that of *Pa. valentini* (see above). The m3s of *Versoporcus* from CB differ from the specimen assigned to *Pa. valentini* from the same site in the more distally tapering occlusal profile at the level of the central lobe, the less inflated cuspids and cuspulids, the longer ectometacristid (merging with the protoprecristid), and the much lesser developed metaprecristid that does not obliterate the protofossid, more closely resembling in shape specimens of both *V.* '*grivensis*' and *V. steinheimensis* s.s. previously reported in the literature (Chen 1984: pl. 1, fig. 11 and pl. 4, fig. 2; Pickford 2014: fig. 31, 2016a: figs. 6, 16–17; Van der Made et al. 2014: figs. 3 and 4a; McKenzie et al. 2023b: fig. 9f). Although the newly reported m3s of *Versoporcus* from CB do not expand much the range of metrical variation for this genus, the range of *V.* '*grivensis*' in the comparative sample already encompassed entirely that of *V. steinheimensis* s.s., thus also failing to support the distinction of these species.

Upper deciduous teeth

Upper deciduous incisors: The upper deciduous incisors from CB assigned to *P. palaeochoerus* (Fig. 12a–b, g–l) generally resemble those from CCN20 assigned to the same taxon, particularly in the case of the DI1 and the DI3 (McKenzie et al. 2023a: fig. 9a–d, h), although the former displays a double endocrista and the latter a more subtriangular crown profile at CB. Their dimensions and proportions of the DI1s from CB (ML = 9.7–9.8 mm, BL = 6.3 mm, BL = 64–65%, n = 2) also fit well with those from CCN20 (MD = 8.0–9.8, BL = 5.0–6.4, BLI = 58–70%, n = 4; McKenzie et al. 2023a). The similarities between the DI2s from CB here assigned to *P. palaeochoerus* (Fig. 12g–j) and those from CCN20 attributed to the same taxon (McKenzie et al. 2023a: fig. 9h), which appear more elongate, are more difficult to evaluate given the larger degree of wear of the latter; nevertheless, we consider that the taxonomical and anatomical identification of those from CB is more secure, given some similarities to the DI1 of the same taxon, coupled with some differences more consistent with a second incisor (see also Hünermann 1968: pl. I, fig. 12). The DI1s from CB assigned to *Pa. valentini* (ML = 7.1–7.8 mm, BL = 4.9–5.6 mm, BL = 68–85%, n = 4; Fig. 12c–f) are smaller and labiolingually wider than those of *P. palaeochoerus*, and further differ in their less asymmetric crown, the shallower lingual surface with a better-defined and single endocrista, less marked preanticline and endosyncline, and slenderer root. Given the lack of comparative material, an alternative attribution to *Versoporcus* cannot be ruled out.

Upper deciduous premolars: The DP2s of *P. palaeocherous* from CB (Fig. 12m–o) resemble in size the largest specimens in the comparative sample (Fig. 14a). In particular, they display similar proportions (BLI = 47–53 %, n = 2) and occlusal pattern to the DP2s previously described from CCN20 (BLI = 47%, n = 1; McKenzie et al. 2023a: fig. 10i–m)—except for some minor details, such as the generally better-developed protocone, the more indistinct metacone, and the lesser-developed lingual and buccal cingula (except at the distolingual extension of the crown). The proportions also fit well with the lower range of variation displayed by the Rudabánya sample (BLI = 47–56%, n = 6, if an additional specimen with exceedingly narrow proportions of 32% is excluded; Fortelius et al. 2005). In contrast, the tetraconodontine DP2s from CB differ from those of *P. palaeochoerus* by being mesiodistally longer and more buccolingually compressed (Fig. 14a), further displaying a markedly tilted distolingual portion of the crown, a less obliquely oriented parapostcrista, a much better-developed metacone, and an even more rudimentary to absent protocone. The two DP2s assigned to *Pa. valentini* (Fig. 12p–q) are very similar in dimensions (Fig. 14a) and proportions (BLI = 34–36%, n = 2) to an upper premolar of the same

species from Sant Quirze (IPS96073 [VP1006]; BLI = 37%; Pickford 2016a: fig. 14a), previously interpreted by the latter author as a P1 but here considered most likely a DP2. Compared with the DP2s assigned to *Pa. valentini*, those of *Versoporcus* (Fig. 12r–t) display stouter proportions and a more asymmetrical occlusal contour, a lesser-developed mesial prestyle, more marked occlusal relief due to the higher metacone, and seemingly deeper anticlines at the cervix (particularly at the lingual side). As far as it can be ascertained, the DP2s of *Versoporcus* from CB are consistent in morphology with the partial specimen figured by Chen (1984: pl. 4, fig. 1), which is missing the mesial end of the crown and is only slightly narrower (BL = 6 mm; Pickford 2016a) than the CB specimens (BL = 6.5–6.7 mm, n = 3).

The DP3s of *P. palaeochoerus* from CB (Fig. 12u–z) fall within or near the convex hull of metrical variation for this species (Fig. 14b) and their occlusal proportions (BLI = 70–77%, n = 5) also agree with those previously reported for the species (BLI = 66–79%, n = 9; Fortelius et al. 2005; McKenzie et al. 2023a). They closely resemble in occlusal shape the best-preserved DP3 of *P. palaeochoerus* from CCN20 (McKenzie et al. 2023a: fig. 10n), which is associated with a DP2 of the same individual that further displays the characteristic morphology of the species (see above). In turn, the tetraconodontine DP3s from CB differ from those of *P. palaeochoerus* in the more marked constriction between the mesial and the distal lobes, the more asymmetrical (distolingually protruding) distal lobe, and the more discontinuous cingulum around the crown base. Previously reported measurements, based on very small sample sizes, suggested that *Pa. valentini* would display slightly broader DP3 proportions than *Versoporcus* (BLI = 72–74%, n = 2 vs. BLI = 64–69%, n = 4; Pickford 2014, 2016a). However, the new specimens from CB expand the previously known ranges of variation and indicate that the DP3 of *Pa. valentini* (BLI = 69–77%, n = 3) and *Versoporcus* (BLI = 67–75%, n = 4) largely overlap, not only with one another, but also with the range of variation of *P. palaeochoerus* (see above). The DP3s from CB assigned to *Pa. valentini* (Fig. 12a'–g') are larger than those of *Versoporcus* and tend to display a better-defined constriction between the mesial and the distal lobe, as well as a less subtriangular occlusal contour—like the specimen from Sant Quirze IPS96070 [VP1011] attributed to *Pa. valentini* but not figured by Pickford (2014; reported with the old number IPS63283), and further resembling the best-preserved DP3 of *Pa. valentini* from CCN20 (IPS114230) reported by McKenzie et al. (2023a: fig. 10r). In contrast, the DP3s from CB assigned to *Versoporcus* (Fig. 12h'–l') are more consistent in morphology with that previously figured by Chen (1984: pl. 4, fig. 1).

The DP4s of *P. palaeochoerus* from CB (Fig. 12m'–s') fall within or very close to the range of size variation previously recorded for this species (Fig. 14c), display occlusal proportions (BLI = 79–92%, n = 7) that fit well with those previously reported (BLI = 77–97%, n = 18; Fortelius et al. 2005; Pickford, 2013a; McKenzie et al. 2023a), and are also consistent in occlusal shape with published DP4s of this species (Hünermann 1968: pl. 1, fig. 17; McKenzie et al. 2023a: fig. 10u–x). The tetraconodontine DP4s from CB differ from those of *P. palaeochoerus* by displaying a less mesiodistally expanded distal lobe as well as a more moderate development of enamel wrinkling in unworn to slightly worn specimens. Those of *Pa. valentini* (Fig. 12t'–v') are similar in size, apparently differing by the indistinct protopreconule, the slightly less developed cingula (particularly on the distobuccal portion of the crown), and the distal cusps more closely located to one another than the mesial. In terms of size (Fig. 14c) and proportions (BLI = 82%, n = 2), the CB specimens of *Pa. valentini* fit with those previously reported for the species (BLI = 81–99%, n = 6; Pickford 2014; McKenzie et al. 2023a). In terms of shape, as far as it can be ascertained, they further agree with previously figured specimens (Pickford 2014: fig.

16A; McKenzie et al. 2023a: fig. 10y–z'), although the DP4 of *Pa. valentini* remains much more difficult to distinguish from that of *P. palaeochoerus* (particularly at advanced wear stages) than those of *Versoporcus*. The DP4s of the latter (Fig. 12w'–y') further differ from those of *P. palaeochoerus* and *Pa. valentini* in the 'twisted' appearance of the mesial lobe, due to the mesial contour—which instead of being straight and uniformly inclined, is mesiobuccally convex and mesiolingually straighter but markedly inclined—as well as the more transversely aligned distal cusps. The proportions of the CB specimens (BLI = 83–85%, n = 3) fall within the range of variation of *V. steinheimensis* s.s. (BLI = 80–92%, n = 11; Pickford 2014, 2016a)—which nevertheless also overlap to a large extent with those of the remaining species—and are consistent with the specimen figured by Chen (1984: pl. 4, fig. 1).

Lower deciduous teeth

Lower deciduous incisors: The di1s from CB attributed to *P. palaeochoerus* (Fig. 13a–d) resemble in size and proportions (MD = 4.1–4.6 mm, BL = 5.3–5.8 mm, BLI = 123–142%, n = 4) those from CCN20 (MD = 4.2–5.2 mm, BL = 5.5–6.1 mm, BLI = 115–136%, n = 5; McKenzie et al. 2023a). The least worn and most completely preserved di1s from CB (Fig. 13a–b) also closely resemble in shape the similarly preserved ones assigned to the same species by McKenzie et al. (2023: fig. 11a–b). In contrast, the tetraconodontine di1s from CB differ from those of *P. palaeochoerus* in the broader endocristid, resulting in deeper prefossid and endofossid with no lingual cingulid, and the greater constriction of the crown from apex to cervix. The di1s from CB assigned to *Pa. valentini* (MD = 5.3 mm, BL = 6.1–6.4 mm, BLI = 115–121%, n = 2; Fig. 13e–f) are more consistent in shape with the di1s from CCN20 attributed to the same species (McKenzie et al. 2023a: fig. 11f–g), while those assigned to *Versoporcus* (Fig. 13g–h)—to our knowledge, not previously figured in the literature—are similar in size and proportions (MD = 4.9 mm, BL = 6.0 mm, BLI = 122%, n = 1) to those of *Pa. valentini* but appear more labiolingually compressed at the apical half of the crown (with a more conspicuous vertical depression), and apparently display a shallower and less markedly V-shaped preanticlinid.

An incompletely preserved di2 from CB (MD = 5.2 mm, BL = 7.2 mm, BLI = 139%; Fig. 13i) is tentatively assigned to *P. palaeochoerus* because it apparently displays a narrower endocrista than those assigned to tetraconodontines, thus more closely resembling the figured di2 assigned to the former species by Hünermann (1968: pl. I, fig. 12), which appears as a miniature of the i2 of the same taxon, although in the CB specimen the endocristid appears more developed. The di1 assigned to *Pa. valentini* (Fig. 13j) displays similar size and proportions (MD = 5.0 mm, BL = 6.9 mm, BLI = 138%), but the crown is more mesially inclined and displays a more curved distal profile than those assigned to the other taxa. Those assigned to *Versoporcus* (Fig. 13k–l) are also similar in size and proportions (MD = 5.3–5.4 mm, BL = 6.5–7.1 mm, BLI = 120–134%), but possess broader endocristid and endofossid, as well as a more moderate degree of distal curvature of the crown. Coupled with the possession of a depressed apical portion of the lingual crown, these differences parallel those displayed by the di1s assigned to the same taxon. However, given that, to our knowledge, this tooth position had not been previously reported in the literature for either of these tetraconodontine taxa, all assignments must remain tentative.

The di3s of *P. palaeochoerus* from CB (MD = 8.2–8.7 mm, BL = 4.3 mm, BLI = 49–52%, n = 2; Fig. 13m–n) are somewhat smaller than, but display similar proportions to, those from CCN20 (MD = 9.4–10.0 mm, BL = 4.5–4.7 mm, BLI = 45–49%, n = 3; McKenzie et al. 2023a). They further resemble the latter specimens

(McKenzie et al. 2023a: fig. 11i–k) in several regards, particularly the possession of an asymmetrical (mesially higher) and labiolingually compressed crown that is convex on the labial side but concave at the lingual, except for a bulging vertical portion where the crown reaches its maximum height. However, in other aspects the di3s from CB more closely resemble (at a smaller size) the similarly elongate i3s of *P. palaeochoerus* from CCN20 (McKenzie et al. 2023a: fig. 7p–t) and elsewhere (Van der Made et al. 1999: pl. 2, fig. 6), especially regarding the possession of a distally directed endocristid that lingually encloses a deep, narrow, and distally oriented endofossid that is not discernible in the CCN20 deciduous specimens. Nevertheless, an alternate identification of the CB specimens as i3s can be ruled out based on their lower crown height and smaller dimensions, which are not only smaller than the i3s of *P. palaeochoerus* from CCN20, but also slightly smaller than the di3s from that locality (McKenzie et al. 2023a). It may be thus concluded that the di3 of *P. palaeochoerus* displays some variability in the development of the endocristid and endofossid. In turn, the germ identified as a tetraconodontine di3 (Fig. 13o) is only tentatively assigned to *Pa. valentini* based on similarities with the i3 of the same taxon, despite differences in occlusal proportions—although it should be taken into account that this tooth position had not been previously reported for this taxon (or *Versoporcus*).

Lower deciduous premolars: Except for a dp3 that can unambiguously be assigned to *P. palaeochoerus* (Fig. 13r), the identification of the dp2s and dp3s from CB is somewhat tentative, because none of the specimens is associated to more diagnostic material from the same individual and also due to the rather scanty evidence for these tooth positions available from the literature—despite the previous efforts by McKenzie et al. (2023a) based on the CCN20 sample. The complete dp2 assigned to *P. palaeochoerus* (Fig. 13p) falls within the size variation previously reported for this species (Fig. 15a). Indeed, it is similar in length but slightly broader (BLI = 52%) than those previously reported from Rudabánya (BLI = 33–44%, n = 6; Fortelius et al. 2005), being more comparable in this regard to the specimens reported from CCN20 (BLI = 51–56%, n = 2; McKenzie et al. 2023a). The dp2 of *P. palaeochoerus* from CB also closely resembles in shape one of the specimens attributed to the same species by McKenzie et al. (2023a: fig. 11n), except for minor details including the more pointed mesial end and the stouter and more diverging roots of the CB specimen. Unfortunately, distal crown morphology cannot be ascertained in neither of these specimens due to wear, thereby precluding an unambiguous assignment to *P. palaeochoerus*. An incomplete dp2 germ from CCN20 described by McKenzie et al. (2023: fig. 11o), associated with more diagnostic teeth of *Pa. palaeochoerus*, displays a distally positioned hypoconid and no trace of metaconid—as it is also the case of the dp3 of the same species but unlike the dp2 and dp3 from CB assigned to *Versoporcus* (see below). On this basis, a more elongate dp2 from CCN20 (IPS114102), tentatively assigned to *Pa. valentini* by McKenzie et al. (2023a: fig. 11p), might alternatively be assigned to *P. palaeochoerus*, given that its proportions fit well with those of Rudabánya (BLI = 35%) and its length are only slightly greater than otherwise recorded for the species (Fig. 15a). Another dp2 from CB (Fig. 13q) is very buccolingually compressed and displays a more trenchant appearance than those of *P. palaeochoerus* despite the low crown height, being assigned to *Versoporcus*. Its bifurcated distal cristid, delimining a distolinguall fossid, is reminiscent of the lower anterior permanent premolars of tretaconodontines, as well as the dp3s assigned to the same taxon.

The single dp3 of *P. palaeochoerus* from CB (Fig. 13r) fits with the lower range of size variation for this species (Fig. 15b) and displays similar proportions (BLI = 48%) than previously available specimens (BLI = 43–55%, n = 12; Fortelius et al. 2005; McKenzie et al. 2023a). It further closely resembles in occlusal shape the

dp3s of *P. palaeochoerus* from CCN20 (McKenzie et al. 2023a: fig. 11q–u), from which it merely differs by displaying a more rounded (instead of pointed) mesial contour. In turn, the dp3s from CB attributed to tetraconodontines differ by displaying a more distinct metaconid located close to the protoconid as well as a bifurcated metapostcristid. The attribution of one of the specimens to *Pa. valentini* (Fig. 13s) is based on minor differences (more marked distolingual cleft and more lingually oriented distal fossid) relative to those assigned to *Versoporcus* (Fig. 13t–v). However, incomplete preservation (which precludes the measurement of mesiodistal length) and the lack of previously figured specimens hinders a more conclusive attribution. In terms of buccolingual breadth, the specimen assigned to *Pa. valentini* (BL = 5.8 mm) is somewhat narrower than that previously available (BL = 6.4 mm; Pickford, 2016a), whereas those attributed to *Versoporcus* (BL = 5.6–6.7 mm, n = 3) only partially overlap with those of *V. steinheimensis* s.s. available from the literature (BL = 6.0–7.1, n = 5; Pickford, 2016a).

The studied sample of dp4s from CB includes four complete specimens as well as a mesial and several distal fragments. Attributing them to the three taxa distinguished here is not always straightforward, since the published iconography is rather limited and the most distinctive features between *P. palaeochoerus* and tetraconodontines become easily erased by occlusal and interproximal wear. Dental proportions (Fig. 15c) indicate that the studied tetraconodontine dp4s do not overlap much with those of *P. palaeochoerus*, generally displaying relatively broader proportions at equal length, whereas those *Pa. valentini* and *Versoporcus* show some overlap despite the former being larger on average. Regarding occlusal shape, moderately worn dp4s of *P. palaeochoerus* (e.g., McKenzie et al. 2023a: fig. 11v–w) differ from those of *Pa. valentini* (Pickford 2014: fig. 16C–D) and *Versoporcus* (Pickford 2016a: fig. 24H) in the possession of thicker cristids with more abundant crenulations of the enamel, a better-developed and distally projecting pentaconid, larger endo- and preconulids, and a more convex lingual contour. Based on these features, a complete dp4 from CB that shows an advanced degree of wear (Fig. 13y) as well as three partial specimens better preserving the occlusal morphology (Fig. 13w–x, z) are assigned to *P. palaeochoerus*. The complete specimen overlaps in dimensions with the three taxa recorded at the site (Fig. 15c), its proportions (BLI = 48%) being relatively broader than those of *P. palaeochoerus* from Rudabánya (BLI = 39–44%, n = 14; Fortelius et al. 2005) but overlapping with the larger specimens from CCN20 (BLI = 44–49%, n = 4; McKenzie et al. 2023a). This specimen also overlaps in proportions with previously reported specimens of *Pa. valentini* (BLI = 41–51%, n = 3; Pickford 2014, 2016a) and *Versoporcus* (BLI = 46–50%, n = 5; Pickford, 2016a), but the convexities of the lingual contour, coupled with the distally projecting and seemingly well-developed hypoconid (even if largely eroded by wear) support an attribution to *P. palaeochoerus*. The remaining dp4s from CB display tetraconodontine affinities, most clearly evinced by the three complete crowns with a slight degree of wear, which display thinner cristids, distinct but smaller pentaconid and conulids, and a straighter lingual profile. One of the specimens (Fig. 13a') resembles those of *Pa. valentini* in size (Fig. 15c), proportions (BLI = 43%), and occlusal shape—particularly in the possession of more transversely aligned cuspids, a better-developed and more projecting distal cingulid, and a more inconspicuous mesial cingulid. In contrast, the other two complete crowns (Fig. 13b'–c') more closely resemble those of *Versoporcus* in the more projecting mesial margin but more rounded distal margin of the crown, as well as in the less transversely aligned pairs of main cuspids (with the buccal ones being more distally located than the mesial, especially the hypoconid relative to the entoconid). The remaining two distal crown fragments (Fig. 13d'–e') are also tentatively assigned to *Versoporcus* based on similarities in the preserved

occlusal profile. The two complete dp4s from CB attributed to *Versoporcus* are somewhat smaller (Fig. 15c) and slightly narrower in relative terms (BLI = 42–46%) than previously reported specimens, but this is not surprising given the small sample sizes available to date.

Discussion

Taxonomic attributions

Attribution of the suine remains: In terms of teeth, approximately half of the studied suid sample from CB belongs to the dicoryphochoerin suine *Propotamochoerus palaeochoerus*. The dicoryphochoerin affinities of the material are most clearly shown by the distinctive morphology of the p4 (with a well-developed metaconid that is not aligned with, but markedly distolingually located relative to, the protoconid) and the mesiodistally elongate I2 with a marked lingual cingulum (Van der Made and Moyà-Solà 1989). The described material fits well with the known dental morphology of *Propotamochoerus* and differs instead from the other Late Miocene dicoryphochoerin genus from Europe, *Hippopotamodon* (including material formerly assigned to *Microstonyx*, here considered its junior synonym following Pickford, 2015) in the smaller size and the retention of some more plesiomorphic details of the dentition, such as the triangular and mesiodistally shorter I3 (Van der Made et al. 1992).

The described material of *Propotamochoerus* from CB fits well in terms of occlusal morphology with that of *P. palaeochoerus* (Mottl 1966; Hünermann 1968; Schmidt-Kittler 1971; Golpe-Posse 1972; Van der Made et al. 1999; Fortelius et al. 2005; Iannucci and Begun,2022; McKenzie et al. 2023a), which is the only species of the genus recorded from the Vallesian of Europe. Two additional species of *Propotamochoerus* are recognized in Europe, *Propotamochoerus provincialis* and *Propotamochoerus aegaeus* (Geraads et al. 2008; Pickford 2013c; Lazaridis 2015; Iannucci et al. 2021; Kostopoulos and Sylvestrou 2022; Lazaridis et al. 2022; Iannucci 2023; but see Iannucci et al. 2021 and Iannucci 2023 regarding the distinction between these species). However, they date to the Turolian and can be distinguished from *P. palaeochoerus* as well as the *Propotamochoerus* material from CB in several details of dental size and proportions (Iannucci 2023; McKenzie et al. 2023a). As evidenced by our dental plots (Figs. 14–15), *P. palaeochoerus* displays considerable variation in dental size for all tooth loci that are well represented. However, the CB sample generally fits well or only minimally expand the range of dental variation of the species as recorded in the comparative sample. Some tooth loci (particularly the second and third molars) appear to be larger than average for the species, as it is also the case for the sample from the roughly coeval site of CCN20 (also in the Vallès-Penedès Basin), which McKenzie et al. (2023a) also attributed to *P. palaeochoerus* without favoring a subspecific distinction.

Attribution of the tetraconodontine remains: The presence of tetraconodontines at CB is evidenced by many tooth loci that clearly display a morphology that is not compatible with *P. palaeochoerus* (or any of the other suids recorded at the site), including multiple upper and lower incisors, some P1s, a P3, multiple P4s and upper molars (especially the M3s), both male and female lower canines, multiple lower premolars and molars (some belonging to a partial mandible), and even upper and lower deciduous teeth.

In turn, the record of two different tetraconodontines at CB is supported by the presence of distinctive morphologies for various tooth loci, particularly (but not exclusively) the P4, M3, the i2, and the p4. Size does not seem to be a good distinctive criterion, because even though *Pa. valentini* is generally larger on average than

Versoporcus, there is considerable overlap. The presence of two different tetraconodontine i2 morphotypes at CB, one of them closely resembling the distinctive shape of the ones previously assigned to *Pa. valentini* by McKenzie et al. (2023a), corroborates the co-occurrence of this species with another tetraconodontine. The same holds for the P4, which is consistent with the presence of *Pa. valentini* and a *Versoporcus* species, despite the advanced degree of wear of those assigned to the latter. Most enlightening from a taxonomic viewpoint, however, are the differences in p4 and M3 morphology. Regarding the former tooth locus, the large tetraconodontine mandible with p2–m3 from CB is most informative. The p2 and p3 appear particularly elongate, but the p4 displays the characteristic morphology of *Versoporcus*, with a moderately stout occlusal contour that is constricted at the level of the protoconid and displays a distinct metaconid distolingually from the protoconid (as in *P. palaeochoerus*, but smaller and less lingually located). The p4 of this mandible resembles two other isolated specimens from CB, also attributed to *Versoporcus*, and clearly differ from the ones those assigned to *Pa. valentini*, which display a more elliptical and stouter occlusal contour, with inflated crown walls and without a distinct metaconid distally from the protoconid.

Similarly, clear differences can be found among the large sample of M3s from CB, which despite variation in size, proportions, and distal development of the talon, evince the presence of more than a single taxon. The M3s from CB assigned to *Pa. valentini* resemble those previously attributed by Pickford and colleagues (Pickford 2013a, 2014, 2016a; Pickford and Laurent 2014) to either *Pa. valentini* or *C. doati* (excluding the lectotype of the latter), displaying an asymmetric distal contour that distally tapers abruptly, with a generally distinct third lobe that is more or less distally expanded only on the lingual side and tilted buccally to some extent (unlike the M3s of *P. palaeochoerus*, where the crown displays a similar contour but a lingually tilted third lobe). In contrast, the M3s from CB assigned to *Versoporcus* display a less distally tapering and more symmetrical contour, with a less distinct third lobe, which does not exhibit a greater distolingual protrusion compared to the distobuccal region, more closely resembling the material included in this genus by Pickford (2014, 2016a).

Implications for tetraconodontine taxonomy

The described dental remains evince that a large tetraconodontine species, not attributable to *Versoporcus,* is present at CB. Together with the material from CCN20 previously assigned to *Pa. valentini* by McKenzie et al. (2023a), this paper therefore lends further support to Pickford's (2014, 2016a) contention that a previously overlooked large tetraconodontine is present in the late Aragonian and early Vallesian of Europe. The CB material improves the knowledge of the dental morphology of this tetraconodontine as well as that of *Versoporcus*, and enlarges the size variation previously recorded for many tooth loci in both taxa. The CB material shows that the two tetraconodontine taxa substantially overlap in dental dimensions—more so than suggested by the comparative sample mostly based on Pickford (2013a, 2014, 2016a), indicating that size is not a reliable criterion to distinguish among them—whereas, in contrast, they display noticeable differences in occlusal shape.

Adequately diagnosing the genera *Conohyus* and *Parachleuastochoerus* and determining what species must be included in each genus has long been a controversial issue (e.g., Bernor et al. 2004). Pickford's recent revision of tetraconodontines (Pickford 2014, 2016a; Pickford and Laurent 2014) has not settled this issue, as shown by Van der Made's (2020) strongly dissenting views. We concur with Pickford (2014, 2016a) and McKenzie et al. (2023a) that *Pa. valentini* is not a junior synonym of *C. simorrensis*—except for the type

material of *C. melendezi*, which was assigned to the former by Pickford (2014, 2016a) but reassigned to *C. simorrensis* not only by Van der Made (2020) but also by McKenzie et al. (2023a). We further agree with Pickford (2014, 2016a) that *Pa. valentini* belongs to a different genus than the species included by him in *Versoporcus*, and hence provisionally follow his taxonomic opinion (see also McKenzie et al. 2023a, 2023b) rather than Van der Made's (2020), who included these species in *Conohyus* and *Parachleuastochoerus*, respectively. An inclusion in *Parachleuastochoerus* is tentatively favored based on the proportions of the posterior premolars relative to the molars, which more closely resemble those of *Pa. crusafonti* (the type species of the genus) and are narrower than in *Conohyus* (Pickford, 2014). Nevertheless, based on currently available evidence, we consider that the genus ascription of *Pa. valentini* is debatable and that an alternative attribution to *Conohyus*, as supported by Van der Made (2020), cannot be entirely ruled out at present. It is outside the scope of this paper to reach a definitive conclusion about the genus allocation of both *Pa. valentini* and *V. steinheimensis* because the studied material does not enable to ascertain cranial morphology and neither includes some key tooth loci for the two species. As noted by Pickford (2014), the generic distinction of *Versoporcus* from *Parachleuastochoerus* largely stems from cranial differences between the former and *Pa. valentini* but, as discussed by subsequent authors (Iannucci and Begun 2022; McKenzie et al. 2023a), such differences would also be compatible with *Versoporcus* being a junior synonym of *Parachleuastochoerus* if *Pa. valentini* belongs in fact to *Conohyus*. However, given that this alternative taxonomic arrangement is not favored by premolar-to-molar proportions and that clearly diagnostic features of *Conohyus* cannot be ascertained based on currently available evidence, we consider that proposing a new combination for this species within the genus *Conohyus* is not warranted at present.

To resolve this issue, more detailed comparisons between *Pa. valentini* and the type species of the three genera involved—*C. simorrensis*, *Pa. crusafonti*, and *V. steinheimensis*—would be required. However, this does not seem feasible until the dental morphology of *Pa. valentini* is better known, including that of the c1m. This seems particularly relevant because the c1m morphology of *C. simorrensis* has been considered diagnostic for the genus (Pickford and Laurent 2014; Pickford 2016a). Pickford (2014) attributed to *Pa. valentini*—but did not figure or describe—a c1m fragment from Sant Quirze (IPS31067), which was incorrectly labeled with the old number [VP1113], when in fact it corresponds to the old number [IPS1113], currently IPS31067 (McKenzie et al. 2023a). The latter authors asserted that this c1m fragment could not belong to *Pa. valentini* because, based on Golpe-Posse's (1971) dissertation, it apparently came from a much older locality. Such assertion is incorrect and stems from a problem of mispagination in Golpe-Posse's (1971) dissertation. When this problem is accounted for, it becomes clear that this lower canine fragment, which displays a verrucosic morphology, comes from Trinxera del Ferrocarril-Sant Quirze and was attributed by Golpe-Posse (1971) to *L. splendens*. Yet this specimen was not cited by Van der Made (1996b) among the material of *L. splendens* from this locality. Certainly, the specimen is fragmentary and not particularly well preserved, but it differs from the c1m of *Listriodon* (e.g., see Van der Made 1996b) in various regards, including the narrower distal side relative to both the labial and lingual ones, and the lack of enamel except at the apical-most portion. If this specimen actually represented the c1m of *Pa. valentini*, it would support the contention that this species does not belong to genus *Conohyus*—which displays a scrofic cross section with a cementum band on the distal side (Pickford 2013b: fig. 6E; Pickford and Laurent 2014), whereas, in contrast, the genus *Parachleuastochoerus* is characterized by a verrucosic c1m (Pickford 2014, 2016a). Nevertheless, the shape and size of this specimen (MD = 18.0 mm, BL =

10.6 mm; Pickford 2014) are consistent with a large c1f of *L. splendens* (MD = 11.2–17.7 mm, BL = 8.3–12.8 mm; Van der Made 1996b), particularly considering that MD is artifactually increased in the former because of preservation. It thus seems that an attribution to *L. splendens* is more likely and that the c1m of *Pa. valentini* is still unknown.

The description of unpublished tetraconodontine material from Abocador de Can Mata (currently underway) might clarify further the c1m morphology of *Pa. valentini* in the future. In the meantime, we consider that the variability displayed by most remains previously included in *C. doati* by Pickford and colleagues (Pickford 2013a, 2014, 2016a; Pickford and Laurent 2014), except those from the type locality, fit well with the variation evidenced by the remains of *Pa. valentini* from CB, as better exemplified by the M3s. McKenzie et al. (2023a) noted that some M3s attributed to *C. doati* by Pickford (2016a) might indeed belong to *Pa. valentini*, but in the light of the variation found within the CB sample we consider it more likely that the purported differences between the M3 of these taxa (presumably larger and wider in *C. doati*) merely represent intraspecific variation. An alternative interpretation would recognize the co-occurrence of yet another large tetraconodontine at the site, which a priori appears unlikely and is neither supported by differences found in other tooth loci. We further include in *Pa. valentini* the type material of *C. ebroensis*, previously considered a distinct species by Van der Made (1989), a junior synonym of *C. doati* by Pickford (2016a), and a junior synonym of *C. simorrensis* by Van der Made (2020). Van der Made (2020) noted that the size of the lectotype M3 of *C. doati* is consistent with this species being a junior synonym of *C. simorrensis*, and the ascription of this specimen to *Conohyus* is further supported by the presence of a cementum band on the distal surface of the c1m from the type locality (Pickford 2013b, 2016a; Pickford and Laurent 2014). Nevertheless, it is noteworthy that the morphology of the M3 lectotype is also quite similar to one of the specimens from CB attributed to *Versoporcus*, an attribution to the latter genus not being unreasonable in our opinion.

In summary, we disagree with Pickford (2013a, 2014, 2016a) and Pickford and Laurent (2014) that *C. doati* is a taxonomically valid species but, unlike Van der Made (2020), we consider that part of the material (including the holotype of *C. ebroensis*) belongs to *Pa. valentini* instead of *C. simorrensis*, while the lectotype might belong to either the latter or to *Versoporcus*. In the light of such uncertainties, we prefer to consider the nominal species *C. doati* as a nomen dubium. Note, however, that if the lectotype of *C. doati* from Bonnefond were eventually found to belong to *Versoporcus* instead of *C. simorrensis*, the former name (erected by Lartet 1851) would take precedence over *V. steinheimensis*, the type species of *Versoporcus*, which was erected by Fraas (1870).

Regarding the distinction of two *Versoporcus* species promoted by Pickford (2014, 2016a), who resurrected *V. grivensis* when establishing the genus, McKenzie et al. (2023b) tentatively supported it despite recognizing that the chronostratigraphic ranges of the two species overlapped to a large extent. This indicated that Pickford's (2014, 2016a) concept of two *Versoporcus* species was not compatible with a single anagenetic lineage increasing in size through time. The existence of two different species of the genus *Versoporcus* remains a viable possibility, but its likelihood is diminished by the size variation displayed for multiple tooth loci by the specimens of *Versoporcus* from CB. Previous species assignments by Pickford (2014, 2016a) and McKenzie et al. (2023b), as reflected in the comparative sample used in this paper, generally indicated a larger dental size for *V.* '*grivensis*' as compared with *V. steinheimensis* s.s., with minimal to vast overlap depending on the tooth locus. The specimens of *Versoporcus* from CB, however, not only expand in some cases the previously known

variation for the genus (e.g., p2, p3, lower molars), but also frequently encompass the whole range of variation of the two species considered together (M3, p4, m1). Unless it is interpreted that the two species were present at CB, as Pickford (2014, 2016a) argued for La Grive, the CB sample of *Versoporcus* strongly supports the view that *V. grivensis* is merely a junior synonym of *V. steinheimensis*, as already argued by Van der Made (2020). Coexistence of two tetraconodontine species of the same genus seems even more unlikely for CB—where most of the remains come from a single stratigraphic horizon and the sequence spans a short time span (Alba et al. 2019)—than for La Grive, which includes multiple fissure fillings of different age (Mein and Ginsburg 2002; Casanovas-Vilar et al. 2011). Furthermore, the range of metrical variation displayed by currently available samples of *Versoporcus* does not exceed that of *Pa. valentini* or *P. palaeochoerus*, indicating that there is no sound reason to assume that it cannot be interpreted as intraspecific variation.

It is noteworthy that, irrespective of the species assignment, the record of *Versoporcus* at CB confirms the persistence of this genus until the earliest Vallesian with a chronostratigraphic range extending from ~14.0–13.5 to 11.2 Ma (McKenzie et al. 2023b and references therein; this paper). It is uncertain whether CB represents the Last Appearance Datum of *Versoporcus*, as Van der Made (1997) reported it (as *Pa. steinheimensis*) from later Vallesian sites of the Vallès-Penedès Basin (Santiga, Can Coniller, Can Poncic 1, and Can Llobateres), while Pickford (2016a) did not. Such discrepancies highlight the need to continue revising the tetraconodontine remains from this basin, which will surely contribute to a better understanding of the evolutionary history of this group of suids in Europe during the Miocene.

Conclusions

Our revision of all the suine and tetraconodontine dentognathic material from CB (comprising more than 200 specimens) leads us to conclude that, at this earliest Vallesian site, *P. palaeochoerus* was a common species that coexisted with two tetraconodontines—as well as with two additional suids (*L. splendens* and *A. castellensis*), previously described in greater detail. The presence of *Propotamochoerus*—whose first appearace is currently considered a marker of the Vallesian (Alba et al. 2022 and references therein)—at CB is in agreement with the earliest Vallesian age recently supported for the site based on magnetostratigraphic and biostratigraphic data (Alba et al. 2019). Although the presence of *Propotamochoerus* at CB had been noted by some previous authors (e.g., Van der Made 1997), it was substantiated only by material reported by Golpe-Posse (1971, 1972) as *Hyotherium palaeochoerus*, which was barely described and not adequately figured. Our study describes in detail much more abundant material and shows that previous identifications by Golpe-Posse (1971, 1972) of both *H. palaeochoerus* and *H. soemmeringi* correspond in fact to the three taxa identified in this paper: *P. palaeochoerus*, *Pa. valentini*, and *V. steinheimensis*.

Our study has even more important implications for current debates about the taxonomy of tetraconodontine suids from the Miocene of Europe. First, we show that, contrary to some previous assertions, the two species recorded at the site are quite large and substantially overlap in size, while the presence of the smaller *Pa. huenermanni* can be discounted. Previous reports of the latter species (e.g., Van der Made 1997) probably stemmed from some specimens of *Pa. crusafonti* from Can Llobateres and *Pa. huenermanni* from Can Poncic that we found mislabeled as coming from CB, but whose provenance can be determined based on old collection numbers listed in Golpe-Posse's (1971) dissertation. Nevertheless, the range of size and shape variation

displayed by the tetraconodontine dental remains from CB is considerable and cannot be attributed to a single species, which was previously identified as *Pa. steinheimensis* by Van der Made (1997). Indeed, if interpreted literally in the light of Pickford's (2014, 2016) taxonomy, the variation displayed by some tooth loci such as the M3 would lead to the distinction of as much as four species—namely, *Pa. valentini*, *C. doati*, and the two *Versoporcus* spp. Nevertheless, we consider that a simpler interpretation of the new data reported here is that most of the material previously attributed to *C. doati* belongs to *Pa. valentini*, while *V. grivensis* is a junior subjective synonym of *V. steinheimensis*. Unfortunately, the material at hand does not allow us to settle other ongoing debates (Van der Made 2020; McKenzie et al. 2023a, 2023b; this paper), such as the plausible alternative genus allocation of *Pa. valentini* into *Conohyus*, the distinctiveness of *Versoporcus* from *Parachleuastochoerus*, or the taxonomic identity of the lectotype of the nominal species *C. doati* (here provisionally considered a nomen dubium). Ongoing research focused on the more abundant and complete craniodental remains of tetraconodontines from the late Aragonian and early Vallesian of Abocador de Can Mata, coupled with more detailed comparisons with *C. simorrensis*, will hopefully help disentangle these issues in the near future.

Acknowledgments: We are indebted to the municipality of Barberà del Vallès for allowing fieldwork at the site in 2014–2015, Salvador Moyà-Solà for codirecting these fieldwork campaigns, Josep M. Robles for assistance with the ICP collections, and the Preparation & Conservation Area of the ICP for the preparation of some specimens. We also acknowledge the collaboration of the Servei de Patrimoni Arqueològic i Paleontològic of the Generalitat de Catalunya and thank the two reviewers (Alessio Iannucci and an anonymous one) for useful comments that helped us improve a previous version of this paper. This work is part of the PhD dissertation of S.M., in the framework of the PhD Programme in Geology of the Universitat Autònoma de Barcelona.

Author contributions: D.M.A. and D.DM. designed the study. S.A. directed fieldwork. S.M. took the photographs, measured the specimens, and drafted the descriptions. D.M.A. prepared the figures. S.M., S.G.A., and D.M.A. identified the material. S.M. and D.M.A. wrote the manuscript with input from the remaining authors, who reviewed several drafts of the manuscript.

Funding: This work is part of R+D+I projects PID2020-117289GBI00, PID2020-116220GBI00, and PID2020-116908GB-I00, funded by the Agencia Estatal de Investigación of the Spanish Ministry of Science and Innovation (MCIN/AEI/10.13039/501100011033/). Research has also been supported by the Generalitat de Catalunya/CERCA Programme, the Agència de Gestió d'Ajuts Universitaris i de Recerca of the Generalitat de Catalunya (2021 SGR 00620), the Departament de Cultura of the Generalitat de Catalunya (CLT0009_22_000018), a predoctoral fellowship from the Confederated Tribes of Grand Ronde (CTGR) to S.M., and the INVESTIGO Program 2022 (reference 100027TC1) financed by the European Union, Next Generation EU to S.G.A.

Data availability: The fossil material studied in this paper is housed and adequately curated in the ICP and is accessible to other researchers. All the data generated in the course of this study are provided in the paper.

Declarations

Conflicts of interest: The authors have no competing interests to declare that are relevant to the content of this article.

References

Aguilar J-P, Agustí J, Gibert J (1979) Rongeurs miocènes dans le Valles-Penedes. 2 - Les Rongeurs de Castell de Barbera. Palaeovertebrata 9:17–32

Agustí J (1981) Roedores Miomorfos del Neógeno de Cataluña. Dissertation, Universidad de Barcelona, Barcelona

Agustí J, Cabrera L, Garcés M, Krijgsman W, Oms O, Parés JM (2001). A calibrated mammal scale for the Neogene of Western Europe. State of the art. Earth-Sci Rev 52:247–260

Agustí J, Cabrera L, Garcés M, Parés JM (1997) The Vallesian mammal succession in the Vallès-Penedès basin (northeast Spain): Paleomagnetic calibration and correlation with global events. Palaeogeogr Palaeoclimatol Palaeoecol 133:149–180

Agustí J, Cabrera L, Moyà-Solà S (1985) Sinopsis estratigráfica del Neógeno de la fosa del Vallés-Penedés. Paleontol Evol 18:57–81

Alba DM (2012) Fossil apes from the Vallès-Penedès Basin. Evol Anthropol 21:254–269

Alba DM, Casanovas-Vilar I, Garcés M, Robles JM (2017) Ten years in the dump: An updated review of the Miocene primate-bearing localities from Abocador de Can Mata (NE Iberian Peninsula). J Hum Evol 102:12–20

Alba DM, Garcés M, Casanovas-Vilar I, Robles JM, Pina M, Moyà-Solà S, Almécija S (2019) Bio- and magnetostratigraphic correlation of the Miocene primate-bearing site of Castell de Barberà to the earliest Vallesian. J Hum Evol 132:32–46

Alba DM, Moyà-Solà S (2012) A new pliopithecid genus (Primates: Pliopithecoidea) from Castell de Barberà (Vallès-Penedès Basin, Catalonia, Spain). Am J Phys Anthropol 147:88–112

Alba DM, Moyà-Solà S, Almécija S (2011) A partial hominoid humerus from the middle Miocene of Castell de Barberà (Vallès-Penedès Basin, Catalonia, Spain). Am J Phys Anthropol 144:365–381

Alba DM, Moyà-Solà S, Casanovas-Vilar I, Galindo J, Robles JM, Rotgers C, Furió M, Angelone C, Köhler M, Garcés M, Cabrera L, Almécija S, Obradó P (2006) Los vertebrados fósiles del Abocador de Can Mata (els Hostalets de Pierola, l'Anoia, Cataluña), una sucesión de localidades del Aragoniense superior (MN6 y MN7+8) de la cuenca del Vallès-Penedès. Campañas 2002-2003, 2004 y 2005. Estud Geol 62:295–312

Alba DM, Robles JM, Casanovas-Vilar I, Beamud E, Bernor RL, Cirilli O, DeMiguel D, Galindo J, Llopart I, Pons-Monjo G, Sánchez IM, Vinuesa V, Garcés M (2022) A revised (earliest Vallesian) age for the hominoid-bearing locality of Can Mata 1 based on new magnetostratigraphic and biostratigraphic data from Abocador de Can Mata (Vallès-Penedès Basin, NE Iberian Peninsula). J Hum Evol 170:103237

Almécija S, Alba DM, Moyà-Solà S (2012) The thumb of Miocene apes: new insights from Castell de Barberà (Catalonia, Spain). Am J Phys Anthropol 148:436–450

Andrews P, Harrison T, Delson E, Bernor RL, Martin L (1996) Distribution and biochronology of European and Southwest Asian Miocene catarrhines. In: Bernor RL, Fahlbusch V, Mittmann H-W (eds). The Evolution of Western Eurasian Neogene Mammal Faunas. NeColumbia University Press, w York, pp 168–207

Arias-Martorell J, Almécija S, Urciuoli A, Nakatsukasa M, Moyà-Solà S, Alba DM (2021). A proximal radius of *Barberapithecus huerzeleri* from Castell de Barberà: Implications for locomotor diversity among pliopithecoids. J Hum Evol 157:103032

Azanza B (1986) Estudio geológico y paleontológico del Mioceno del sector oeste de la Comarca de Borja. Cuad Estud Borj 17–18:63–126

Azanza B, Menéndez E (1990) Los ciervos fósiles del neógeno español. *Paleontologia i Evolució* 23:75–82.

Bernor RL, Bi S, Radovčić J (2004) A contribution to the evolutionary biology of *Conohyus olujici* n. sp. (Mammalia, Suidae, Tetraconodontinae) from the early Miocene of Lučane, Croatia. Geodiversitas 26:509–534

Casanovas-Vilar I, Alba DM, Garcés M, Robles JM, Moyà-Solà S (2011) Updated chronology for the Miocene hominoid radiation in Western Eurasia. Proc Natl Acad Sci USA 108:5554–5559

Casanovas-Vilar I, Garcés M, Van Dam J, García-Paredes I, Robles JM, Alba DM (2016b) An updated biostratigraphy for the late Aragonian and the Vallesian of the Vallès-Penedès Basin (Catalonia). Geol Acta 14:195–217

Casanovas-Vilar I, Jovells-Vaqué S, Alba DM (2022) The Miocene high-resolution record of the Vallès-Penedès Basin (Catalonia). In: Casanovas-Vilar I, Alba DM (eds). NOW 25th Anniversary Meeting. Sabadell (Barcelona), 16–18 November 2022. Abstract Book & Fieldtrip Guide. Paleontol Evol memòria especial 9:79–122

Casanovas-Vilar I, Madern A, Alba DM, Cabrera L, García-Paredes I, Van den Hoek Ostende LW, DeMiguel D, Robles JM, Furió M, Van Dam J, Garcés M, Angelone C, Moyà-Solà S (2016a) The Miocene mammal record of the Vallès-Penedès Basin (Catalonia). C R Palevol 15:791–812

Chen G (1984) Suidae and Tayassuidae (Artiodactyla, Mammalia) from the Miocene of Steinheim a. A. (Germany). Palaeontogr Abt A 184:79–93

Crusafont Pairó M (1950) La cuestión del llamado Meótico español. Arrahona 1950:41–48

Crusafont Pairó M (1951) El sistema miocénico en la depresión española del Vallés-Penedés. In: International Geological Congress "Report of the Eighteenth Session, Great Britain, 1948", Part XI, pp 33–42

Crusafont Pairó M (1953) El sistema miocénico en la depresión española del Vallés-Penedés. Mem Com Inst Geol Prov 10:13–23

Crusafont-Pairó M (1975a) El gibón fósil (*Pliopithecus*) del Vindoboniense terminal del Vallès. Bol Inf Inst Paleontol Sabadell 7:36–38

Crusafont-Pairó M (1975b) Transición Vindoboniense-Vallesiense en los alrededores de Sabadell. Bol Inf Inst Paleontol Sabadell 7:33–35

Crusafont-Pairó M (1976) Corrigenda (A dos notas sobre la presencia del género *Anchitherium* en el Mioceno del Vallès). Bol Inf Inst Paleontol Sabadell 8:27–28

Crusafont-Pairó M, Golpe-Posse JM (1971) Biozonation des Mammifères néogènes d'Espagne. In: V Congrés du Néogène Mediterranéen. Mém Bur Rech Géol Min 78:121–129

Crusafont-Pairó M, Golpe JM (1972) Dos nuevos yacimientos del Vindoboniense en el Vallés. Acta Geol Hisp 7:71–72

Crusafont-Pairó M, Golpe-Posse JM (1972) Hallazgo del género *Anchitherium* Meyer, 1844 en el Vindoboniense terminal del Vallés-Penedés. Bol R Soc Esp Hist Nat (Geol) 69:297–298

Crusafont-Pairó M, Golpe-Posse JM (1974) Asociación de *Anchitherium* Mey., 1834, con *Hipparion* Christ, 1832, en el Alto Mioceno del Vallés. Bol R Soc Esp Hist Nat (Geol) 72:75–93

Crusafont-Pairó M, Golpe-Posse JM (1981a) Estudio de la dentición inferior del primer pliopitécido hallado en España (Vindoboniense terminal de Castell de Barberà, Cataluña, España). Butll Inf Inst Paleontol Sabadell 13:25–38

Crusafont-Pairó M, Golpe-Posse JM (1981b) Hallazgo de una nueva especie del género *Semigenetta (S. grandis)* del Vindoboniense terminal de Castell de Barberá (Depresión prelitoral catalana; España). Bol R Soc Esp Hist Nat 79:67–76

Crusafont Pairó M, Golpe Posse JM (1982a) Los Pliopitécidos en España. Col Cátedra Paleontol 37:41–46.

Crusafont-Pairó M, Golpe-Posse JM (1982b) Hallazgo de *Palaeomeles Pachecoi* Vill. et Crus., 1943, en Castell de Barberà (Vallés-Penedés). Acta Geol Hisp 17:27–37

Crusafont Pairó M, Hürzeler J (1969) Catálogo comentado de los Póngidos fósiles de España. Acta Geol Hisp 4:44–48

Crusafont Pairó M, Truyols Santonja J (1951) Hallazgo del *plesiodimylus chantrei* Gaillard en el Meótico del Vallés. Not Com Inst Geol Min Esp 22:97–126

Crusafont Pairó M, Truyols Santonja J (1960) Sobre la caracterización del Vallesiense. Not Com Inst Geol Min Esp 60:109–125

de Beaumont G, Crusafont-Pairó M (1982) Les Félidés (Mammifères, Carnivores) du Vallésien du Vallès, Catalogne, Espagne. Arch Sci Gen 35:41–64

de Bruijn H, Daams R, Daxner-Höck G, Fahlbusch V, Ginsburg L, Mein P, Morales J, Heinzmann E, Mayhew DF, van der Meulen AJ, Schmidt-Kittler N, Telles Antunes M (1992) Report of the RCMNS working group on fossil mammals, Reisensburg 1990. Newslett Stratigr 26:65–118

DeMiguel D, Domingo L, Sánchez IM, Casanovas-Vilar I, Robles JM, Alba DM (2021) Palaeoecological differences underlie rare co-occurrence of Miocene European primates. BMC Biol 19:6

Depéret C (1892) La faune de Mammifères Miocènes de La Grive-Saint-Alban (Isère) et de quelques autres localités du bassin du Rhone. Arch Mus Hist Nat Lyon 5:1–95

Filhol H (1882) Note relative à une nouvelle espèce de *Sus* fossile trouvée dans les argiles à *Dinotherium* de Valentine (Haute-Garonne). Bull Soc Philom Paris 6:123–124

Fortelius M, Armour-Chelu M, Bernor RL, Fessaha N (2005) Systematics and palaeobiology of the Rudabánya Suidae. In: Bernor RL, Kordos L, Rook L (eds). Multidisciplinary Research at Rudabánya. Palaeontogr Ital 90:259–278

Fortelius M, Van der Made J, Bernor RL (1996) Middle and Late Miocene Suoidea of Central Europe and the Eastern Mediterranean: Evolution, Biogeography, and Paleoecology. In: Bernor RL, Fahlbusch V, Mittmann H-M (eds). The Evolution of Western Eurasian Neogene Faunas. Columbia University Press, New York, pp 348–377

Fraas O (1870) Die Fauna von Steinheim. Mit Rüecksicht auf die miocänen Säugethier- und Vogelreste des Steinheimer Beckens. Jahresh Ver vaterl Naturkd Wb 26:145–306

Fujita M, Kawamura Y, Murase N (2000) Middle Pleistocene wild boar remains from NT Cave, Niimi, Okayama Prefecture, west Japan. J Geosci Osaka City Univ 43:57–95

Gaillard C (1899) Mammifères miocènes nouveaux ou peu connus de La Grive-Saint-Alban (Isère). Arch Mus Hist Nat Lyon 7:1–78

Garcés M, Agustí J, Cabrera L, Parés JM (1996) Magnetostratigraphy of the Vallesian (late Miocene) in the Vallès-Penedès Basin (northeast Spain). Earth Planet Sci Lett 142:381–396.

Geraads D, Spassov N, Garevski R (2008) New specimens of *Propotamochoerus* (Suidae, Mammalia) from the late Miocene of the Balkans. N Jb Geol Paläont Abh 248:103–113

Gibert J (1974) Étude des Insectivores du Miocène de Vallès-Penedès, Calatayud-Daroca et Rubielos de Mora. Dissertation, Universidad de Barcelona, Barcelona

Gibert J (1975a) New insectivores from the Miocene of Spain. I. Proc Kon Ned Akad Wetensch B 78:108–123

Gibert J (1975b) New insectivores from the Miocene of Spain. II. Proc Kon Ned Akad Wetensch B 78:124–133

Gibert Clols J (1975) Distribución bioestratigráfica de los Insectívoros del Mioceno en el NE. de España. Biotopos, comparación de cuencas y localidades. Relaciones faunísticas con América del Norte. Acta Geol Hisp 10:167–169

Ginsburg L (1974) Les faunes de Mammifères burdigaliens et vindoboniens des bassins de la Loire et de la Garonne. Mém Bur Rech Géol Min 78:153–167

Ginsburg L (1980) *Xenohyus venitor*, suidé nouveau *(Mammalia, Artiodactyla)* du Miocène Inférieur de France. Geobios 13:861–877

Golpe-Posse JM (1971) Suiformes del Terciario Español y Sus Yacimientos. Dissertation, Universidad de Barcelona, Barcelona

Golpe-Posse JM (1972) Suiformes del Terciario español y sus yacimientos (Tesis doctoral-Resumen) (revisado y reimprimido en Diciembre de 1972). Paleontol Evol 2:1–197

Golpe-Posse JM (1974) Faunas de yacimientos con suiformes en el Terciario español. Paleontol Evol 8:1–87

Golpe-Posse JM (1975) Un nuevo tayasuido en el Vindoboniense terminal de Castell de Barberà (Cuenca del Vallès, España). Bol Inf Inst Paleontol Sabadell 7:39–43

Golpe-Posse JM (1977) *Barberahyus castellensis* n.g.n.sp., Tayasuido del Vindoboniense terminal de Castell de Barberà (Cuenca del Vallès, España). Paleontol Evol 12:31–43

Golpe Posse JM (1978) Presencia del género *Microstonyx* Pilgrim, 1926, en el Vallesiense superior de Terrassa (Barcelona, Cuenca del Vallès). Butll Inf Inst Paleontol Sabadell 10:28–33

Golpe-Posse JM (1981a) Estudio comparativo entre la mandíbula de *Semigenetta grandis* del Vindoboniense de Castell de Barberà (Depresión Prelitoral Catalana, España) y otros ejemplares europeos de *Semigenetta*. Paleontol Evol 16:15–24

Golpe-Posse JM (1981b) Datos comparativos de tres formas viverrinas del Vindoboniense superior y Vallesiense medio del Vallès-Penedès (depresión prelitoral catalana, España). Acta Geol Hisp 16:191–194

Golpe-Posse JM (1984) Las formas melinoideas de la transición Vindoboniense superior-Vallesiense medio del Vallès-Penedès (Depresión prelitoral catalana, España). Acta Geol Hisp 19:11–18

Golpe Posse JM (1993) Los Hispanopitecos (Primates, Pongidae) de los yacimientos del Vallès-Penedès (Cataluña, España). II: Descripción del material existente en el Instituto de Paleontología de Sabadell. Acta Geol Hisp 26–27:151–224

Gray JE (1821) On the natural arrangement of vertebrose animals. Lond Med Repos Rec 15:296–310

Harris JH, Liu L-P (2007) Superfamily Suoidea. In: Prothero DR, Foss EF (eds). The Evolution of Artiodactyls. Johns Hopkins University Press, Baltimore, pp 130–150

Harrison T (1991) Some observations on the Miocene hominoids from Spain. J Hum Evol 19:515–520

Heissig K (1989) *Conohyus huenermanni* n. sp., eine kleine Schweineart aus der Oberen Süßwassermolasse Bayerns. Mitt Bayer Staatssamml Paläontol Hist Geol 29:235–240

Hellmund M (1995) The Vertebrate Locality Maramena (Macedonia, Greece) at the Boundary Turolian-Ruscinian Boundary (Neogene). 13. Suidae (Artiodactyla, Mammalia). Munch Geowiss Abh 28:143–156

Hünermann KA (1968) Die Suidae (Mammalia, Artiodactyla) aus den Dinotheriensanden (Unterpliozän = Pont) Rheinhessens (Sudwestdeutschland). Schweiz Paläontol Abh 86:1–96

Iannucci A (2023) A reappraisal of the lost suids from the Late Miocene of Gravitelli (Sicily, Italy) and paleobiogeographical implications. Palaeoworld https://doi.org/10.1016/j.palwor.2023.02.001

Iannucci A, Begun DR (2022) Suidae (Mammalia, Artiodactyla) from the Late Miocene hominoid locality of Alsótelekes (Hungary). Geobios 71:39–49

Iannucci A, Cherin M, Sorbelli L, Sardella R (2021) Suidae transition at the Miocene-Pliocene boundary: a reassessment of the taxonomy and chronology of *Propotamochoerus provincialis*. J Mamm Evol 28:323–335

International Commission on Zoological Nomenclature (1999) International Code of Zoological Nomenclature. The International Trust for Zoological Nomenclature, London

Kaup J-J (1833) Description d'Ossements Fossiles de Mammifères Inconnus jusqu'à Présent, qui se Trouvent au Muséum Grand-Ducal de Darmstadt. Second Cahier. J.G. Heyer, Darmstadt

Kostopoulos DS, Sylvestrou I (2022) The fossil record of suoids (Mammalia: Artiodactyla: Suoidea) in Greece. In: Vlachos E (ed). Fossil Vertebrates of Greece Vol. 2. Laurasiatherians, Artiodactyles, Perissodactyles, Carnivorans, and Island Endemics. Springer, Cham, pp 249–269

Lartet E (1851) Notice sur la Colline de Sansan, suivie d'une Récapitulation des Diverses Espèces d'Animaux Vertébrés Fossiles, Trouvés soit a Sansan, soit dans d'autres Gisements du Terrain Tertiaire Miocène dans le Bassin Sous-Pyréneen. J.-A. Portes, Auch

Lazaridis G (2015) Study of the late Miocene vertebrate locality of Kryopigi and other localities of Kassandra Peninsula, Chalkidiki (Greece). Systematics, Taphonomy, Paleoecology, Biochronology. Dissertation, Aristotle University of Thessaloniki, Thessaloniki (in Greek)

Lazaridis G, Tsoukala E, Kostopoulos DS (2022) Validation of a prematurely abolished new *Propotamochoerus* Pilgrim, 1925 species (Mammalia, Suidae) from SE Mediterranean. C R Palevol 21:531–549

López Martínez N (1989) Revisión sistemática y biostratigráfica de los Lagomorpha (Mammalia) del Terciario y Cuaternario de España. Mem Mus Paleontol Univ Zaragoza 3:1–353

Luján ÀH, Delfino M, Robles JM, Alba DM (2016) The Miocene tortoise *Testudo catalaunica* Bataller, 1926 and a revised phylogeny of extinct species of genus *Testudo* (Testudines: Testudinidae). Zool J Linn Soc 178:312–342

Lydekker R (1876) Molar teeth and other remains of Mammalia. In: Indian Tertiary and post-Tertiary Vertebrata. In: Palaeontologia Indica. Ser. X (Part II). Indian Tertiary and post-Tertiary Vertebrata. Vol. I. Memoirs of the Geological Survey of India, Calcutta, pp 19–87.

Marigó J, Susanna I, Minwer-Barakat R, Madurell-Malapeira J, Moyà-Solà S, Casanovas-Vilar I, Robles JM, Alba DM (2014) The primate fossil record in the Iberian Peninsula. J Ib Geol 40:179–211

McKenzie S, Casanovas-Vilar I, Alba DM (2023b) Tetraconodont dental remains (Suidae, Tetraconodontinae) from the Middle Miocene site of Ca l'Almirall (Vallès-Penedès Basin, NE Iberian Peninsula). Hist Biol 35:597–606

McKenzie S, Sorbelli L, Cherin M, Almécija S, Pina M, Abella J, Luján ÀH, DeMiguel D, Alba DM (2023a) Earliest Vallesian suid remains from Creu de Conill 20 (Vallès-Penedès Basin, NE Iberian Peninsula). J Mamm Evol 30:155–212

Mein P, Ginsburg L (2002) Sur l'âge relatif des différents dépôts karstiques miocènes de La Grive-Saint-Alban (Isère). Cah Sci 2/2002:7–47

Mottl M (1955) Neue Säugetierfunde aus dem Jungtertiär der Steiermark. III. *Hyotherium palaeochoerus*, ein neuer Suide aus dem Unterpliozän der Steiermark. Mitt Mus Bergb Geol Techn Landesmus Joanneum Graz 15:69–76

Mottl M (1966) Neue Säugetierfunde aus dem Jungtertiär der Steiermark. VII. Ein vollständiger *Hyotherium palaeochoerus*-Schädel aus dem Altpliozän (Pannon) Südost-Österreichs. Mitt Mus Bergb Geol Techn Landesmus Joanneum Graz 28:73–101

Moyà-Solà S (1983) Los Boselaphini (Bovidae Mammalia) del Neógeno de la península Ibérica. Universitat Autònoma de Barcelona, Bellaterra

Ogg JG (2020) Geomagnetic Polarity Time Scale. In: Gradstein FM, Ogg JG, Schmitz MD, Ogg GM (eds). Geologic Time Scale 2020. Elsevier, Amsterdam, pp 159–192.

Owen R (1848) Description of teeth and portions of jaws of two extinct Anthracotherioid quadrupeds (*Hyopotamus vectianus* and *Hyop. bovinus*) discovered by the Marchioness of Hastings in the Eocene deposits on the N.W. coast of the Isle of Wight: with an attempt to develop Cuvier's idea of the classification of pachyderms by the number of their toes. Quart J Geol Soc Lond 4:103–141

Petter G (1976) Étude d'un nouvel ensemble de petits carnivores du Miocène d'Espagne. Geol Mediterran 3:135–154

Pickford M (2012) Les Suoidea (Artiodactyla) de Sansan : systématique, paléoécologie, biogéographie et biochronologie. In: Peigné S, Sen S (eds). Mammifères de Sansan. Mém Mus Natl Hist Nat 203:249–277

Pickford M (2013a) Reassessment of Dinotheriensande Suoidea: Biochronological and biogeographic implications (Miocene Eppelsheim Formation). Mainz Naturwiss Arch 50:155–193

Pickford M (2013b) *Conohyus simorrensis* (Lartet, 1851) (Suidae, Mammalia) from the Middle Miocene of Carpetana (Madrid, Spain). Spanish J Palaeontol 28:91–102

Pickford M (2013c) Re-assessment of the suids from the Sables marins de Montpellier and selection of a lectotype for *Sus provincialis* Blainville, 1847. Geodiversitas 35:655–689

Pickford M (2014) *Sus valentini* Filhol (1882) from St Gaudens (MN 8–9) France: blighted from the outset but a key to understanding late Middle Miocene Tetraconodontinae (Suidae, Mammalia) of Europe. Mainz Naturwiss Arch 51:167–220

Pickford M (2015) Late Miocene Suidae from Eurasia: *Hippopotamodon* and *Microstonyx* problem revisited. Münch Geowiss Abh A 42:1–126

Pickford M (2016a) Biochronology of European Miocene Tetraconodontinae (Suidae, Artiodactyla, Mammalia) flowing from recent revision of the subfamily. Ann Naturhist Mus Wien A 118:175–244

Pickford M (2016b) Revision of European Hyotheriinae (Suidae) and *Doliochoeridae* (Mammalia). Münch Geowiss Abh A 44:1–270

Pickford M, Laurent Y (2014) Valorisation of palaeontological collections: nomination of a lectotype for *Conohyus simorrensis* (Lartet, 1851), Villefranche d'Astarac, France, and description of a new genus of tetraconodont. Estud Geol 70:e002

Pilgrim G (1925) Presidential address to the geological section of the 12th Indian Science Congress. In: Proceedings of the 12th Indian Science Congress, pp 200–218

Pilgrim GE (1926) The fossil Suidae of India. In: Memoirs of the Geological Survey of India. Palaeontologia Indica 8 (4):1–65.

Robles JM (2014) Miocene Carnivorans from the Vallès-Penedès Basin (NE Iberian Peninsula). Dissertation, Universitat Autònoma de Barcelona, Cerdanyola del Vallès

Robles JM, Alba DM, Fortuny J, De Esteban-Trivigno S, Rotgers C, Balaguer J, Carmona R, Galindo J, Almécija S, Bertó JV, Moyà-Solà S (2013) New craniodental remains of the barbourofelid *Albanosmilus jourdani* (Filhol, 1883) from the Miocene of the Vallès-Penedès (NE Iberian Peninsula) and the phylogeny of the Barbourofelini. J Syst Palaeontol 11:993–1022

Robles JM, Alba DM, Moyà-Solà S, Casanovas-Vilar I, Galindo J, Rotgers C, Almécija S, Carmona R (2010) New craniodental remains of *Trocharion albanense* Major, 1903 (Carnivora, Mustelidae), from the Vallès-Penedès Basin (Middle to Late Miocene, Barcelona, Spain). J Vertebr Paleontol 30:547–562

Roman F (1907) Le Néogène Continental dans la Basse Vallée du Tage (rive droite). 1re Partie—Paléontologie. Commission du Service Géologique du Portugal, Lisbonne

Rotgers C, Alba DM (2011) The genus *Anchitherium* (Equidae: Anchitheriinae) in the Vallès-Penedès Basin (Catalonia, Spain). In: Pérez-García A, Gascó F, Gasulla JM, Escaso F (eds). Viajando a Mundos Pretéritos. Ayuntamiento de Morella, Morella, pp 347–354

Sánchez IM, DeMiguel D, Almécija S, Moyà-Solà S, Morales J, Alba DM (2019) New *Hispanomeryx* (Mammalia, Ruminantia, Moschidae) from Spain and a reassessment of the systematics and paleobiology of the genus *Hispanomeryx* Morales, Moyà-Solà, and Soria, 1981. J Vertebr Paleontol 39:e1602536

Sánchez IM, Morales J (2006) Distribución biocronológica de los Moschidae (Mammalia, Ruminantia) en España. Estud Geol 62:533–546

Santafé Llopis JV (1978a) Rinocerótidos Fósiles de España. Dissertation, Universidad de Barcelona, Barcelona

Santafé Llopis JV (1978b) Revisión de los Rinocerótidos miocénicos del Vallès-Penedès. Acta Geol Hisp 13:43–45

Schmidt-Kittler N (1971) Die obermiozäne Fossillagerstätte Sandelzhausen 3. Suidae (Artiodactyla, Mammalia). Mitt Bayer Staatssamml Paläontol Hist Geol 11:129–170

Smith JB, Dodson P (2003) A proposal for a standard terminology of anatomical notation and orientation in fossil vertebrate dentitions. J Vertebr Paleontol 23:1–12

Stehlin HG (1899) Ueber die Geschichte des Suiden-Gebisses. Erster Teil. Abh Schweiz Paläontol Ges 26:1–336

Stehlin HG (1900) Ueber die Geschichte des Suiden-Gebisses. Zweiter Teil. Abh Schweiz Paläontol Ges 27:337–527

Stromer E (1928) Wirbeltiere im obermiocänen Flinz Münchens. Abh Bayer Akad Wiss Math-naturwiss Abteil 32:1–71

Sukselainen L, Fortelius M, Harrison T (2015) Co-occurrence of pliopithecoid and hominoid primates in the fossil record: An ecometric analysis. J Hum Evol 84:25–41

Thaung-Htike, Tsubamoto T, Takai M, Egi N, Zin-Maung-Maung-Thein, Chit-Sein, Maung-Maung (2006) Discovery of *Propotamochoerus* (Artiodactyla, Suidae) from the Neogene of Myanmar. Asian Paleprimatol 4:173–185

Thenius E (1956) Die Suiden und Tayassuiden des steirischen Tertiärs. Beiträge zur Kenntnis der Säugetierreste des steirischen Tertiärs VIII. Sitz Österr Akad Wiss Math-naturwiss Kl 165:337–382

Van den Hoek Ostende LW, Furió M (2005) Spain. In: Van den Hoek Ostende LW, Doukas CS, Reumer JWF (eds). The Fossil Record of the Eurasian Neogene Insectivores (Erinaceomorpha, Soricomorpha, Mammalia), Part I. Scripta Geol Special Issue 5:149–284

Van der Made J (1989) A *Conohyus*-lineage (Suidae, Artiodactyla) from the Miocene of Europe. Rev Esp Paleontol 4:19–28

Van der Made J (1990a) Iberian Suoidea. Paleontol Evol 23:83–97

Van der Made J (1990b) A range-chart for European Suidae and Tayassuidae. Paleontol Evol 23:99–104

Van der Made J (1996a) *Albanohyus*, a small Miocene pig. Acta Zool Cracov 39:293–303

Van der Made J (1996b) Listriodontinae (Suidae, Mammalia), their evolution, systematics and distribution in time and space. Contrib Tert Quater Geol 33:3–254

Van der Made J (1997) Los Suoidea de la Península Ibérica. In: Calvo JP, Morales J (eds). Avances en el Conocimiento del Terciario Ibérico. Cuenca, pp 109–112

Van der Made J (1998) *Aureliachoerus* from Oberdorf and other Aragonian pigs from Styria. Ann Naturhist Mus Wien 99A:225–277

Van der Made J (1999) Biometrical trends in the Tetraconodontinae, a subfamily of pigs. Trans R Soc Edinburgh Earth Sci 89:199–225

Van der Made J (2010) The pigs and "Old World peccaries" (Suidae and Palaeochoeridae, Suoidea, Artiodactyla) from the Miocene of Sandelzhausen (southern Germany): phylogeny and an updated classification of the Hyotheriinae and Palaeochoeridae. Paläontol Zeits 84:43–121

Van der Made J (2020) The Suoidea from the Middle Miocene of Gračanica (Bugojno Basin, Bosnia and Herzegovina)—evolution, taxononomy, and biostratigraphy. Palaeobiodiv Palaeoenvir 100:321–349

Van der Made J, Aiglstorfer M, Böhme M (2014) Taxonomic study of the pigs (Suidae, Mammalia) from the late Middle Miocene of Gratkorn (Austria, Syria). Palaeobiodiv Palaeoenvir 94:595–617

Van der Made J, Krakhmalnaya T, Kubiak H (1999) The pig *Propotamochoerus palaeochoerus* from the Upper Miocene of Grytsiv, Ukraine. Estud Geol 55:283–292

Van der Made J, Montoya P, Alcalá L (1992) *Microstonyx* (Suidae, Mammalia) from the Upper Miocene of Spain. Geobios 25:395–413

Van der Made J, Moyà-Solà S. (1989) European Suinae (Artiodactyla) from the Late Miocene onwards. Boll Soc Paleontol Ital 28:329–339

Van der Made J, Tuna V (1999) A tetraconodontine pig from the Upper Miocene of Turkey. Trans R Soc Edinburgh Earth Sci 89:227–230

Villa A, Delfino M, Luján ÀH, Almécija S, Alba DM (2019) First record of *Latonia gigantea* (Anura, Alytidae) from the Iberian Peninsula. Hist Biol 31:371–382

von Meyer H (1834) Die fossilen Zähne und Knochen und ihre Ablagerung in der Gegen von Georgensmünd in Bayern. J. D. Sauerländer, Frankfurt am Mein

von Meyer H (1846) Mittheilungen an Professor Bronn gerichtet. N Jb Min Geol Geog Petref 1846:462–476

Zapfe H (1949) Die Säugetierfauna aus dem Unterpliozän von Gaiselberg bei Zistersdorf in Niederösterreich. Jb Geol Bundes 93:83–97

Figure captions

Fig. 1 a. Ortophotomap showing the location of Castell de Barberà (CB) and nearby toponyms, modified from Alba et al. (2019: fig. 2A), base map © Institut Cartogràfic i Geològic de Catalunya under CC BY 4.0 license. **b**. Excavation of layer CB-D (where the main fossiliferous level was originally situated) during 2015, reproduced from Alba et al. (2019: fig. 2B). **c**. Location (left inset) and simplified geological map of the Vallès-Penedès Basin indicating the situation of CB (black star), reproduced from Alba et al. (2019: fig. 3).

Fig. 2 Suid maxillary remains from Castell de Barberà. **a.** IPS33308a, palate with R P3–P4 and M2–M3 and L P3–M3 of *Propotamochoerus palaeochoerus*, in occlusal (*left*), right lateral (*right above*), and left lateral (*right below*) views; **b**. IPS1751–IPS1760, upper postcanine dentition of a single individual of *P. palaeochoerus*, including L P2 (IPS1760), R P2–P3 (IPS1755), L P4 (IPS1754), R P4 (IPS1759), L M1 (IPS1758), R M1 (IPS1753), L M2 (IPS1757), R M2 (IPS1752), L M3 (IPS1756), and R M3 (IPS1751) in occlusal view (*left and middle*), as well as R P2–P3 in lingual (*right above*) and buccal (*right below*) views; **c**. IPS1712, L maxillary fragment with DP2–M1 of *Versoporcus steinheimensis*, in occlusal (*left*), lingual (*right above*), and buccal (*right below*) views; **d**. IPS92379, R maxillary fragment with P4 of *P. palaeochoerus*, in occlusal (*left*), lingual (*middle*), and buccal (*right*) views; **e**. IPS93159, L maxillary fragment with P2 and partial P1 alveolus of *P. palaeochoerus*, in occlusal (*left*), lingual (*middle*), and buccal (*right*) views. Scale bar equals 1 cm.

Fig. 3 Suid permanent upper incisors from Castell de Barberà. Each specimen is depicted (from left to right) in lingual, mesial, labial, and distal views. **a**. IPS1717, R I1 of *Propotamochoerus palaeochoerus*; **b**. IPS93091, R I1 of *P. palaeochoerus*; **c**. IPS93087, L I1 of *P. palaeochoerus*; **d**. IPS1749, L I1 of *Parachleuastochoerus*

valentini; **e**. IPS100375, L I1 of *Pa. valentini*; **f**. IPS93085, L I1 of *Pa. valentini*; **g**. IPS92709 L I1 germ of *Pa. valentini*; **h**. IPS1719, R I2 of *P. palaeochoerus*; **i**. IPS92857, L I2 of *Pa. valentini*; **j**. IPS92710, L I2 of *Pa. valentini*; **k**. IPS33287a, L I3 of *P. palaeochoerus*; **l**. IPS92661, L I3 of *P. palaeochoerus*. Scale bar equals 1 cm.

Fig. 4 Suid permanent upper canines of female individuals from Castell de Barberà. Each specimen is depicted (from left to right) in lingual, mesial, labial, and distal views. **a**. IPS1718, L C1f of *Propotamochoerus palaeochoerus*; **b**. IPS92387, R C1f of *P. palaeochoerus*; **c**. IPS33287b, R C1f of *P. palaeochoerus*; **d**. IPS33287c, L C1f of *P. palaeochoerus*; **e**. IPS93150, R C1f of *Parachleuastochoerus valentini*; **f**. IPS1715, R C1f of *Pa. valentini*. Scale bar equals 1 cm.

Fig. 5 Suid permanent upper premolars from Castell de Barberà. Anterior premolars (P1s and P2s) and some P3s are depicted (from left to right) in occlusal (mesial on top), lingual, and buccal views, whereas other P3s and all P4s are depicted in occlusal view only. **a**. IPS33287d, R P1 of *Propotamochoerus palaeochoerus*; **b**. IPS33287e, L P1 of *P. palaeochoerus*; **c**. IPS92392a, R P1 of *P. palaeochoerus*; **d**. IPS92392b, L P1 of *P. palaeochoerus*; **e**. IPS92699, L P1 of *P. palaeochoerus*; **f**. IPS92695, L P1 of *P. palaeochoerus*; **g**. IPS92700, L P1 crown of *P. palaeochoerus*; **h**. IPS93107, L P1 crown of *Parachleuastochoerus valentini*; **i**. IPS93100, R P1 of *Pa. valentini*; **j**. IPS1760, L P2 of *P. palaeochoerus*; **k**. IPS92697, L P2 of *P. palaeochoerus*; **l**. IPS92788, R P2 of *P. palaeochoerus*; **m**. IPS1755, R P2 of *P. palaeochoerus*; **n**. IPS92848, R P2 distal fragment of *P. palaeochoerus*; **o**. IPS33287f, R P2 of *P. palaeochoerus*; **p**. IPS93159, L P2 of *P. palaeochoerus*; **q**. IPS92692, L P2 distal fragment of *V. steinheimensis*; **r–s**. IPS33308a, R (**r**) and L (**s**) P3 of *P. palaeochoerus*; **t**. IPS1755, R P3 of *P. palaeochoerus*; **u**. IPS92787, R P3 of *P. palaeochoerus*; **v**. IPS33288, L P3 of *P. palaeochoerus*; **w**. IPS93081, R P3 of *P. palaeochoerus*; **x**. IPS93101, damaged R P3 of *Pa. valentini*; **y**. IPS93112, partial R P3 of *Pa. valentini*; **z**. IPS1759, R P4 of *P. palaeochoerus*; **a'**. IPS1754 L P4 of *P. palaeochoerus*; **b'**. IPS92380, L P4 of *P. palaeochoerus*; **c'**. IPS92379, R P4 of *P. palaeochoerus*; **d'**. IPS93158, L P4 crown of *P. palaeochoerus*; **e'**. IPS33294, partial L P4 of *P. palaeochoerus*; **f'–g'**. IPS33308a, R (**f'**) and L (**g'**) of *P. palaeochoerus*; **h'–i'**. IPS33289, R (**h'**) and L (**i'**) P4 of *P. palaeochoerus*; **j'**. IPS92737, R P4 of *P. palaeochoerus*; **k'**. IPS92747, damaged L P4 of *Pa. valentini*; **l'**. IPS33269a, damaged R P4 of *Pa. valentini*; **m'**. IPS33269b, damaged L P4 of *Pa. valentini*; **n'**. IPS92746, R P4 of *V. steinheimensis*; **o'**. IPS33265, L P4 of *V. steinheimensis*. Scale bar equals 1 cm.

Fig. 6 Suid upper molars from Castell de Barberà, in occlusal view (mesial on top). **a**. IPS33289, L M1 of *Propotamochoerus palaeochoerus*; **b**. IPS1753, R M1 of *P. palaeochoerus*; **c**. IPS1758, L M1 of *P. palaeochoerus*; **d**. IPS92381, L M1 crown of *P. palaeochoerus*; **e**. IPS33302, L M1 mesial fragment of *P. palaeochoerus*; **f**. IPS92850, R M1 distal fragment of *P. palaeochoerus*; **g**. IPS93157, damaged R M1 crown of *Parachleuastochoerus valentini*; **h**. IPS93155, damaged L M1 of *Pa. valentini*; **i**. IPS33296a, R M1 of *Pa. valentini*; **j**. IPS33296b, L M1 of *Pa. valentini*; **k**. IPS33269c, L M1 of *Pa. valentini*; **l**. IPS92843, R M1 of *Pa. valentini*; **m**. IPS93156, damaged R M1 of *Pa. valentini*; **n**. IPS93096, partial L M1 of *Pa. valentini*; **o**. IPS92764, R M1 distal fragment of *Pa. valentini*; **p**. IPS1712, L M1 of *Versoporcus steinheimensis*; **q**. IPS33297b, L M1 germ of *V. steinheimensis*; **r**. IPS33289d, R M2 of *P. palaeochoerus*; **s**. IPS33289e, L M2 of *P. palaeochoerus*; **t**. IPS1752, R M2 of *P. palaeochoerus*; **u**. IPS1757, L M2 of *P. palaeochoerus*; **v**. IPS33308a,

R M2 of *P. palaeochoerus*; **w**. IPS92840, L M2 of *P. palaeochoerus*; **x**. IPS93093, L M2 lingual fragment of *P. palaeochoerus*; **y**. IPS33296c, R M2 of *Pa. valentini*; **z**. IPS92842, L M2 of *Pa. valentini*; **a'**. IPS92367, L M2 germ distal end of *Pa. valentini*; **b'–c'**. IPS33289, R (**b'**) and L (**c'**) M3 of *P. palaeochoerus*; **d'**. IPS1751, R M3 of *P. palaeochoerus*; **e'**. IPS1756, L M3 of *P. palaeochoerus*; **f'**. IPS125636, R M3 of *P. palaeochoerus*; **g'**. IPS125637, L M3 of *P. palaeochoerus*; **h'**. IPS125638, damaged R M3 of *P. palaeochoerus*; **i'–j'**. IPS33308a, R (**i'**) and L (**j'**) M3 of *P. palaeochoerus*; **k'**. IPS125640, partial L M3 of *P. palaeochoerus*; **l'**. IPS33296d, R M3 of *Pa. valentini*; **m'**. IPS33296e, L M3 of *Pa. valentini*; **n'**. IPS33237, R M3 of *Pa. valentini*; **o'**. IPS125635, R M3 of *Pa. valentini*; **p'**. IPS125639, partial R M3 f *Pa. valentini*; **q'**. IPS93094 L M3 of *Pa. valentini*; **r'**. IPS93095 damaged R M3 of *Pa. valentini*; **s'**. IPS92759 partial L M3 of *Pa. valentini*; **t'**. IPS33270 R M3 mesial fragment of *Pa. valentini*; **u'**. IPS92841, L M3 distolingual fragment of *Pa. valentini*; **v'**. IPS33300, L M3 of *V. steinheimensis*; **w'**. IPS33309, L M3 of *V. steinheimensis*; **x'**. IPS93070, R M3 of *V. steinheimensis*; **y'**. IPS33303, R M3 of *V. steinheimensis*; **z'**. IPS33301 L M3 of *V. steinheimensis*; **a''**. IPS92383, R M3 *V. steinheimensis*. Scale bar equals 1 cm.

Fig. 7 Suid mandibular remains from Castell de Barberà. **a**. IPS33286, L mandibular fragment with dp3 of *Propotamochoerus palaeochoerus*, in occlusal (*left*), lingual (*middle*), and buccal (*right*) views; **b**. IPS93147, R mandibular fragment with p2 roots and p3–p4 of *P. palaeochoerus*, in occlusal (*left*), lingual (*middle*), and buccal (*right*) views; **c**. IPS33308b, edentulous L mandibular fragment with m1–m3 alveoli of *P. palaeochoerus*, in occlusal (*left*), lingual (*right above*), and buccal (*right below*) views; **d**. IPS87621, R mandibular fragment with m2 of *P. palaeochoerus*, in occlusal (*left*), lingual (*right above*), and buccal (*right below*) views; **e**. IPS93146a, R mandibular fragment with m1–m3 of *P. palaeochoerus*, in occlusal (*left*), lingual (*right above*), and buccal (*right below*) views; **f**. IPS93146b, L mandibular fragment with m3 of *P. palaeochoerus*, in occlusal (*left*), lingual (*right above*), and buccal (*right below*) views; **g**. IPS1713, L mandibular fragment with p2–m3 of *Versoporcus steinheimensis*, in occlusal (*left*), lingual (*right above*), and buccal (*right below*) views; **h**. IPS33240, L mandibular fragment with m1–m3 of *V. steinheimensis*, in occlusal (*left*), lingual (*right above*), and buccal (*right below*) views. Scale bar equals 1 cm.

Fig. 8 Suid permanent lower incisors from Castell de Barberà. Each specimen is depicted (from left to right) in lingual, mesial, labial, and distal views. **a**. IPS93088 L i1 crown of *Propotamochoerus palaeochoerus*; **b**. IPS93089 R i1 of *P. palaeochoerus*; **c**. IPS93090 L i1 of *P. palaeochoerus*; **d**. IPS1716, L i1 of *P. palaeochoerus*; **e**. IPS93152, R i1 of *V. steinheimensis*; **f**. IPS92815, R i2 of *P. palaeochoerus*; **g**. IPS1721, L i2 of *P. palaeochoerus*; **h**. IPS92406, L i2 of *P. palaeochoerus*; **i**. IPS35103, L i2 of *P. palaeochoerus*; **j**. IPS92738, L i2 crown of *Parachleuastochoerus valentini*; **k**. IPS92739, R i2 of *Pa. valentini*; **l**. IPS92374, L i2 crown of *Pa. valentini*; **m**. IPS92373, R i2 of *Pa. valentini*; **n**. IPS33290, R i2 of *V. steinheimensis*; **o**. IPS93103, R i3 of *Pa. valentini*; **p**. IPS92861 L i3 germ of *Pa. valentini*; **q**. IPS92672 R i3 germ of *Pa. valentini*; **r**. IPS92708 L i3 crown of *Pa. valentini*; **s**. IPS93078, R i3 crown of *Pa. valentini*; **t**. IPS92862 L i3 crown of *Pa. valentini*; **u**. IPS93077, R i3 of *V. steinheimensis*. Scale bar equals 1 cm.

Fig. 9 Suid permanent lower canines from Castell de Barberà. Each specimen is depicted (from left to right) in lingual, mesial, labial, and distal views. **a**. IPS92656, L c1m tip of *Propotamochoerus palaeochoerus*; **b**.

IPS93079, R c1m of *V. steinheimensis*; **c**. IPS92657, L c1m fragment of *V. steinheimensis*; **d**. IPS1722, L c1f of *P. palaeochoerus*; **e**. IPS93086, R c1f of *P. palaeochoerus*; **f**. IPS93084, L c1f of *Parachleuastochoerus valentini*; **g**. IPS1723, R c1f of *Pa. valentini*. Scale bar equals 1 cm.

Fig. 10 Suid permanent lower premolars from Castell de Barberà. Each specimen is depicted (from left to right) in occlusal (mesial on top), lingual, and buccal views. **a**. IPS33304, R p1 of *Propotamochoerus palaeochoerus*; **b**. IPS39522, L p1 of *P. palaeochoerus*; **c**. IPS92385, L p1 of *P. palaeochoerus*; **d**. IPS93104, L p1 of *Parachleuastochoerus valentini*; **e**. IPS92763, R p1 of *Pa. valentini*; **f**. IPS92726, L p1 germ of *Pa. valentini*; **g**. IPS92669, L p1 crown of *Pa. valentini*; **h**. IPS92670, partial R p1 of *Pa. valentini*; **i**. IPS92678, R p1 crown of *V. steinheimensis*; **j**. IPS92671, R p1 of *V. steinheimensis*; **k**. IPS92694, L p2 of *P. palaeochoerus*; **l**. IPS92698, R p2 of *P. palaeochoerus*; **m**. IPS92720, L p2 crown of *V. steinheimensis*; **n**. IPS92723, partial L p2 of *V. steinheimensis*; **o**. IPS1713, L p2 of *V. steinheimensis*; **p**. IPS92679, R p2 distal fragment of *V. steinheimensis*; **q**. IPS93147, R p3 of *P. palaeochoerus*; **r**. IPS92396, R p3 distal fragment of *P. palaeochoerus*; **s**. IPS92395, R p3 of *P. palaeochoerus*; **t**. IPS1713, L p3 of *V. steinheimensis*; **u**. IPS93154, L p4 of *P. palaeochoerus*; **v**. IPS93147, R p4 of *P. palaeochoerus*; **w**. IPS92382, L p4 crown of *P. palaeochoerus*; **x**. IPS92415, R p4 of *P. palaeochoerus*; **y**. IPS92416, L p4 distal fragment of *P. palaeochoerus*; **z**. IPS92719, L p4 of *Pa. valentini*; **a'**. IPS93082, L p4 partial germ of *Pa. valentini*; **b'**. IPS1713, L p4 of *V. steinheimensis*; **c'**. IPS92867, L p4 of *V. steinheimensis*; **d'**. IPS93106 R p4 mesial fragment of *V. steinheimensis*. Scale bar equals 1 cm.

Fig. 11 Suid permanent lower molars from Castell de Barberà, in occlusal view (mesial on top). **a**. IPS93146a, R m1 of *Propotamochoerus palaeochoerus*; **b**. IPS92760, damaged R m1 of *P. palaeochoerus*; **c**. IPS92732, R m1 germ of *P. palaeochoerus*; **d**. IPS92400, L m1 of *Parachleuastochoerus valentini*; **e**. IPS92375, L m1 of *Pa. valentini*; **f**. IPS33297a, L m1 germ of *Versoporcus steinheimensis*; **g**. IPS33305, R m1 germ of *V. steinheimensis*; **h**. IPS92852, L m1 distal fragment of *V. steinheimensis*; **i**. IPS1713, L m1 of *V. steinheimensis*; **j**. IPS33240, L m1 of *V. steinheimensis*; **k**. IPS93146a, R m2 of *P. palaeochoerus*; **l**. IPS92391, R m2 of *P. palaeochoerus*; **m**. IPS87621, R m2 of *P. palaeochoerus*; **n**. IPS92402, R m2 of *Pa. valentini*; **o**. IPS33291, R m2 of *V. steinheimensis*; **p**. IPS92761, L m2 distal fragment of *V. steinheimensis*; **q**. IPS1713, L m2 of *V. steinheimensis*; **r**. IPS33240, L m2 of *V. steinheimensis*; **s**. IPS93146a, R m3 of *P. palaeochoerus*; **t**. IPS93146b, L m3 of *P. palaeochoerus*; **u**. IPS33285, R m3 of *P. palaeochoerus*; **v**. IPS33254, L m3 of *Pa. valentini*; **w**. IPS33282, damaged L m3 of *V. steinheimensis*; **x**. IPS92718, R m3 distal fragment of *V. steinheimensis*; **y**. IPS1713, L m3 of *V. steinheimensis*; **z**. IPS33240, L m3 of *V. steinheimensis*. Scale bar equals 1 cm.

Fig. 12 Suid deciduous upper teeth from Castell de Barberà. Incisors are depicted (from left to right) in lingual, mesial, labial, and distal views, whereas DP2s are illustrated (from left to right) in occlusal (mesial on top), lingual, and buccal views, and DP3s and DP4s in occlusal view (mesial on top) only. **a**. IPS92856, L DI1 of *Propotamochoerus palaeochoerus*; **b**. IPS92858, R DI1 of *P. palaeochoerus*; **c**. IPS92863, L DI1 of *Parachleuastochoerus valentini*; **d**. IPS92864, R DI1 of *Pa. valentini*; **e**. IPS92865, L DI1 of *Pa. valentini*; **f**. IPS92398, L DI1 of *Pa. valentini*; **g**. IPS92384, R DI2 crown of *P. palaeochoerus*; **h**. IPS92859, R DI2 crown of *P. palaeochoerus*; **i**. IPS92866, R DI2 of *P. palaeochoerus*; **j**. IPS92860, L DI2 germ of *P. palaeochoerus*; **k**. IPS92711, L DI3 of *P. palaeochoerus*; **l**. IPS92691, R DI3 crown of *P. palaeochoerus*; **m**. IPS92696, L DP2 of

P. palaeochoerus; **n**. IPS92693 L DP2 of *P. palaeochoerus*; **o**. IPS92401, partial R DP2 of *P. palaeochoerus*; **p**. IPS93110, R DP2 of *Pa. valentini*; **q**. IPS93105, R DP2 of *Pa. valentini*; **r**. IPS1712, L DP2 of *Versoporcus steinheimensis*; **s**. IPS93108, R DP2 of *V. steinheimensis*; **t**. IPS93109, L DP2 of *Versoporcus steinheimensis*; **u**. IPS92412, L DP3 germ of *P. palaeochoerus*; **v**. IPS92405, L DP3 germ of *P. palaeochoerus*; **w**. IPS92397, L DP3 crown of *P. palaeochoerus*; **x**. IPS92846, L DP3 of *P. palaeochoerus*; **y**. IPS92413, L DP3 of *P. palaeochoerus*; **z**. IPS92839, R DP3 distal fragment of *P. palaeochoerus*; **a'**. IPS33264, R DP3 of *Pa. valentini*; **b'**. IPS93102, R DP3 of *Pa. valentini*; **c'**. IPS93099, R DP3 of *Pa. valentini*; **d'**. IPS93097, partial L DP3 of *Pa. valentini*; **e'**. IPS93111, L DP3 mesial fragment of *Pa. valentini*; **f'**. IPS92849, L DP3 distal fragment of *Pa. valentini*; **g'**. IPS92806, R DP3 distal fragment of *Pa. valentini*; **h'**. IPS1712, L DP3 of *V. steinheimensis*; **i'**. IPS92722, L DP3 of *V. steinheimensis*; **j'**. IPS92735, R DP3 of *V. steinheimensis*; **k'**. IPS93098, damaged L DP3 of *V. steinheimensis*; **l'**. IPS92414, R DP3 mesial fragment of *V. steinheimensis*; **m'**. IPS92404, L DP4 germ of *P. palaeochoerus*; **n'**. IPS92407, damaged R DP4 germ of *P. palaeochoerus*; **o'**. IPS33306, L DP4 germ of *P. palaeochoerus*; **p'**. IPS92337, R DP4 germ of *P. palaeochoerus*; **q'**. IPS92410, damaged L DP4 of *P. palaeochoerus*; **r'**. IPS92408, L DP4 of *P. palaeochoerus*; **s'**. IPS92734, L DP4 of *P. palaeochoerus*; **t'**. IPS92411, R DP4 crown of *Pa. valentini*; **u'**. IPS33272, partial L DP4 of *Pa. valentini*; **v'**. IPS92399, partial L DP4 of *Pa. valentini*; **w'**. IPS1712, L DP4 of *V. steinheimensis*; **x'**. IPS33299, R DP4 of *V. steinheimensis*; **y'**. IPS92409, L DP4 of *V. steinheimensis*. Scale bar equals 1 cm.

Fig. 13 Suid deciduous lower teeth from Castell de Barberà. Incisors are depicted (from left to right) in lingual, mesial, labial, and distal views, whereas dp2s and dp3s are illustrated (from left to right) in occlusal (mesial on top), lingual, and buccal views, and dp4s in occlusal view (mesial on top) only. **a**. IPS33277a, R di1 of *Propotamochoerus palaeochoerus*; **b**. IPS33277b, L di1 of *P. palaeochoerus*; **c**. IPS92359, R di1 of *P. palaeochoerus*; **d**. IPS92882, R di1 of *P. palaeochoerus*; **e**. IPS93066, L di1 of *Parachleuastochoerus valentini*; **f**. IPS33276, L di1 germ of *Pa. valentini*; **g**. IPS93069, R di1 germ of *V. steinheimensis*; **h**. IPS93068, L di1 germ of *Versoporcus steinheimensis*; **i**. IPS92701, damaged L di2 of *P. palaeochoerus*; **j**. IPS92703, R di2 of *Pa. valentini*; **k**. IPS92702, R di2 of *V. steinheimensis*; **l**. IPS92704, L di2 partial crown of *V. steinheimensis*; **m**. IPS1750, R di3 of *P. palaeochoerus*; **n**. IPS92690, L di3 of *P. palaeochoerus*; **o**. IPS92885, L di3 of *Pa. valentini*; **p**. IPS92874, L dp2 of *P. palaeochoerus*; **q**. IPS93083, damaged R dp2 of *V. steinheimensis*; **r**. IPS33286, L dp3 of *P. palaeochoerus*; **s**. IPS92881, R dp3 distal fragment of *Pa. valentini*; **t**. IPS92779, partial L dp3 of *V. steinheimensis*; **u**. IPS93153, partial R dp3 of *V. steinheimensis*; **v**. IPS92388, R dp3 germ of *V. steinheimensis*; **w**. IPS28175, L dp4 germ mesial fragment of *P. palaeochoerus*; **x**. IPS92348, R dp4 distal fragment of *P. palaeochoerus*; **y**. IPS92758, L dp4 of *P. palaeochoerus*; **z**. IPS92847, R dp4 distal fragment of *P. palaeochoerus*; **a'**. IPS92731, R dp4 of *Pa. valentini*; **b'**. IPS93149, R dp4 of *V. steinheimensis*; **c'**. IPS93148, L dp4 of *V. steinheimensis*; **d'**. IPS92420, R dp4 distolingual fragment of *V. steinheimensis*; **e'**. IPS92762, R dp4 distal fragment of *V. steinheimensis*. Scale bar equals 1 cm.

Fig. 14 Bivariate plots of BL vs. MD in the deciduous and permanent upper cheek teeth of *Propotamochoerus palaeochoerus* and tetraconodontines from Castell de Barberà as compared with *P. palaeochoerus* and selected tetraconodontines from elsewhere: **a**. DP2; **b**. DP3; **c**. DP4; **d**. P1; **e**. P2; **f**. P3; **g**. P4; **h**. M1; **i**. M2; **j**. M3. Metrical data for the Castell de Barberà remains are reported in Appendix Table 2, while those for the

comparative sample have been taken from the literature (see Material and methods for details on the published sources).

Fig. 15 Bivariate plots of BL vs. MD in the deciduous and permanent lower cheek teeth of *Propotamochoerus palaeochoerus* and tetraconodontines from Castell de Barberà as compared with *P. palaeochoerus* and selected tetraconodontines from elsewhere: **a**. dp2; **b**. dp3; **c**. dp4; **d**. p1; **e**. p2; **f**. p3; **g**. p4; **h**. m1; **i**. m2; **j**. m3. Metrical data for the Castell de Barberà remains are reported in Appendix Table 2, while those for the comparative sample have been taken from the literature (see Material and methods for details on the published sources).


a
Ca n'Altimira
Can Gili
Ripoll River
el Castell
Castell de Barberà
Ca n'Ermengol
* CB
100 m


b

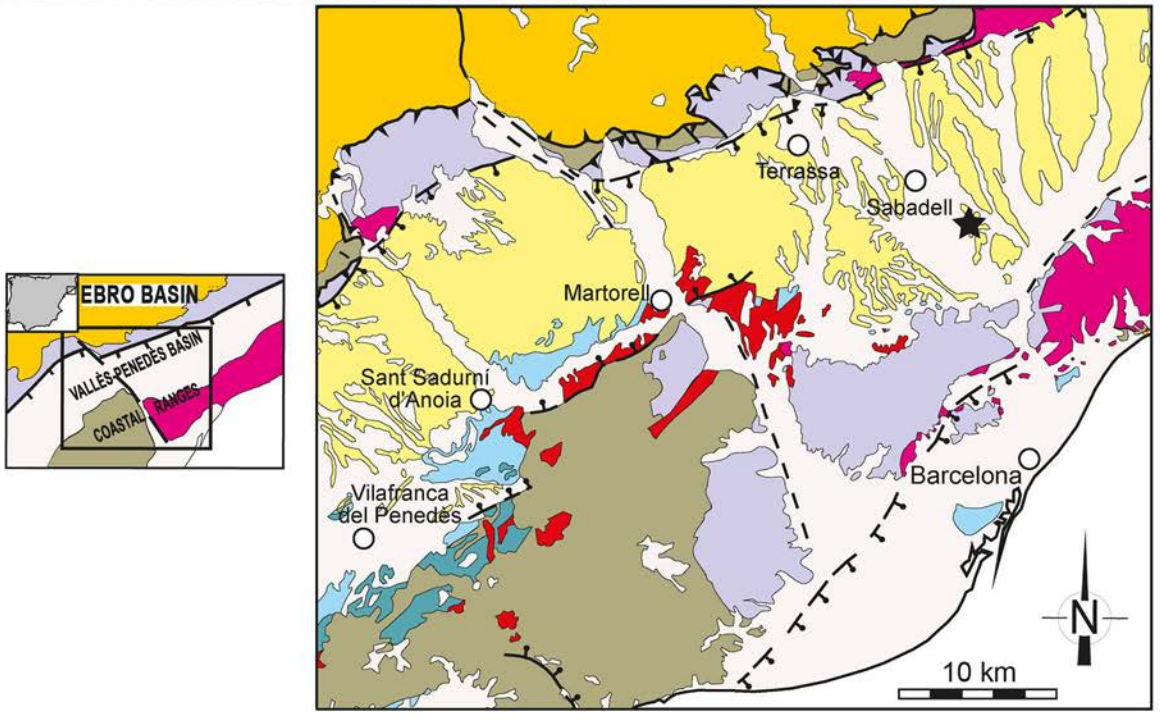
c
EBRO BASIN
VALLÈS-PENEDÈS BASIN
COASTAL RANGES
Terrassa
Sabadell
Martorell
Sant Sadurní d'Anoia
Vilafranca del Penedès
Barcelona
N
10 km
NEOGENE-QUATERNARY
Pliocene and Quaternary sediments
Middle to Late Miocene continental units (Langhian-Tortonian): alluvial fan facies
Miocene marine and transitional units (Late Burdigalian-Langhian): coralgal carbonate facies
Miocene marine and transitional units (Late Burdigalian-Serravallian): marls, silts, bioclastic sands and sandstones
Early Miocene continental units (Early and Late Burdigalian): alluvial fan and shallow lacustrine facies
EBRO FORELAND BASIN INFILL
Paleogene (conglomerates, sandstones, lutites)
PALEOZOIC BASEMENT AND MESOZOIC COVER
Mesozoic (carbonates, sandstones, lutites)
Hercynian intrusive rocks (mostly granitoids)
Paleozoic sedimentary and metamorphic rocks
Fault
Inferred fault
Normal fault
Thrust fault

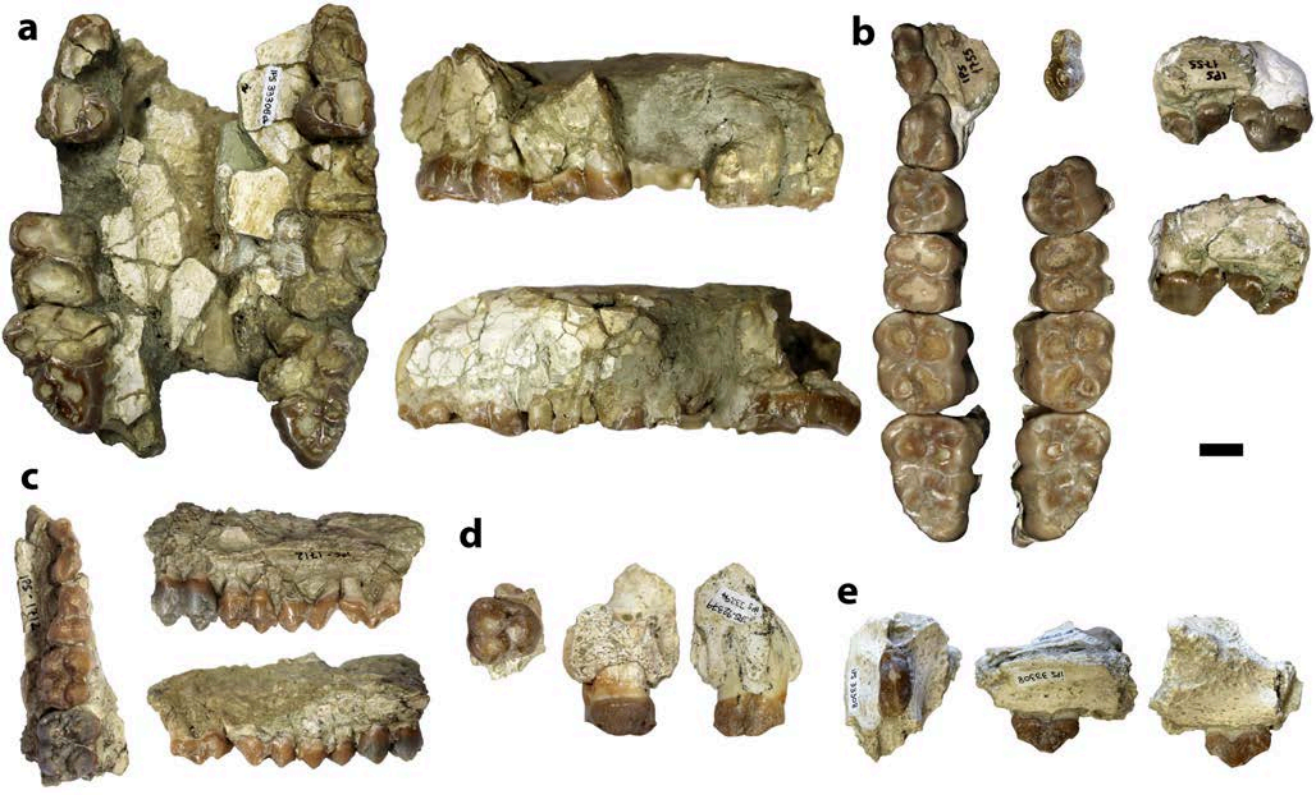
a
b
c
d
e

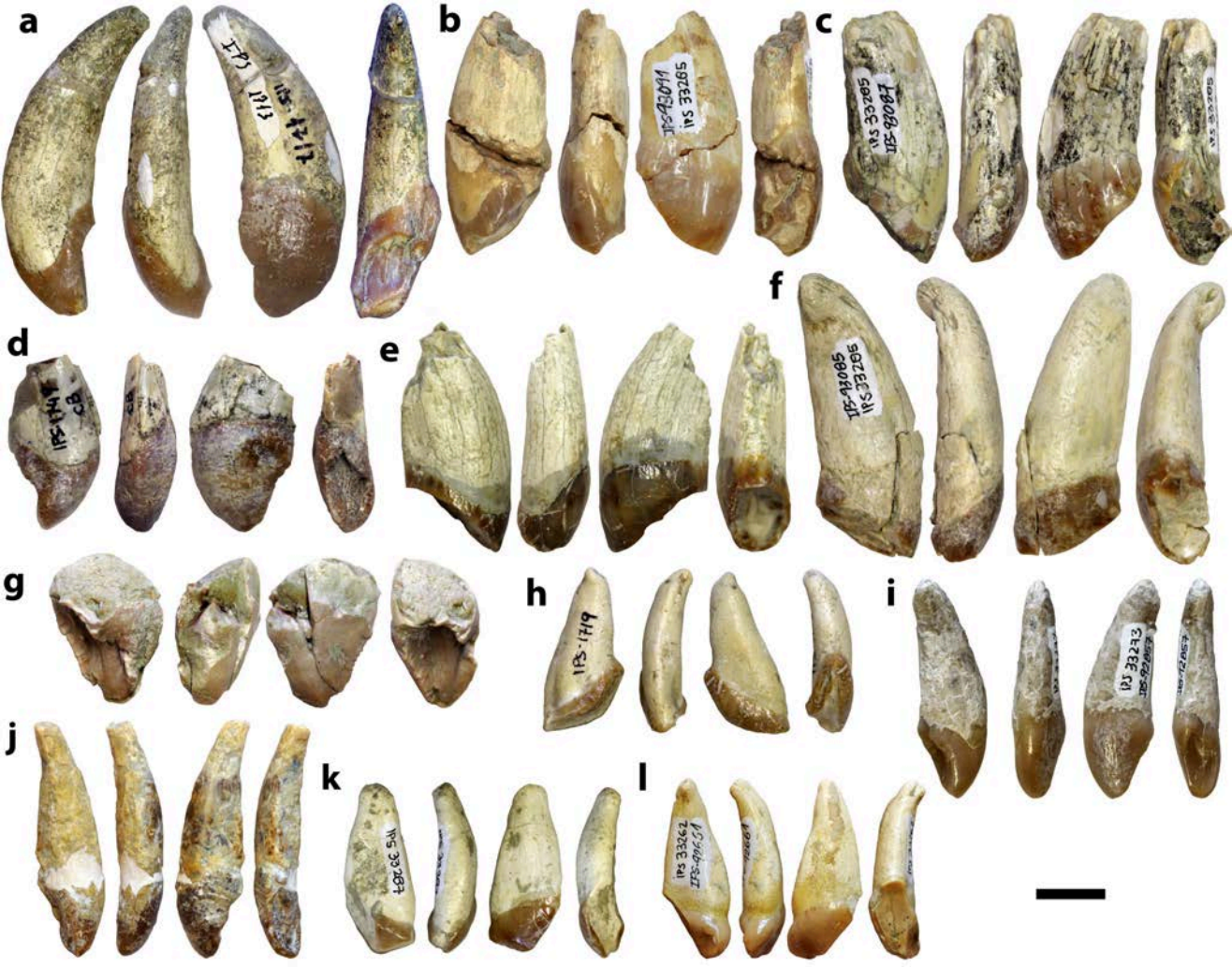
a
b
c
d
e
f
g
h
i
j
k
l

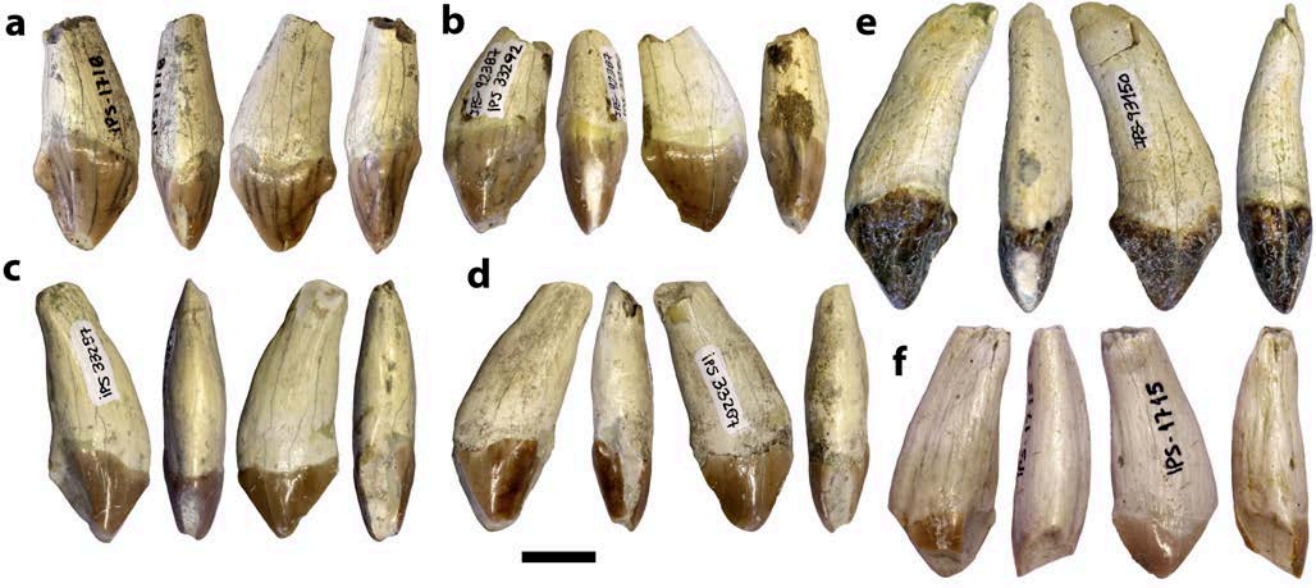
a
b
c
d
e
f
IPS-17116
IPS 33292
IPS 33294
IPS 33293
IPS-91150
IPS-17115


a
b
c
d
e
f
g
h
i
j
k
l
m
n
o
p
q
r
s
t
u
v
w
x
y
z
a′
b′
c′
d′
e′
f′
g′
h′
i′
j′
k′
l′
m′
n′
o′

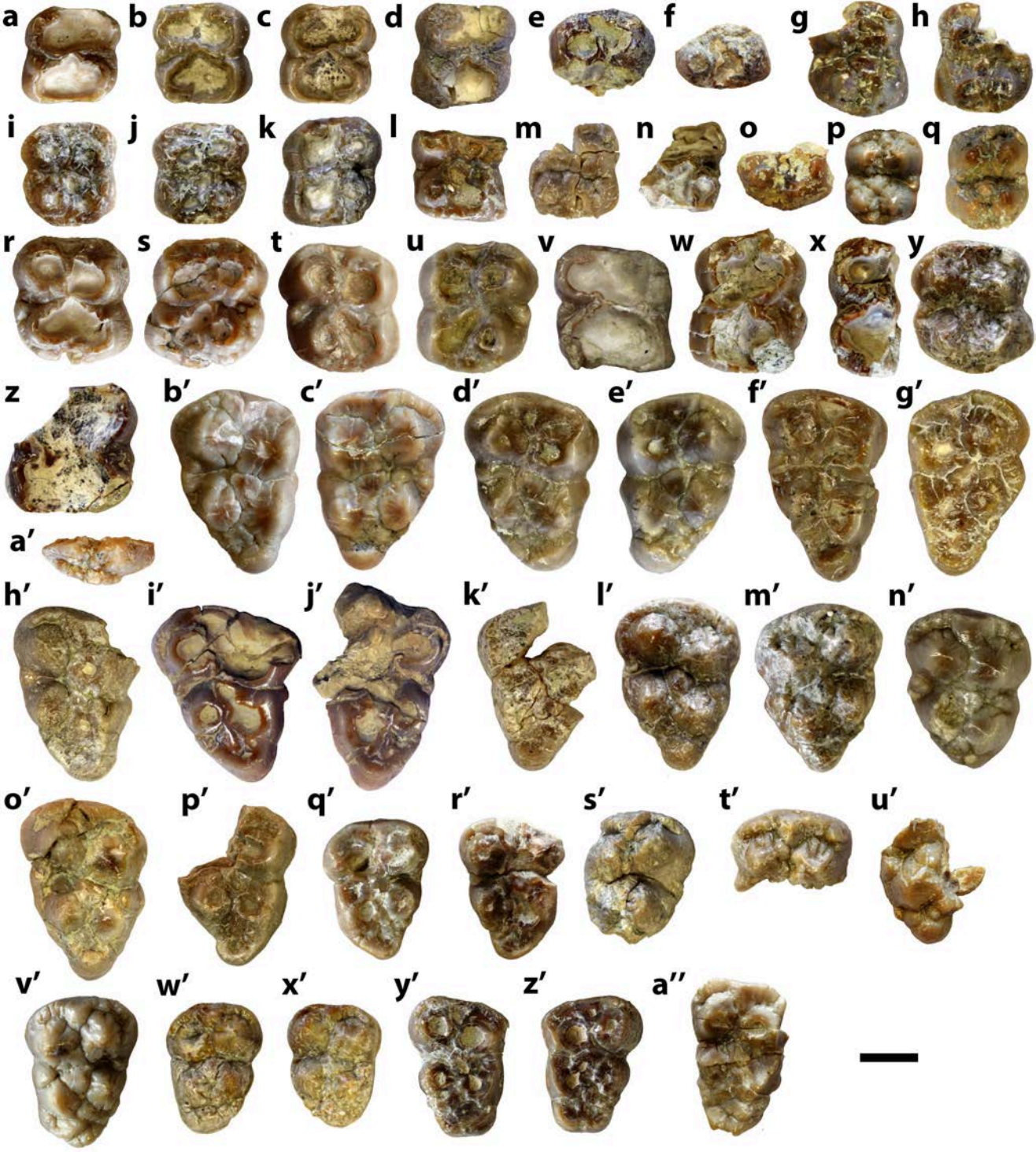
a
b
c
d
e
f
g
h
i
j
k
l
m
n
o
p
q
r
s
t
u
v
w
x
y
z
b′
c′
d′
e′
f′
g′
a′
h′
i′
j′
k′
l′
m′
n′
o′
p′
q′
r′
s′
t′
u′
v′
w′
x′
y′
z′
a″


a
b
c
d
e
f
g
h
IPS 33206
IPS 4521
IPS 33340
IPS 33316
IPS 33308
IPS-1713
IPS 4553
IPS 33240


a
b
c
d
e
f
g
h
i
j
k
l
m
n
o
p
q
r
s
t
u
IPS 1716
IPS 1721


a
b
c
d
e
f
g
IPS-92656
IPS 33262
IPS 33262
IPS-92657
IPS 35103
IPS-1722
IPS-92691
IPS 33263
IPS-1723


a
b
c
d
e
f
g
h
i
j
k
l
m
n
o
p
q
r
s
t
u
v
w
x
y
z
a′
b′
c′
d′

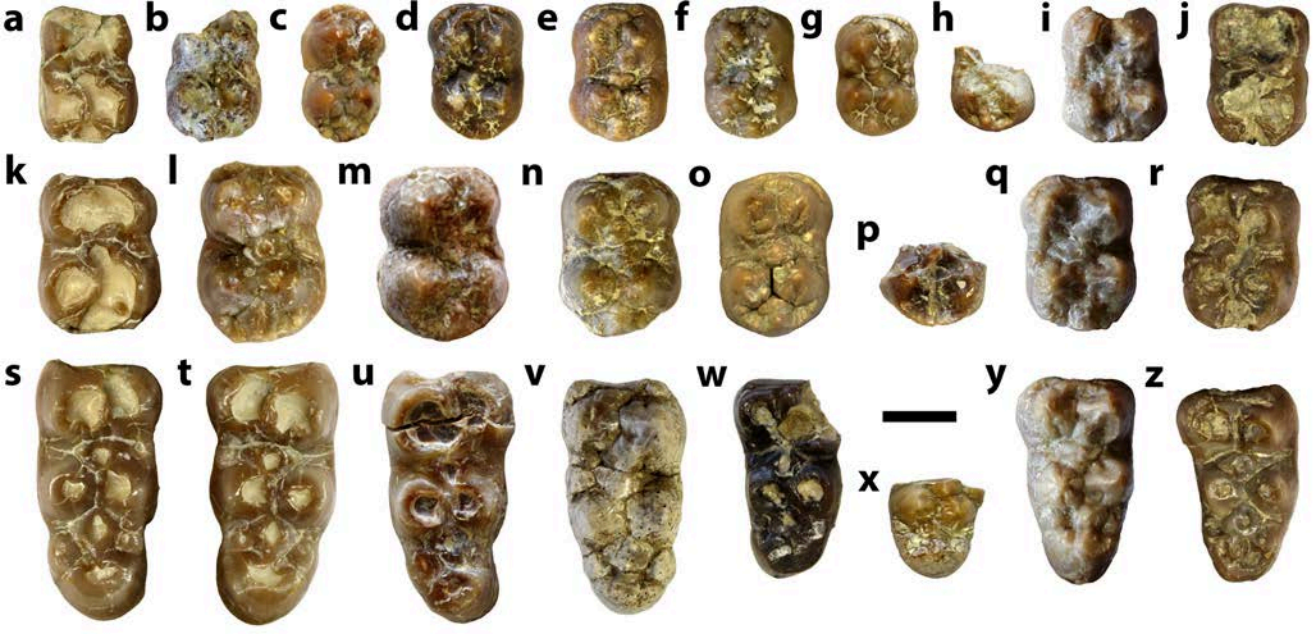
a
b
c
d
e
f
g
h
i
j
k
l
m
n
o
p
q
r
s
t
u
v
w
x
y
z


a
b
c
d
e
f
g
h
i
j
k
l
m
n
o
p
q
r
s
t
u
v
w
x
y
z
a′
b′
c′
d′
e′
f′
g′
h′
i′
j′
k′
l′
m′
n′
o′
p′
q′
r′
s′
t′
u′
v′
w′
x′
y′

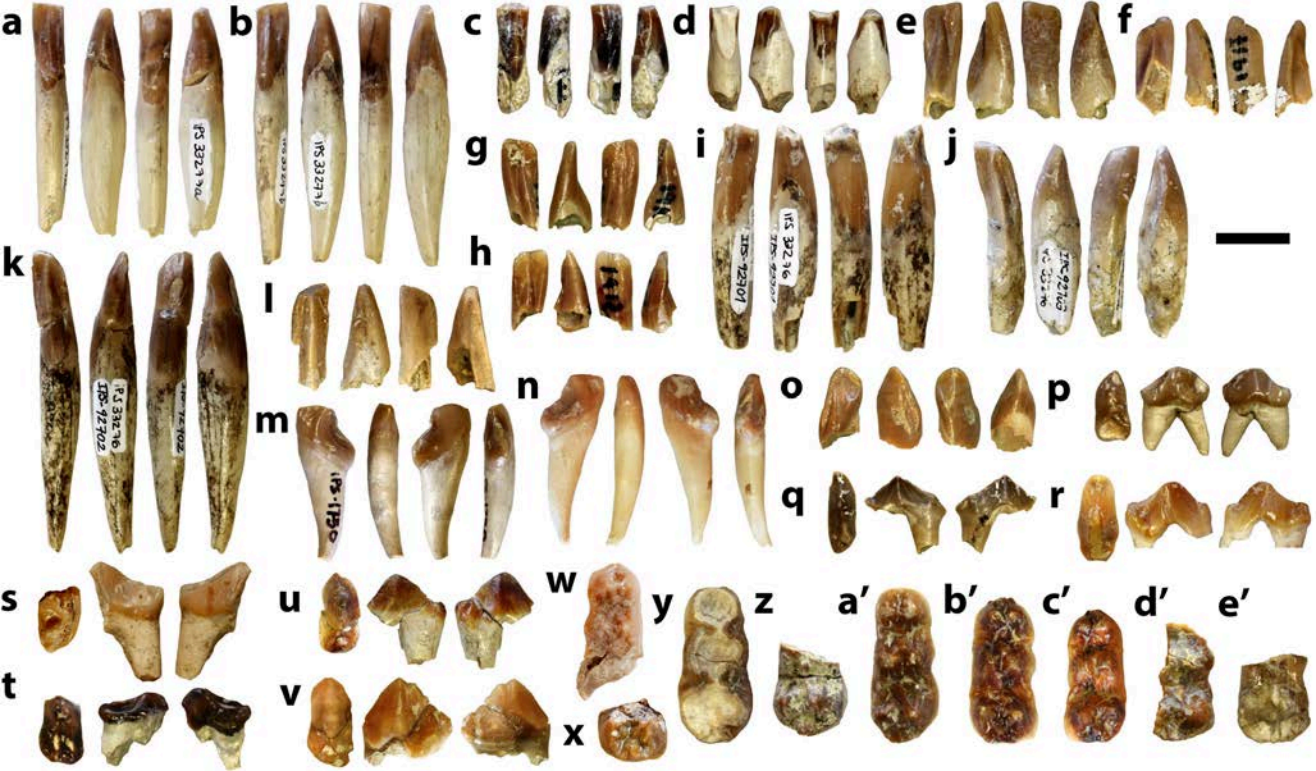
a
b
c
d
e
f
g
h
i
j
k
l
m
n
o
p
q
r
s
t
u
v
w
x
y
z
a′
b′
c′
d′
e′

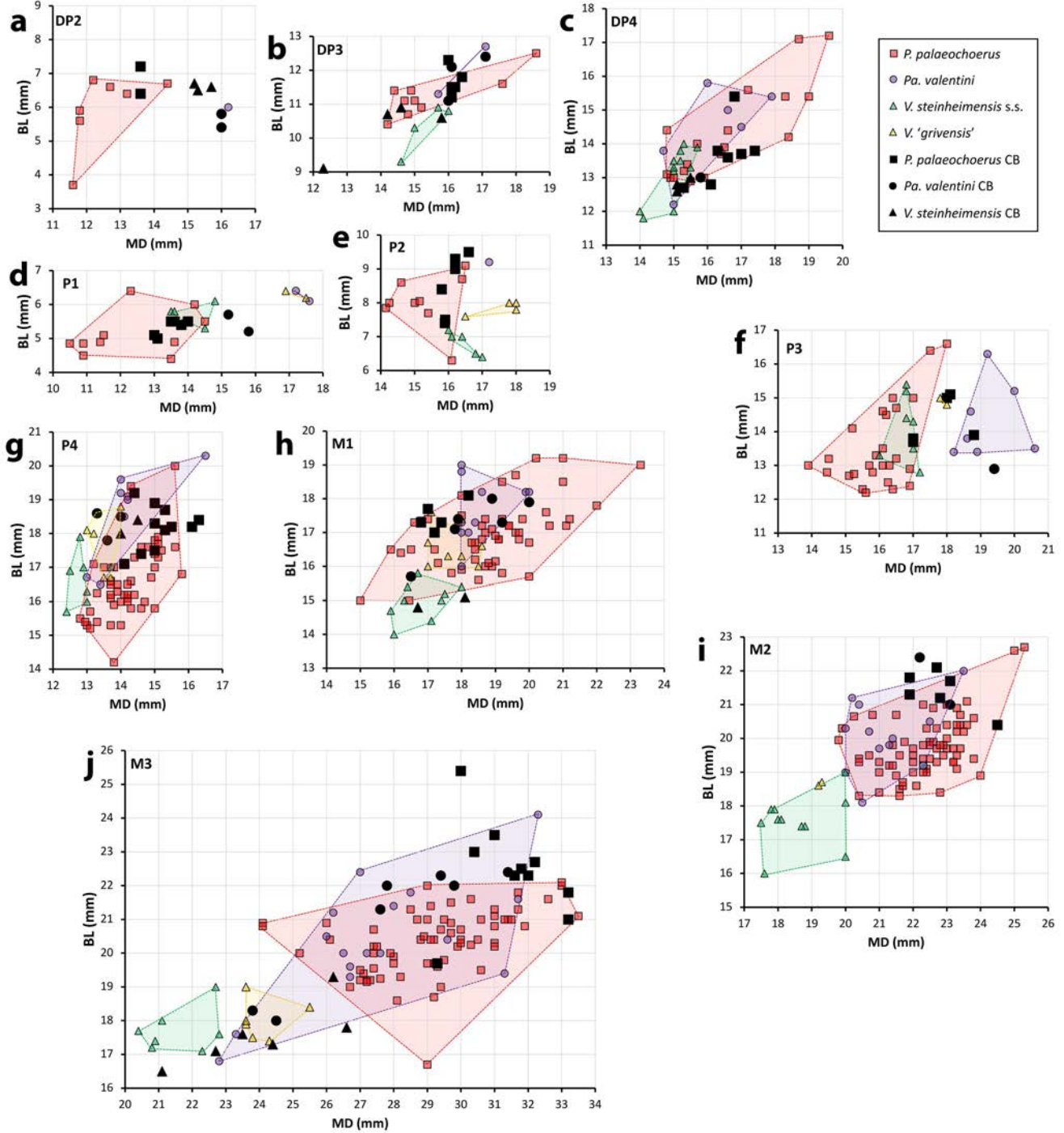
a
DP2
b
DP3
c
DP4
d
P1
e
P2
f
P3
g
P4
h
M1
i
M2
j
M3
BL (mm)
MD (mm)
P. palaeochoerus
Pa. valentini
V. steinheimensis s.s.
V. 'grivensis'
P. palaeochoerus CB
Pa. valentini CB
V. steinheimensis CB

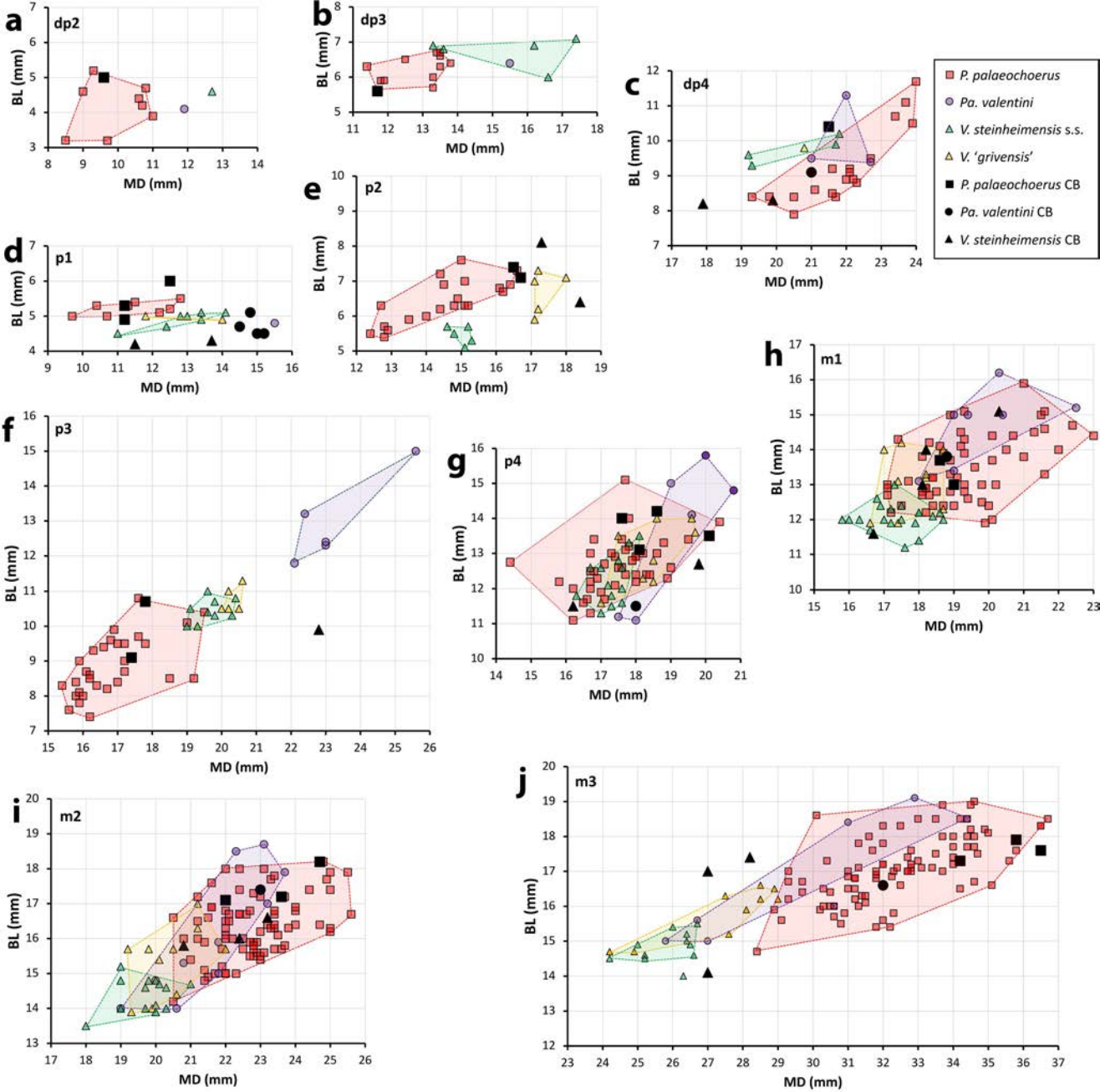
a
dp2
b
dp3
c
dp4
d
p1
e
p2
f
p3
g
p4
h
m1
i
m2
j
m3
BL (mm)
MD (mm)
P. palaeochoerus
Pa. valentini
V. steinheimensis s.s.
V. 'grivensis'
P. palaeochoerus CB
Pa. valentini CB
V. steinheimensis CB

Appendix

Table 1 List of suid dental remains from Castell de Barberà described in this paper, including taxonomic attribution, anatomical identification, and the figure(s) where each specimen is depicted. Old numbers used by Golpe-Posse (1971, 1972) are included within brackets

Catalog No.	Species	Description	Figures
IPS1712[a,b]	*V. steinheimensis*	L maxillary fragment with DP2–M1	Figs. 2c, 6p, 12r, h', w'
IPS1713[a]	*V. steinheimensis*	L mandibular fragment with p2–m3	Figs. 7g, 10o, t, b', 11i, q, y
IPS1715[a]	*Pa. valentini*	R C1f	Fig. 4f
IPS1716[a]	*P. palaeochoerus*	L i1	Fig. 8d
IPS1717 [IPS1713][c]	*P. palaeochoerus*	R I1	Fig. 3a
IPS1718[a]	*P. palaeochoerus*	L C1f	Fig. 4a
IPS1719 [IPS1719][c]	*P. palaeochoerus*	R I2	Fig. 3h
IPS1721[a]	*P. palaeochoerus*	L i2	Fig. 8g
IPS1722[a]	*P. palaeochoerus*	L c1f	Fig. 9d
IPS1723[a]	*Pa. valentini*	R c1f	Fig. 9g
IPS1749[a,b]	*Pa. valentini*	L I1	Fig. 3d
IPS1750[a]	*P. palaeochoerus*	R di3	Fig. 13m
IPS1751–IPS1760[a,d]	*P. palaeochoerus*	Upper postcanine dentition: L P2 (IPS1760), R P2–P3 (IPS1755), L P4 (IPS1754), R P4 (IPS1759), L M1 (IPS1758), R M1 (IPS1753), L M2 (IPS1757), R M2 (IPS1752), L M3 (IPS1756), and R M3 (IPS1751)	Figs. 2b, 5j, m, t, z–a', 6b–c, t–u, d'–e'
IPS28175 [IPS1542][e]	*P. palaeochoerus*	L dp4 germ mesial fragment	Fig. 13w

IPS33237 [IPS1986][a,f]	*Pa. valentini*	R M3	Fig. 6n’
IPS33240 [IPS1553][e]	*V. steinheimensis*	L mandibular fragment with m1–m3	Fig. 7h, 11j, r, z
IPS33254[a]	*Pa. valentini*	L m3	Fig. 11v
IPS33264[a]	*Pa. valentini*	R maxillary fragment with DP3	Fig. 12a’
IPS33265[a]	*V. steinheimensis*	L P4	Fig. 5o’
IPS33269a–d [IPS1541+IPS1544+IPS1545+IPS1546][e,g]	*Pa. valentini*	R maxillary fragment with damaged P4 (a, IPS1541) + damaged L P4 (b; IPS1546) + L M1 (c; IPS1544 = IPS93092) + R M2 fragment (d; IPS1545)	Fig. 5l’–m’, 6k
IPS33270[a,h]	*Pa. valentini*	R M3 mesial fragment	Fig. 6t’
IPS33272[a]	*Pa. valentini*	L DP4 (partial)	Fig. 12u’
IPS33276 [IPS1917][e]	*Pa. valentini*	L di1 germ	Fig. 13f
IPS33277a–b[a]	*P. palaeochoerus*	R di1 (a) + L di1 (b)	Fig. 13a–b
IPS33282[a]	*V. steinheimensis*	L m3 (damaged)	Fig. 11w
IPS33285[a]	*P. palaeochoerus*	R m3	Fig. 11u
IPS33286 [IPS1521][e]	*P. palaeochoerus*	L mandibular fragment with dp3	Fig. 7a, 13r
IPS33287a–f[a]	*P. palaeochoerus*	L I3 (a), R C1f (b), L C1f (c), R P1 (d), L P1 (e), and R P2 (f)	Figs. 3k, 4c–d, 5a–b, o
IPS33288[a,i]	*P. palaeochoerus*	Maxillary fragment with L P3	Fig. 5v
IPS33289a–g[a]	*P. palaeochoerus*	R P4 (a), L P4 (b), L M1 (c), R M2 (d), L M2 (e), R M3 (f), and L M3 (g)	Fig. 5h’–i’, 6a, r–s, b’–c’

IPS33290 [IPS1524][e]	*V. steinheimensis*	R i2	Fig. 8n
IPS33291[a]	*V. steinheimensis*	R m2	Fig. 11o
IPS33294 [IPS1531][e]	*P. palaeochoerus*	L P4 (partial)	Fig. 5e’
IPS33296a–e[a]	*Pa. valentini*	R M1 (a), L M1 (b), R M2 (c), R M3 (d), and L M3 (e)	Fig. 6i–j, y, l’–m’
IPS33297a–b [IPS1556+IPS1557][e,g]	*V. steinheimensis*	L m1 germ (a) [IPS1557] + L M1 germ (b) [IPS1556]	Figs. 6q, 11f
IPS33299 [IPS1566][e,j]	*V. steinheimensis*	R DP4	Fig. 12x’
IPS33300[a]	*V. steinheimensis*	L M3	Fig. 6v’
IPS33301 [IPS1539][e]	*V. steinheimensis*	L M3	Fig. 6z’
IPS33302 [IPS1540][a,f]	*P. palaeochoerus*	L M1 mesial fragment	Fig. 6e
IPS33303 [IPS1547][e]	*V. steinheimensis*	R M3	Fig. 6y’
IPS33304[a]	*P. palaeochoerus*	R p1	Fig. 10a
IPS33305[a,i]	*V. steinheimensis*	R m1 germ	Fig. 11g
IPS33306[a]	*P. palaeochoerus*	L DP4 germ	Fig. 12o’
IPS33308a–b[a,h]	*P. palaeochoerus*	Palate with R P3–P4, R M2–M3, and L P3–M3/ (a) + edentulous L mandibular fragment with m1– m3 alveoli (b)	Figs. 2a, 5r–s, f’–g’, 6v, i’–j’, 7c
IPS33309[a,k]	*V. steinheimensis*	L M3	Fig. 6w’

IPS35103 [IPS1958][a,f]	*P. palaeochoerus*	L i2	Fig. 8i
IPS39522 [IPS1523][e]	*P. palaeochoerus*	L p1	Fig. 10b
IPS87621[a,l]	*P. palaeochoerus*	R mandibular fragment with m2	Fig. 7j–l, 11m
IPS92337[a,i]	*P. palaeochoerus*	R DP4 germ	Fig. 12p’
IPS92348[a]	*P. palaeochoerus*	R dp4 distal fragment	Fig. 13x
IPS92359[a]	*P. palaeochoerus*	R di1	Fig. 13c
IPS92367[a]	*Pa. valentini*	L M2 germ distal end	Fig. 6a’
IPS92373[a]	*Pa. valentini*	R i2	Fig. 8m
IPS92374[a]	*Pa. valentini*	L i2 crown	Fig. 8l
IPS92375[a]	*Pa. valentini*	L m1	Fig. 11e
IPS92379[a]	*P. palaeochoerus*	R maxillary fragment with P4	Figs. 2d, 5c’
IPS92380[a]	*P. palaeochoerus*	L P4	Fig. 5b’
IPS92381[a]	*P. palaeochoerus*	L M1 crown	Fig. 6d
IPS92382[a]	*P. palaeochoerus*	L p4 crown	Fig. 10w
IPS92383	*V. steinheimensis*	R M3	Fig. 6a”
IPS92384[a,h]	*P. palaeochoerus*	R DI2 crown	Fig. 12g
IPS92385 [IPS1532?][e]	*P. palaeochoerus*	L p1	Fig. 10c
IPS92387[a]	*P. palaeochoerus*	R C1f	Fig. 4b
IPS92388[a]	*V. steinheimensis*	R dp3 germ	Fig. 13v
IPS92391[a,m]	*P. palaeochoerus*	R m2	Fig. 11l
IPS92392a–b[a,i]	*P. palaeochoerus*	R P1 (a) and L P1 (b)	Fig. 5c–d

IPS92395[a]	*P. palaeochoerus*	R p3	Fig. 10s
IPS92396[a]	*P. palaeochoerus*	R p3 distal fragment	Fig. 10r
IPS92397[a]	*P. palaeochoerus*	L DP3 crown	Fig. 12w
IPS92398[a]	*Pa. valentini*	L DI1	Fig. 12f
IPS92399 [IPS1339][a,n]	*Pa. valentini*	L DP4 (partial)	Fig. 12v’
IPS92400 [IPS1550][e]	*Pa. valentini*	L m1	Fig. 11d
IPS92401 [IPS1915][e]	*P. palaeochoerus*	R DP2 (partial)	Fig. 12p
IPS92402 [IPS1715][c]	*Pa. valentini*	R m2	Fig. 11n
IPS92404 [IPS1951][a,f]	*P. palaeochoerus*	L DP4 germ	Fig. 12m’
IPS92405 [IPS1814][a,f]	*P. palaeochoerus*	L DP3 germ	Fig. 12v
IPS92406[a]	*P. palaeochoerus*	L i2	Fig. 8h
IPS92407[a]	*P. palaeochoerus*	R DP4 germ (damaged)	Fig. 12n’
IPS92408[a]	*P. palaeochoerus*	L maxillary fragment with DP4	Fig. 12r’
IPS92409 [IPS1913?][e]	*V. steinheimensis*	L DP4	Fig. 12y’
IPS92410[a]	*P. palaeochoerus*	L DP4 (damaged)	Fig. 12q’
IPS92411[a]	*Pa. valentini*	R DP4 crown	Fig. 12t’
IPS92412[a]	*P. palaeochoerus*	L DP3 germ	Fig. 12u

IPS92413[a]	*P. palaeochoerus*	L DP3	Fig. 12y
IPS92414[a]	*V. steinheimensis*	R DP3 mesial fragment	Fig. 12l’
IPS92415[a]	*P. palaeochoerus*	R p4	Fig. 10x
IPS92416[a]	*P. palaeochoerus*	L p4 distal fragment	Fig. 10y
IPS92420[a]	*V. steinheimensis*	R dp4 distolingual fragment	Fig. 13d’
IPS92656[a]	*P. palaeochoerus*	L c1m (tip)	Fig. 9a
IPS92657[a]	*V. steinheimensis*	L c1m (fragment)	Fig. 9c
IPS92661[a]	*P. palaeochoerus*	L I3	Fig. 3l
IPS92669[a]	*Pa. valentini*	L p1 crown	Fig. 10g
IPS92670[a]	*Pa. valentini*	R p1 (partial)	Fig. 10h
IPS92671[a]	*V. steinheimensis*	R p1	Fig. 10j
IPS92672[a]	*Pa. valentini*	R i3 germ	Fig. 8q
IPS92678[a]	*V. steinheimensis*	R p1 crown	Fig. 10i
IPS92679[a]	*V. steinheimensis*	R p2 distal fragment	Fig. 10p
IPS92690[a]	*P. palaeochoerus*	L di3	Fig. 13n
IPS92691[a]	*P. palaeochoerus*	R DI3 crown	Fig. 12l
IPS92692[a]	*V. steinheimensis*	L P2 distal fragment	Fig. 5q
IPS92693[a]	*P. palaeochoerus*	L DP2	Fig. 12n
IPS92694[a]	*P. palaeochoerus*	L p2	Fig. 10k
IPS92695[a]	*P. palaeochoerus*	L P1	Fig. 5f
IPS92696[a]	*P. palaeochoerus*	L DP2	Fig. 12m
IPS92697[a]	*P. palaeochoerus*	L P2	Fig. 5k
IPS92698[a]	*P. palaeochoerus*	R p2	Fig. 10l
IPS92699[a]	*P. palaeochoerus*	L P1	Fig. 5e

IPS92700[a]	*P. palaeochoerus*	L P1 crown	Fig. 5g
IPS92701[a]	*P. palaeochoerus*	L di2 (damaged)	Fig. 13i
IPS92702[a]	*V. steinheimensis*	R di2	Fig. 13k
IPS92703[a]	*Pa. valentini*	R di2	Fig. 13j
IPS92704[a]	*V. steinheimensis*	L di2 partial crown	Fig. 13l
IPS92708[a,h]	*Pa. valentini*	L i3 crown	Fig. 8r
IPS92709[a,h]	*Pa. valentini*	L I1 germ	Fig. 3g
IPS92710[a,h]	*Pa. valentini*	L I2	Fig. 3j
IPS92711[a]	*P. palaeochoerus*	L DI3	Fig. 12k
IPS92718[a]	*V. steinheimensis*	R m3 distal fragment	Fig. 11x
IPS92719[a]	*Pa. valentini*	L p4	Fig. 10z
IPS92720[a]	*V. steinheimensis*	L p2 crown	Fig. 10m
IPS92722[a]	*V. steinheimensis*	L DP3	Fig. 12i’
IPS92723[a]	*V. steinheimensis*	L p2 (partial)	Fig. 10n
IPS92726[a,h]	*Pa. valentini*	L p1 germ	Fig. 10f
IPS92731 [IPS1522][e]	*Pa. valentini*	R dp4	Fig. 13a’
IPS92732 [IPS1525][e]	*P. palaeochoerus*	R m1 germ	Fig. 11c
IPS92734 [IPS1558][e]	*P. palaeochoerus*	L DP4	Fig. 12s’
IPS92735 [IPS1559][e]	*V. steinheimensis*	R DP3	Fig. 12j’

IPS92737 [IPS????][o]	*P. palaeochoerus*	R P4	Fig. 5j’
IPS92738[a]	*Pa. valentini*	L i2 crown	Fig. 8j
IPS92739[a]	*Pa. valentini*	R i2	Fig. 8k
IPS92746[a]	*V. steinheimensis*	R P4	Fig. 5n’
IPS92747[a]	*Pa. valentini*	L P4 (damaged)	Fig. 5k’
IPS92758[a,m]	*P. palaeochoerus*	L dp4	Fig. 13y
IPS92759[a,m]	*Pa. valentini*	L M3 (partial)	Fig. 6s’
IPS92760[a]	*P. palaeochoerus*	R m1 (damaged)	Fig. 11b
IPS92761[a,m]	*V. steinheimensis*	L m2 distal fragment	Fig. 11p
IPS92762[a,m]	*V. steinheimensis*	R dp4 distal fragment	Fig. 13e’
IPS92763[a]	*Pa. valentini*	R p1	Fig. 10e
IPS92764[a,m]	*Pa. valentini*	R M1 distal fragment	Fig. 6o
IPS92779[a,k]	*V. steinheimensis*	L dp3 (partial)	Fig. 13t
IPS92787[a,i]	*P. palaeochoerus*	R P3	Fig. 5u
IPS92788[a,i]	*P. palaeochoerus*	R P2	Fig. 5l
IPS92806[a,k]	*Pa. valentini*	R DP3 distal fragment	Fig. 12g’
IPS92815[a]	*P. palaeochoerus*	R i2	Fig. 8f
IPS92839[a]	*P. palaeochoerus*	R DP3 distal fragment	Fig. 12z
IPS92840[a,m]	*P. palaeochoerus*	L M2	Fig. 6w
IPS92841[a,m]	*Pa. valentini*	L M3 distolingual fragment	Fig. 6u’
IPS92842[a]	*Pa. valentini*	L M2	Fig. 6z
IPS92843[a,m]	*Pa. valentini*	R M1	Fig. 6l
IPS92846[a,m]	*P. palaeochoerus*	L DP3 germ	Fig. 12x

IPS92847[a,m]	*P. palaeochoerus*	R dp4 distal fragment	Fig. 13z
IPS92848[a,m]	*P. palaeochoerus*	R P2 distal fragment	Fig. 5n
IPS92849[a,m]	*Pa. valentini*	L DP3 distal fragment	Fig. 12f’
IPS92850[a,m]	*P. palaeochoerus*	R M1 distal fragment	Fig. 6f
IPS92852[a,m]	*V. steinheimensis*	L m1 distal fragment	Fig. 11h
IPS92856[a]	*P. palaeochoerus*	L DI1	Fig. 12a
IPS92857[a]	*Pa. valentini*	L I2	Fig. 3i
IPS92858[a]	*P. palaeochoerus*	R DI1	Fig. 12b
IPS92859[a]	*P. palaeochoerus*	R DI2 crown	Fig. 12h
IPS92860[a]	*P. palaeochoerus*	L DI2 germ	Fig. 12j
IPS92861[a]	*Pa. valentini*	L i3 germ	Fig. 8p
IPS92862[a]	*Pa. valentini*	L i3 crown	Fig. 8t
IPS92863[a]	*Pa. valentini*	L DI1	Fig. 12c
IPS92864[a]	*Pa. valentini*	R DI1	Fig. 12d
IPS92865[a]	*Pa. valentini*	L DI1	Fig. 12e
IPS92866 [IPS1717][c]	*P. palaeochoerus*	R DI2	Fig. 12i
IPS92867[a]	*V. steinheimensis*	L p4	Fig. 10c’
IPS92874[a]	*P. palaeochoerus*	L dp2	Fig. 13p
IPS92881[a]	*Pa. valentini*	R dp3 distal fragment	Fig. 13s
IPS92882[a]	*P. palaeochoerus*	R di1 (very worn)	Fig. 13d
IPS92885[a]	*Pa. valentini*	L di3	Fig. 13o
IPS93066[a]	*Pa. valentini*	L di1	Fig. 13e

IPS93068 [IPS1912][c]	*V. steinheimensis*	L di1 germ	Fig. 13h
IPS93069 [IPS1916][e]	*V. steinheimensis*	R di1 germ	Fig. 13g
IPS93070[a,k]	*V. steinheimensis*	R M3	Fig. 6x’
IPS93077 [IPS1961][a,f]	*V. steinheimensis*	R i3	Fig. 8u
IPS93078[a]	*Pa. valentini*	R i3 crown	Fig. 8s
IPS93079[a]	*V. steinheimensis*	R c1m	Fig. 9b
IPS93081[a]	*P. palaeochoerus*	R P3	Fig. 5w
IPS93082[a]	*Pa. valentini*	L p4 germ (partial)	Fig. 10a’
IPS93083[a]	*V. steinheimensis*	R dp2 (damaged)	Fig. 13q
IPS93084[a]	*Pa. valentini*	L c1f	Fig. 9f
IPS93085[a]	*Pa. valentini*	L I1	Fig. 3f
IPS93086[a]	*P. palaeochoerus*	R c1f	Fig. 9e
IPS93087[a]	*P. palaeochoerus*	L I1	Fig. 3c
IPS93088[a]	*P. palaeochoerus*	L i1 crown	Fig. 8a
IPS93089[a]	*P. palaeochoerus*	R i1	Fig. 8b
IPS93090[a]	*P. palaeochoerus*	L i1	Fig. 8c
IPS93091[a]	*P. palaeochoerus*	R I1	Fig. 3b
IPS93093 [IPS1548][a,f]	*P. palaeochoerus*	L M2 lingual fragment	Fig. 6x
IPS93094 [IPS1549][e]	*Pa. valentini*	L M3	Fig. 6q’

IPS93095 [IPS1551][e]	*Pa. valentini*	R M3 (damaged)	Fig. 6r’
IPS93096 [IPS1552][a,f]	*Pa. valentini*	L M1 (partial)	Fig. 6n
IPS93097 [IPS1567][e]	*Pa. valentini*	L DP3 (partial)	Fig. 12d’
IPS93098 [IPS1910][c]	*V. steinheimensis*	L DP3 (damaged)	Fig. 12k’
IPS93099 [IPS1911][c]	*Pa. valentini*	R DP3	Fig. 12c’
IPS93100 [IPS1988][a]	*Pa. valentini*	R P1 crown	Fig. 5i
IPS93101[a]	*Pa. valentini*	R P3 (damaged)	Fig. 5x
IPS93102 [IPS1914?][a]	*Pa. valentini*	R DP3	Fig. 12b’
IPS93103[a]	*Pa. valentini*	R i3	Fig. 8o
IPS93104[a]	*Pa. valentini*	L p1	Fig. 10d
IPS93105[a]	*Pa. valentini*	R DP2	Fig. 12q
IPS93106[a]	*V. steinheimensis*	R p4 mesial fragment	Fig. 10d’
IPS93107[a]	*Pa. valentini*	L P1 crown	Fig. 5h
IPS93108[a]	*V. steinheimensis*	R DP2	Fig. 12s
IPS93109[a]	*V. steinheimensis*	L DP2	Fig. 12t
IPS93110[a]	*Pa. valentini*	R DP2	Fig. 12p
IPS93111[a]	*Pa. valentini*	L DP3 mesial fragment	Fig. 12e’

IPS93112[a]	*Pa. valentini*	R P3 (partial)	Fig. 5y
IPS93146a–b[a]	*P. palaeochoerus*	R mandibular fragment with m1–m3 (a) and L mandibular fragment with m3 (b)	Fig. 7e, f, 11a, k, s–t
IPS93147[a]	*P. palaeochoerus*	R mandibular fragment with p2 roots and p3–p4	Fig. 7b, 10q, v
IPS93148[a]	*V. steinheimensis*	L dp4	Fig. 13c’
IPS93149[a]	*V. steinheimensis*	R dp4	Fig. 13b’
IPS93150[a]	*Pa. valentini*	R C1f	Fig. 4e
IPS93152[a]	*V. steinheimensis*	R i1	Fig. 8e
IPS93153[a]	*V. steinheimensis*	R dp3 (partial)	Fig. 13u
IPS93154[a]	*P. palaeochoerus*	L p4	Fig. 10u
IPS93155 [IPS1577?][c]	*Pa. valentini*	L M1 (damaged)	Fig. 6h
IPS93156[a]	*Pa. valentini*	R M1 (damaged)	Fig. 6m
IPS93157[a]	*Pa. valentini*	R M1 crown (damaged)	Fig. 6g
IPS93158[a]	*P. palaeochoerus*	L P4 crown	Fig. 5d’
IPS93159[a]	*P. palaeochoerus*	L maxillary fragment with P2 and partial P1 alveolus	Figs. 2e, 5o
IPS100375[a,p]	*Pa. valentini*	L I1	Fig. 3e
IPS125635[a]	*Pa. valentini*	R M3	Fig. 6o’
IPS125636[a]	*P. palaeochoerus*	R M3	Fig. 6f’
IPS125637 [IPS1716][c]	*P. palaeochoerus*	L M3	Fig. 6g’
IPS125638[a]	*P. palaeochoerus*	R M3 (damaged)	Fig. 6h’
IPS125639[a]	*Pa. valentini*	R M3 (partial)	Fig. 6p’
IPS125640[a]	*P. palaeochoerus*	L M3 (partial)	Fig. 6k’

[a] Material not included in Golpe-Posse (1971, 1972).

[b] Current IPS catalog number should not be confused with the former number used in Golpe-Posse (1971), which correspond to a specimen of *Pa. crusafonti* from Can Llobateres.

[c] Assigned to *Hyotherium palaeochoerus* by Golpe-Posse (1971), in some cases with different anatomical identifications: [IPS1713] as R I2, [IPS1719] as R I3, [IPS1717] as R I3, [IPS1912] as L i1. [IPS1577] probably corresponds IPS93155, which is the only L M1 with similar measurements to those reporte by Golpe-Posse (1971) and has no old number written on the specimen.

[d] Originally each specimen (isolated tooth or maxillary fragment) was given a different number but they clearly belong to the same individual based on shape, wear, and interproximal facets (not ascertainable in IPS1760, which nevertheless is so similar to IPS1755 that can be considered its antimere).

[e] Assigned to *Hyotherium soemmeringi* by Golpe-Posse (1971), in some cases with different anatomical identifications: [IPS1521] as L p1, [IPS1523] as L P2, [IPS1525] as R M1, [IPS1542] as dp3, [IPS1915] as L dp3, [IPS1916] as R i2, and [IPS1917] as L i2. IPS33294 has two old numbers recorded ([IPS1531] and [IPS1572]), but only the former is written on the specimen and can be found in Golpe-Posse (1971). The old number [IPS1542] was listed twice by Golpe-Posse (1971), as a dp3 mesial fragment of *H. soemmeringi* from Castell de Barberà and as a R ?m2 of *Pa. crusafonti* from Can Llobateres; only a dp4 mesial fragment IPS28175 has been found among the ICP collections, labeled as coming from Can Llobateres but most likely corresponding to the Castell de Barberà specimen, which is a dp4 mesial fragment. The old number [IPS1558] corresponding to IPS92734 was also listed twice by Golpe-Posse (1971) as L and R, and even a third time corresponding to a specimen of *Pa. crusafonti* from Can Llobateres. [IPS1913] probably corresponds to IPS92409 as it is the only L DP4 from the sample that has similar measurements to those reported by Golpe-Posse (1971) and does not have an old number written on the specimen. [IPS1914] probably corresponds to IPS33264, which is the only R DP3 from the sample that has similar measurements to those reported by Golpe-Posse (1971) and does not have an old number written on the specimen. [IPS1532] might correspond to IPS92385 as it is the L p1 that more closely resembles in dimensions those reported by Golpe-Posse (1971).

[f] This specimen has an old number written on the specimen but we have been unable to find it listed in Golpe-Posse (1971).

[g] In these cases in which several old catalog numbers are reunited into a single current number is because Golpe-Posse (1971) indicated they belong to a single individual.

[h] Collected in 1978 according to museum records.

[i] Collected in 1980 according to museum records.

[j] IPS33299 in all probability corresponds to specimen listed in Golpe-Posse (1971) as [IPS1560], but the old number written in the specimen is indeed [IPS1566].

[k] Collected in 1977 according to museum records.

[l] Collected in 2014 from Castell de Barberà s.l. (section 1 of Alba et al., 2019), probably about 2 m stratigraphically below the main fossiliferous layer (level D) of Castell de Barberà s.s.

[m] Old label indicates it was collected in Castell de Barberà "new place", i.e., likely in the surroundings but not the same exact outcrop as most of the material.

[n] This specimen has an old number written on the label but we have been unable to find it listed in Golpe-Posse (1971) and it is not sure whether it is right or not.

[o] This specimen has an old number written on the specimen (but it is no longer readable), so it might have been included in Golpe-Posse (1971), or else it has an older valid IPS number that we have been unable to determine.

[p] Collected in 2015 from Castell de Barberà-D (equivalent to the main fossiliferous level excavated by Crusafont and coworkers; Alba et al., 2019).

Appendix

Table 2 Measurements (in mm) of the suid dental remains from CB described in this paper. See Table 1 for equivalence with old numbers used by Golpe-Posse (1971, 1972) and the figure(s) where each specimen is depicted. La, Li, and Di measurements refer to c1m only. Measurements within parentheses are estimates, whereas a 'greater than' (>) symbol denotes that the actual measurement would have been higher than that provided due to damage, and an 'em dash' (—) indicates that no meaningful measurement can be taken owing to incomplete preservation

Catalog No.	Species	Description	MD	BL/Li	BLm/La	BLd/Di	BLI
IPS1712	*V. steinheimensis*	L DP2	15.7	6.6			42.0
IPS1712	*V. steinheimensis*	L DP3	14.2	10.7			75.4
IPS1712	*V. steinheimensis*	L DP4	15.1	12.8	12.8	11.8	84.8
IPS1712	*V. steinheimensis*	L M1	16.7	14.8	14.8	14.3	88.6
IPS1713	*V. steinheimensis*	L p2	18.4	6.4			34.8
IPS1713	*V. steinheimensis*	L p3	22.8	9.9			43.4
IPS1713	*V. steinheimensis*	L p4	19.8	12.7			64.1
IPS1713	*V. steinheimensis*	L m1	20.3	15.1	14.4	15.1	74.4
IPS1713	*V. steinheimensis*	L m2	23.2	16.6	16.6	16.1	71.6
IPS1713	*V. steinheimensis*	L m3	28.2	17.4	17.4	15.2	61.7
IPS1715	*Pa. valentini*	R C1f	14.6	10.4			71.2
IPS1716	*P. palaeochoerus*	L i1	7.9	12.0			151.9
IPS1717	*P. palaeochoerus*	R I1	15.3	10.5			68.6
IPS1718	*P. palaeochoerus*	L C1f	14.7	10.0			68.0
IPS1719	*P. palaeochoerus*	R I2	13.3	8.1			60.9
IPS1721	*P. palaeochoerus*	L i2	9.0	13.2			146.7
IPS1722	*P. palaeochoerus*	L c1f	13.2	8.0			60.6
IPS1723	*Pa. valentini*	R c1f	16.0	9.1			56.9
IPS1749	*Pa. valentini*	L I1	15.0	10.0			66.7
IPS1750	*P. palaeochoerus*	R di3	8.7	4.3			49.4
IPS1751[a]	*P. palaeochoerus*	R M3	31.0	23.5	23.5	19.1	75.8
IPS1752[a]	*P. palaeochoerus*	R M2	22.7	22.1	22.1	19.8	97.4
IPS1753[a]	*P. palaeochoerus*	R M1	17.4	17.3	16.3	17.3	99.4
IPS1754[a]	*P. palaeochoerus*	L P4	16.3	18.4			112.9
IPS1755[a]	*P. palaeochoerus*	R P2	16.2	9.3			57.4
IPS1755[a]	*P. palaeochoerus*	R P3	18.0	15.0			83.3
IPS1756[a]	*P. palaeochoerus*	L M3	31.6	22.3	22.3	18.3	70.6
IPS1757[a]	*P. palaeochoerus*	L M2	22.8	21.2	21.2	19.8	93.0
IPS1758[a]	*P. palaeochoerus*	L M1	17.2	17.0	17.0	16.4	98.8
IPS1759[a]	*P. palaeochoerus*	R P4	16.1	18.2			113.0
IPS1760[a]	*P. palaeochoerus*	L P2	16.6	9.5			57.2
IPS28175	*P. palaeochoerus*	L dp4	—	>9.1			

IPS33237	*Pa. valentini*	R M3	27.6	21.3	21.3	17.5	77.2
IPS33240	*V. steinheimensis*	L m1	18.2	14.0	13.8	14.0	76.9
IPS33240	*V. steinheimensis*	L m2	20.8	15.8	15.7	15.8	76.0
IPS33240	*V. steinheimensis*	L m3	27.0	17.0	17.0	14.1	63.0
IPS33254	*Pa. valentini*	L m3	32.0	16.6	16.6	15.2	51.9
IPS33264	*Pa. valentini*	R DP3	16.0	11.1			69.4
IPS33265	*V. steinheimensis*	L P4	14.0	18.0			128.6
IPS33269a	*Pa. valentini*	R P4	(14.0)	18.5			(132.1)
IPS33269b	*Pa. valentini*	L P4	13.3	18.6			139.8
IPS33269c	*Pa. valentini*	L M1	18.9	18.0	16.8	18.0	95.2
IPS33270	*Pa. valentini*	R M3	--	21.0	21.0	--	--
IPS33272	*Pa. valentini*	L DP4	—	14.3			—
IPS33276	*Pa. valentini*	L di1	5.3	6.1			115.1
IPS33277a	*P. palaeochoerus*	R di1	4.6	5.8			126.1
IPS33277b	*P. palaeochoerus*	L di1	4.4	5.7			129.5
IPS33282	*V. steinheimensis*	L m3	27.0	(14.1)	13.0	(14.1)	(52.2)
IPS33285	*P. palaeochoerus*	R m3	34.2	17.3	17.3	15.6	50.6
IPS33286	*P. palaeochoerus*	L dp3	11.7	5.6			47.9
IPS33287a	*P. palaeochoerus*	L I3	11.1	6.5			58.6
IPS33287b	*P. palaeochoerus*	R C1f	14	8.1			57.9
IPS33287c	*P. palaeochoerus*	L C1f	13.7	8.2			59.9
IPS33287d	*P. palaeochoerus*	R P1	13.0	5.1			39.2
IPS33287e	*P. palaeochoerus*	L P1	13.1	5.0			38.2
IPS33287f	*P. palaeochoerus*	R P2	15.9	7.5			47.2
IPS33288	*P. palaeochoerus*	L P3	17.0	13.7			80.6
IPS33289a	*P. palaeochoerus*	R P4	15.0	18.3			122.0
IPS33289b	*P. palaeochoerus*	L P4	15.3	18.7			122.2
IPS33289c	*P. palaeochoerus*	L M1	16.8	17.3	17.3	17.3	103.0
IPS33289d	*P. palaeochoerus*	R M2	21.9	21.8	21.8	21.6	99.5
IPS33289e	*P. palaeochoerus*	L M2	23.1	21.7	21.7	21.0	93.9
IPS33289f	*P. palaeochoerus*	R M3	32.2	22.7	22.7	18.2	70.5
IPS33289g	*P. palaeochoerus*	L M3	31.8	22.5	22.5	18.5	70.8
IPS33290	*V. steinheimensis*	R i2	7.9	11.1			140.5
IPS33291	*V. steinheimensis*	R m2	22.4	16.0	16.0	15.0	71.4
IPS33294	*P. palaeochoerus*	L P4	(15.0)	17.5			(116.7)
IPS33296a	*Pa. valentini*	R M1	17.9	17.4	17.4	17.2	97.2
IPS33296b	*Pa. valentini*	L M1	17.8	17.1	17.1	17	96.1
IPS33296c	*Pa. valentini*	R M2	23.1	21.0	20.5	21.0	90.9
IPS33296d	*Pa. valentini*	R M3	29.8	22	22	19.1	73.8
IPS33296e	*Pa. valentini*	L M3	29.4	22.3	22.3	19.3	75.9

IPS33297a	*V. steinheimensis*	L m1	18.1	13.0	12.3	13.0	71.8
IPS33297b	*V. steinheimensis*	L M1	18.1	15.1	15.1	14.7	83.4
IPS33299	*V. steinheimensis*	R DP4	15.5	13.0			83.9
IPS33300	*V. steinheimensis*	L M3	26.2	19.3	19.3	15.5	73.7
IPS33301	*V. steinheimensis*	L M3	23.5	17.6	17.6	14.3	74.9
IPS33302	*P. palaeochoerus*	L M1	—	(18.5)	18.5	—	
IPS33303	*V. steinheimensis*	R M3	24.4	17.3	17.3	14.5	70.9
IPS33304	*P. palaeochoerus*	R p1	12.5	6.0			48.0
IPS33305	*V. steinheimensis*	R m1	16.7	11.6	11.6	11.4	69.5
IPS33306	*P. palaeochoerus*	L DP4	16.3	13.8			84.7
IPS33308a	*P. palaeochoerus*	R P3	17.1	>11.9			—
IPS33308a	*P. palaeochoerus*	L P3	18.8	13.9			73.9
IPS33308a	*P. palaeochoerus*	R P4	15.0	18.9			126.0
IPS33308a	*P. palaeochoerus*	L P4	14.4	19.2			133.3
IPS33308a	*P. palaeochoerus*	L M1	17.0	17.7	16.2	17.7	104.1
IPS33308a	*P. palaeochoerus*	R M2	21.9	21.3	21.3	20.7	97.3
IPS33308a	*P. palaeochoerus*	R M3	30.0	25.4	25.4	19.0	84.7
IPS33308a	*P. palaeochoerus*	L M3	33.2	21.0	21.0	18.7	63.3
IPS33309	*V. steinheimensis*	L M3	22.7	17.1	17.1	14.5	75.3
IPS35103	*P. palaeochoerus*	L i2	>7.6	13.7			—
IPS39522	*P. palaeochoerus*	L p1	11.2	4.9			43.8
IPS87621	*P. palaeochoerus*	R m2	23.6	17.2	16.5	17.2	72.9
IPS92337	*P. palaeochoerus*	R DP4	16.6	13.6			81.9
IPS92348	*P. palaeochoerus*	R dp4	—	9.6			—
IPS92359	*P. palaeochoerus*	R di1	4.3	5.3			123.3
IPS92367	*Pa. valentini*	L M2	—	—	—	>19.5	—
IPS92373	*Pa. valentini*	R i2	(8.5)	>10.9			—
IPS92374	*Pa. valentini*	L i2	7.8	12.7			162.8
IPS92375	*Pa. valentini*	L m1	18.8	13.8	13.0	13.8	73.4
IPS92379	*P. palaeochoerus*	R P4	15.5	18.2			117.4
IPS92380	*P. palaeochoerus*	L P4	15.3	18.1			118.3
IPS92381	*P. palaeochoerus*	L M1	18.2	18.1	18.1	18.1	99.5
IPS92382	*P. palaeochoerus*	L p4	18.6	14.2			76.3
IPS92383	*V. steinheimensis*	R M3	26.6	17.8	17.8	14.5	66.9
IPS92384	*P. palaeochoerus*	R DI2	8.8	5.7			64.8
IPS92385	*P. palaeochoerus*	L p1	11.2	5.3			47.3
IPS92387	*P. palaeochoerus*	R C1f	14.7	10.0			68.0
IPS92388	*V. steinheimensis*	R dp3	>12.2	6.7			—
IPS92391	*P. palaeochoerus*	R m2	24.7	18.2	16.7	18.2	73.7
IPS92392a	*P. palaeochoerus*	R P1	13.5	5.5			40.7

IPS92392b	*P. palaeochoerus*	L P1	13.8	5.4			39.1
IPS92395	*P. palaeochoerus*	R p3	17.4	9.1			52.3
IPS92396	*P. palaeochoerus*	R p3	—	8.9			—
IPS92397	*P. palaeochoerus*	L DP3	16.2	11.5			71.0
IPS92398	*Pa. valentini*	L DI1	7.2	4.9			68.1
IPS92399	*Pa. valentini*	L DP4	15.8	(13.0)		1	-82.3
IPS92400	*Pa. valentini*	L m1	18.8	13.8	13.8	13.4	73.4
IPS92401	*P. palaeochoerus*	R DP2	>11.2	5.6			—
IPS92402	*Pa. valentini*	R m2	23.0	17.4	16.8	17.4	75.7
IPS92404	*P. palaeochoerus*	L DP4	17.0	13.7			80.6
IPS92405	*P. palaeochoerus*	L DP3	16.1	11.2			69.6
IPS92406	*P. palaeochoerus*	L i2	9.8	12.9			131.6
IPS92407	*P. palaeochoerus*	R DP4	17.4	13.8			79.3
IPS92408	*P. palaeochoerus*	L DP4	16.8	15.4			91.7
IPS92409	*V. steinheimensis*	L DP4	15.1	12.6			83.4
IPS92410	*P. palaeochoerus*	L DP4	16.1	12.8			79.5
IPS92411	*Pa. valentini*	R DP4	15.8	13.0			82.3
IPS92412	*P. palaeochoerus*	L DP3	16.4	11.8			72.0
IPS92413	*P. palaeochoerus*	L DP3	16.0	12.3			76.9
IPS92414	*V. steinheimensis*	R DP3	—	>8.4			—
IPS92415	*P. palaeochoerus*	R p4	18.1	13.1			72.4
IPS92416	*P. palaeochoerus*	L p4	—	12.0			—
IPS92420	*V. steinheimensis*	R dp4	>16.8	—			—
IPS92656	*P. palaeochoerus*	L c1m		(13.0)	(12.2)	13.0	
IPS92657	*V. steinheimensis*	L c1m		(16.7)	11.4	12.3	
IPS92661	*P. palaeochoerus*	L I3	10.8	6.7			62.0
IPS92669	*Pa. valentini*	L p1	14.8	5.1			34.5
IPS92670	*Pa. valentini*	R p1	>14.1	4.6			—
IPS92671	*V. steinheimensis*	R p1	11.5	4.2			36.5
IPS92672	*Pa. valentini*	R i3	6.1	13.2			216.4
IPS92678	*V. steinheimensis*	R p1	13.7	4.3			31.4
IPS92679	*V. steinheimensis*	R p2	>11.1	6.1			—
IPS92690	*P. palaeochoerus*	L di3	8.2	4.3			52.4
IPS92691	*P. palaeochoerus*	R DI3	8.2	4.2			51.2
IPS92692	*V. steinheimensis*	L P2	>9.0	6.6			—
IPS92693	*P. palaeochoerus*	L DP2	13.6	7.2			52.9
IPS92694	*P. palaeochoerus*	L p2	16.5	7.4			44.8
IPS92695	*P. palaeochoerus*	L P1	14.0	5.5			39.3
IPS92696	*P. palaeochoerus*	L DP2	13.6	6.4			47.1
IPS92697	*P. palaeochoerus*	L P2	15.8	8.4			53.2

IPS92698	*P. palaeochoerus*	R p2	16.7	7.1			42.5
IPS92699	*P. palaeochoerus*	L P1	13.6	5.5			40.4
IPS92700	*P. palaeochoerus*	L P1	13.4	6.0			44.8
IPS92701	*P. palaeochoerus*	L di2	5.2	7.2			138.5
IPS92702	*V. steinheimensis*	R di2	5.3	7.1			134.0
IPS92703	*Pa. valentini*	R di2	5.0	6.9			138.0
IPS92704	*V. steinheimensis*	L di2	5.4	6.5			120.4
IPS92708	*Pa. valentini*	L i3	6.6	12.6			190.9
IPS92709	*Pa. valentini*	L I1	15.3	10.1			66.0
IPS92710	*Pa. valentini*	L I2	8.6	6.6			76.7
IPS92711	*P. palaeochoerus*	L DI3	6.4	4.0			62.5
IPS92718	*V. steinheimensis*	R m3	—	—	—	12.9	—
IPS92719	*Pa. valentini*	L p4	18.0	11.5			63.9
IPS92720	*V. steinheimensis*	L p2	17.3	8.1			46.8
IPS92722	*V. steinheimensis*	L DP3	12.3	9.1			74.0
IPS92723	*V. steinheimensis*	L p2	>14.9	6.4			—
IPS92726	*Pa. valentini*	L p1	14.5	4.7			32.4
IPS92731	*Pa. valentini*	R dp4	21.0	9.1			43.3
IPS92732	*P. palaeochoerus*	R m1	18.7	>11.9	>11.9	>11.0	18.7
IPS92734	*P. palaeochoerus*	L DP4	15.3	12.7			83.0
IPS92735	*V. steinheimensis*	R DP3	14.6	10.9			74.7
IPS92737	*P. palaeochoerus*	R P4	14.1	17.1			121.3
IPS92738	*Pa. valentini*	L i2	8.1	13.8			170.4
IPS92739	*Pa. valentini*	R i2	8.4	13.8			164.3
IPS92746	*V. steinheimensis*	R P4	14.5	18.4			126.9
IPS92747	*Pa. valentini*	L P4	13.6	17.8			130.9
IPS92758	*P. palaeochoerus*	L dp4	21.5	10.4			48.4
IPS92759	*Pa. valentini*	L M3	>23.2	18.7	18.7	16.5	—
IPS92760	*P. palaeochoerus*	R m1	(19.0)	(13.0)	—	13.0	(68.4)
IPS92761	*V. steinheimensis*	L m2	—	—	—	14.7	—
IPS92762	*V. steinheimensis*	R dp4	—	10.0			—
IPS92763	*Pa. valentini*	R p1	15.0	4.5			30.0
IPS92764	*Pa. valentini*	R M1	—	—	—	16.6	—
IPS92779	*V. steinheimensis*	L dp3	>14.0	6.1			—
IPS92787	*P. palaeochoerus*	R P3	17.0	13.8			81.2
IPS92788	*P. palaeochoerus*	R P2	16.2	9.0			55.6
IPS92806	*Pa. valentini*	R DP3	--	11.4			—
IPS92815	*P. palaeochoerus*	R i2	8.7	13.7			157.5
IPS92839	*P. palaeochoerus*	R DP3	—	11.7			—
IPS92840	*P. palaeochoerus*	L M2	24.5	20.4	19.5	20.4	83.3

IPS92842	*Pa. valentini*	L M2	22.2	(22.4)	—	22.4	(100.9)
IPS92843	*Pa. valentini*	R M1	(16.3)	—	15.5	—	—
IPS92846	*P. palaeochoerus*	L DP3	16.1	11.5			71.4
IPS92847	*P. palaeochoerus*	R dp4	>14.3	10.1			—
IPS92848	*P. palaeochoerus*	R P2	—	7.4			—
IPS92849	*Pa. valentini*	L DP3	—	10.3			—
IPS92850	*P. palaeochoerus*	R M1	—	—	—	16.6	—
IPS92852	*V. steinheimensis*	L m1	—	—	—	11.5	—
IPS92856	*P. palaeochoerus*	L DI1	9.8	6.3			64.3
IPS92857	*Pa. valentini*	L I2	10.2	7.0			68.6
IPS92858	*P. palaeochoerus*	R DI1	9.7	6.3			64.9
IPS92859	*P. palaeochoerus*	R DI2	9.0	5.7			63.3
IPS92860	*P. palaeochoerus*	L DI2	8.9	6.5			73.0
IPS92861	*Pa. valentini*	L i3	7.4	>9.0			—
IPS92862	*Pa. valentini*	L i3	(6.7)	>8.5			—
IPS92863	*Pa. valentini*	L DI1	7.8	5.6			71.8
IPS92864	*Pa. valentini*	R DI1	7.1	6.0			84.5
IPS92865	*Pa. valentini*	L DI1	7.4	6.0			81.1
IPS92866	*P. palaeochoerus*	R DI2	8.0	5.4			67.5
IPS92867	*V. steinheimensis*	L p4	16.2	11.5			71.0
IPS92874	*P. palaeochoerus*	L dp2	9.6	5.0			52.1
IPS92881	*Pa. valentini*	R dp3	>9.2	5.8			—
IPS92882	*P. palaeochoerus*	R di1	4.1	5.8			141.5
IPS92885	*Pa. valentini*	L di3	6.3	5.5			87.3
IPS93066	*Pa. valentini*	L di1	5.3	6.4			120.8
IPS93068	*V. steinheimensis*	L di1	4.9	>4.5			—
IPS93069	*V. steinheimensis*	R di1	4.9	6.0			122.4
IPS93070	*V. steinheimensis*	R M3	21.1	16.5	16.5	14.6	78.2
IPS93077	*V. steinheimensis*	R i3	6.4	10.1			157.8
IPS93078	*Pa. valentini*	R i3	6.6	12.3			186.4
IPS93079	*V. steinheimensis*	R c1m		16.8	14.0	10.4	
IPS93081	*P. palaeochoerus*	R P3	18.1	15.1			83.4
IPS93082	*Pa. valentini*	L p4	>19.9	12.5			—
IPS93083	*V. steinheimensis*	R dp2	>11.2	3.9			—
IPS93084	*Pa. valentini*	L c1f	12.3	9.4			76.4
IPS93085	*Pa. valentini*	L I1	16.4	10.5			64.0
IPS93086	*P. palaeochoerus*	R c1f	13.9	8.6			61.9
IPS93087	*P. palaeochoerus*	L I1	15.2	10.0			65.8
IPS93088	*P. palaeochoerus*	L i1	7.4	11.1			150.0
IPS93089	*P. palaeochoerus*	R i1	7.7	11.7			151.9

IPS93090	*P. palaeochoerus*	L i1	7.5	11.5			153.3
IPS93091	*P. palaeochoerus*	R I1	15.4	10.4			67.5
IPS93093	*P. palaeochoerus*	L M2	(24.3)	—	—	—	—
IPS93094	*Pa. valentini*	L M3	23.8	18.3	18.3	14.9	76.9
IPS93095	*Pa. valentini*	R M3	24.5	18.0	18.0	14.3	73.5
IPS93096	*Pa. valentini*	L M1	(15.8)	—	—	>14.0	—
IPS93097	*Pa. valentini*	L DP3	>16.6	12.1			—
IPS93098	*V. steinheimensis*	L DP3	15.8	10.6			67.1
IPS93099	*Pa. valentini*	R DP3	16.1	12.1			75.2
IPS93100	*Pa. valentini*	R P1	15.2	5.7			37.5
IPS93101	*Pa. valentini*	R P3	(19.4)	(12.9)			(66.5)
IPS93102	*Pa. valentini*	R DP3	17.1	12.4			72.5
IPS93103	*Pa. valentini*	R i3	6.0	10.7			178.3
IPS93104	*Pa. valentini*	L p1	15.2	4.5			29.6
IPS93105	*Pa. valentini*	R DP2	16.0	5.8			36.3
IPS93106	*V. steinheimensis*	R p4	—	9.7			—
IPS93107	*Pa. valentini*	L P1	15.8	5.2			32.9
IPS93108	*V. steinheimensis*	R DP2	15.2	6.7			44.1
IPS93109	*V. steinheimensis*	L DP2	15.3	6.5			42.5
IPS93110	*Pa. valentini*	R DP2	16.0	5.4			33.8
IPS93112	*Pa. valentini*	R P3	17.8	>12.0			—
IPS93146a	*P. palaeochoerus*	R m1	18.6	13.7	12.5	13.7	73.7
IPS93146a	*P. palaeochoerus*	R m2	22.0	17.1	15.8	17.1	77.7
IPS93146a	*P. palaeochoerus*	R m3	35.8	17.9	17.9	17.1	50.0
IPS93146b	*P. palaeochoerus*	L m3	36.5	17.6	17.6	17.1	48.2
IPS93147	*P. palaeochoerus*	R p3	17.8	10.7			60.1
IPS93147	*P. palaeochoerus*	R p4	17.6	14.0			79.5
IPS93148	*V. steinheimensis*	L dp4	17.9	8.2			45.8
IPS93149	*V. steinheimensis*	R dp4	19.9	8.3			41.7
IPS93150	*Pa. valentini*	R C1f	15.3	9.9			64.7
IPS93152	*V. steinheimensis*	R i1	6.3	9.7			154.0
IPS93153	*V. steinheimensis*	R dp3	>10.5	5.6			—
IPS93154	*P. palaeochoerus*	L p4	20.1	13.5			67.2
IPS93155	*Pa. valentini*	L M1	19.2	(17.3)	—	17.3	(90.1)
IPS93156	*Pa. valentini*	R M1	(16.5)	(15.7)	>14.2	15.7	95.2
IPS93157	*Pa. valentini*	R M1	20	(17.9)	(17.8)	17.9	(89.5)
IPS93158	*P. palaeochoerus*	L P4	14.6	17.4			119.2
IPS93159	*P. palaeochoerus*	L P2	15.9	7.4			46.5
IPS100375	*Pa. valentini*	L I1	15.7	10.3			65.6
IPS125635	*Pa. valentini*	R M3	31.4	22.4	22.4	18.6	71.3

IPS125636	*P. palaeochoerus*	R M3	33.2	21.8	21.8	19.1	65.7
IPS125637	*P. palaeochoerus*	L M3	32.0	22.3	22.3	20.2	69.7
IPS125638	*P. palaeochoerus*	R M3	30.4	23.0	23.0	19.0	75.7
IPS125639	*Pa. valentini*	R M3	27.8	(22.0)	(22.0)	18.5	(79.1)
IPS125640	*P. palaeochoerus*	L M3	29.3	(19.7)	(19.7)	(18.0)	(67.2)

[a] Specimens IPS1751–IPS1760 were given different catalog numbers but clearly belong to the same individual based on shape, wear, and interproximal facets.